



รายงานวิจัยฉบับสมบูรณ์

โครงการ การพัฒนาอุปกรณ์ตรวจวัดบนกระดาษสำหรับวิเคราะห์ตัวอย่างอาหาร

โดย ดร. วิจิตรา เดือนฉาย

รายงานวิจัยฉบับสมบูรณ์

โครงการ การพัฒนาอุปกรณ์ตรวจวัดบนกระดาษสำหรับวิเคราะห์ตัวอย่างอาหาร

ผู้วิจัย ดร. วิจิตรา เดือนฉาย ภาควิชาเคมี คณะวิทยาศาสตร์ มหาวิทยาลัยเทคโนโลยีพระจอมเกล้าธนบุรี

สนับสนุนโดยสำนักงานคณะกรรมการการอุดมศึกษา สำนักงานกองทุนสนับสนุนการวิจัย และมหาวิทยาลัยเทคโนโลยีพระจอมเกล้าธนบุรี (ความเห็นในรายงานนี้เป็นของผู้วิจัย สกอ. และ สกว. ไม่จำเป็นต้องเห็นด้วยเสมอไป)

Contents

Торіс	Pages
บทคัดย่อ	1
Abstract	2
Executive Summary	3
CHAPTER I	4-6
INTRODUCTION	
CHAPTER II	7-18
Silver nanoparticle colorimetric sensing for paper-based device	
CHAPTER III	19-27
Colorimetric determination of nitrite and nitrate in meat using paper-	
based device	
CHAPTER IV	28-45
Determination of Aerosol Oxidative Activity using Silver Nanoparticle	
Aggregation on Paper-Based Analytical Devices	
CHAPTER V	46
CONCLUSIONS AND FUTURE PERSPECTIVE	
ภาคผนวก	47

บทคัดย่อ

รหัสโครงการ : MRG5580234

ชื่อโครงการ : การพัฒนาอุปกรณ์ตรวจวัดบนกระดาษสำหรับวิเคราะห์ตัวอย่างอาหาร

ชื่อนักวิจัย: ดร. วิจิตรา เดือนฉาย

อีเมลล์: wijitar_29@hotmail.com

ระยะเวลาโครงการ : 2 ปี 6 เดือน ระหว่างวันที่ 2 กรกฎาคม 2555 ถึงวันที่ 31 ธันวาคม 2557

บทคัดย่อ:

ความปลอดภัยทางด้านอาหารเป็นสิ่งที่สำคัญต่อการบริหารประเทศเนื่องจากการแข่งขันทางด้านอาหารและ การสร้างชื่อเสียงในด้าน "ครัวไทยสู่ครัวโลก" ดังนั้นโครงการนี้เน้นการพัฒนาชุดตรวจวัดอาหารที่มีราคาถูก เหมาะกับประเทศกำลังพัฒนาและด้อยพัฒนา รวมทั้งเหมาะกับประเทศไทย ชุดตรวจวัดราคาถูกที่กล่าวนี้ คือ ชุดตรวจวัดบนกระดาษ เนื่องจากกระดาษเป็นวัสดุที่ไม่แพง กระบวนการผลิตที่ง่าย แต่อย่างไรก็ดี งานวิจัยในปัจจุบันประยุกต์ชุดตรวจวัดบนกระดาษเพี่ยงเพื่อการวินิจฉัยโรคเท่านั้น โครงการนี้เป็นโครงการ แรกที่พัฒนาชุดตรวจวัดบนกระดาษเพื่อวิเคราะห์ตัวอย่างอาหาร โดยทำการสร้างชุดตรวจวัดด้วย เครื่องพิมพ์ขี้ผึ้งแบบแข็ง สำหรับส่วนตรวจวัดใช้การตรวจวัดโดยอาศัยหลักการเปลี่ยนสีของการเกาะกลุ่ม กันของอนุภาคเงินระดับนาโนเมตร ซึ่งอนุภาคเงินระดับนาโนเมตรสามารถประยุกต์เพื่อใช้วิเคราะห์ไอออน ทองแดงในน้ำดื่มได้อย่างรวดเร็ว ราคาไม่แพง และสามารถวิเคราะห์ได้ด้วยตาเปล่า สารปนเบื้อนในอาหาร ที่ทำการศึกษาเพิ่มเติมคือ ในเตรต และในไตรต เนื่องจากเป็นสารเติมแต่งในการกระบวนการแปรรูปเนื้อ เพื่อป้องกันการเบื้อยและเสื่อมสภาพ เก็บรักษาสภาพสีและกลิ่นในดูน่ากิน แต่สารทั้งสองตัวนี้หากปนเบื้อน ในอาหารเกินปริมาณที่กำหนด จะก่อนให้เกิดโรคมะเร็งได้ ดังนั้นชุดตรวจวัดบนกระดาษในโครงงานวิจัยนี้ พัฒนาเพื่อตรวจวัดในเตรตและในไตรตในตัวอย่างอาหารประเภทเนื้อ เพื่อให้ได้ชุดตรวจวัดที่ราคาไม่แพง รวดเร็ว และสามารถวิเคราะห์ได้ด้วยตาเปล่า

คำหลัก: ทองแดง; ในเตรต; ในไตรต; การวิเคราะห์ปริมาณ; อาหาร

Abstract

Project Code: MRG5580234

Project Title: Development of paper-based devices for food analysis

Investigator: Dr. Wijitar Dungchai

E-mail Address: Wijitar_29@hotmail.com

Project Period: 2 years and 6 months during 2nd July 2012 to 31st December 2014

Abstract:

The food safety improvement is the one important strategy of Thai's government to boost food competitiveness and promote Thailand as "kitchen of the world". This project therefore needs to develop low-cost devices for food analysis being suitable for both developed and developing nations including Thailand. As developed these devices show significant support in the food safety improvement. Of the available formats, paper-based microfluidic devices have attracted significant attention because of the ultra-low cost of the materials and manufacturing processes used. To date, however, paper-based devices have been utilities for diagnostics. Here, we will develop the first paper-based devices coupled with colorimetric detection for food analysis. The paper-based microfluidic channels were prepared by wax printer. For colorimetric detection, silver nanoparticles aggregation is the attractive technique for rapid and low-cost detection of copper in drinking water samples by naked eyes. Nitrite and nitrate have also been used as food additives using in processed meat to prevent the spoilage, kept the meat red and produce the good smell. Nitrite and nitrate are food contaminants that as a result of degenerative diseases that effects on human health when given in high levels and cause of Eutrophication and cancer. Therefore, our proposed devices promise to be suitable for the low-cost and high-throughput screening by naked eyes for the determination of nitrate, nitrite and copper in meat.

Keywords: Copper; Nitrate; Nitrite; Determination; Food

Executive Summary

วัตถุประสงค์

- 1. เพื่อออกแบบชุดตรวจวัดบนกระดาษ เพื่อการตรวจวัดไอออนทองแดง ในเตรต และ ในไตรตด้วยตาเปล่า
- 2. ศึกษาภาวะที่เหมาะสมสำหรับการตรวจวัดไอออนทองแดง ในเตรต และในไตรต โดยอาศัยหลักการเกาะ กลุ่มกันของอนุภาคเงินระดับนาโนเมตร ตัวอย่างเช่น ชนิดของไทออลที่ใช้ดัดแปรอนุภาคเงินระดับนาโน เมตรสำหรับตรวจวัดไอออนทองแดง สารละลายบัฟเฟอร์ ผลของ pH ความจำเพาะในการตรวจวัด เป็นต้น
- 3. ประยุกต์วิธีการการวิเคราะห์ที่ได้รับการพัฒนาแล้วสำหรับใช้หาปริมาณของไอออนทองแดงในตัวอย่างน้ำ ดื่มจริง และในเตรต ในไตรต ในตัวอย่างเนื้อแปรรูป

การดำเนินงานวิจัย และผลงานวิจัยที่ได้รับอย่างย่อ ๆ

- 1. คันคว้าข้อมูลและเอกสารที่เกี่ยวข้อง
- 2. ได้รูปแบบอุปกรณ์ที่เหมาะสมสำหรับการตรวจวัดไอออนทองแดง ในเตรต และในไตรตด้วยตาเปล่า
- 3. ศึกษาขนาดอนุภาคนาโนเมตรและตรวจสอบสมบัติของโลหะที่สังเคราะห์ได้ด้วยเครื่องมือTransmission electron microscopy (TEM) และเครื่องมือทางสเปกโทรสโคปี เพื่อใช้โลหะช่วยในการเพิ่มสัญญาณการ ตรวจวัด
- 4. ศึกษาภาวะที่เหมาะสมสำหรับการตรวจวัดไอออนทองแดง ในเตรต และในไตรต โดยอาศัยหลักการเกาะ กลุ่มกันของอนุภาคเงินระดับนาโนเมตร ตัวอย่างเช่น ชนิดของไทออลที่ใช้ดัดแปรอนุภาคเงินระดับนาโน เมตรสำหรับตรวจวัดไอออนทองแดง สารละลายบัฟเฟอร์ ผลของ pH ความจำเพาะในการตรวจวัด เป็นต้น
- 5. ศึกษาค่าตัวแปรที่สำคัญทางการวิเคราะห์ ได้แก่ ค่าความเข้มขันต่ำสุดของการวิเคราะห์ ช่วงความสัมพันธ์ ของสัญญาณและความเข้มขัน ความสามารถในการทำซ้ำได้
- 6. นำภาวะที่เหมาะสมที่ได้จากการศึกษาในสารตัวอย่างจริง ได้แก่ น้ำดื่ม เนื้อแปรรูป ไส้กรอก แฮม
- 7. สรุปผลการทดลอง และเขียน manuscript เพื่อตีพิมพ์ในวารสารระดับนานาชาติ
- 8. ผลลงานได้รับการตีพิมพ์ในวารสารระดับนานาชาติ ชื่อวารสาร Talanta (impact factor = 3.722) ดัง เกกสารแนบ
- 9. ได้ทำการศึกษาเบื้องต้นเกี่ยวกับการพัฒนาชุดตรวจวัดบนกระดาษเพื่อตรวจวัด Oxidative Activity ใน อากาศ โดยอาศัยปฏิริยาระหว่าง Oxidative subtract ในอากาศกับกลูตาไทโอน หลังจากนั้นทำการวัดก ลูตาไทโอนที่เหลือด้วยอนุภาคเงินระดับนาโนเมตร โดยอาศัยการเกาะกลุ่มกัน
- 10.หาภาวะที่เหมาะสมของการตรวจวัด Oxidative Activity ในอากาศ เช่น ระยะเวลาการเกิดปฏิกิริยา
- 11.ศึกษาตัวแปรทางการวิเคราะห์ ได้แก่ ขีดจำกัดต่ำสุดของ ช่วงความสัมพันธ์เชิงเส้นตรง ความสามารถใน การวัดซ้ำ
- 12.พัฒนาขึ้นไปใช้สำหรับการตรวจวัดปริมาณโปรตีนในสารตัวอย่างจริง ได้แก่ ควันบุหรี่ และทำการ เปรียบเทียบผลการทดลองที่ได้กับวิธีการทดลองอื่นๆ
- 13.ผลงานได้รับการตอบรับให้ตีพิมพ์ในวารสาร Analyst (impact factor = 3.913)ดังเอกสารแนบ

CHAPTER I

INTRODUCTION

The important plan of Thai's government to increase the economic growth is a boost to "kitchen of the world". Kitchen of the world means Thailand as one of the world's largest and most advanced producers and exporters of processed food products. Thailand is known as the food basket of Asia, since Thailand has a total area of 513,115 km², 45% of which is used for agricultural production. Furthermore, Thailand has the fertile soil bountiful water. Although, Thailand riches agricultural roots and resources, the investments in international quality standards, technology, and research and development (R&D) for food safety still required to boost food competitiveness and promote Thailand as "kitchen of the world". Pointof-care testing (POCT) has become relatively commonplace in the developed nations as a way to augment food safety. The goal of point-of-care applications is to provide a total answer where a sample is introduced to the device and data is generated that can be used to make an informed decision. POCT is also needed in the developing world because it can reduce the cost of food safety test, increase customer satisfaction, improve the outcomes of safe food, and decrease the amount of food rejection. The development of devices for food analysis has been spurred at least in part by the desire to produce rapid, accurate and automatic devices. For example, Chailapakul O.'s group has successfully generated a semiautomatic sequential injection device for the determination of trace heavy metals in herbs using screenprinted carbon nanotubes electrodes. Moreover, alternative electrochemical detection with HPLC was developed for the separation and determination of Sudan dyes in soft drink by this group.² Both methods were more sensitive, selective and rapid than the previous reports. However, these examples aren't adequate for point-of-care applications. In recent years, different commercial point-of-care tests have been manufactured by several companies under different trade names (e.g., BR test, Eclipse test, Copan test, Delvotest, Lumac, and Arla) for microbiological test. Microbiological tests in food can be performed by non-professionals on-farm or laboratory. Unfortunately, these commercial test kits are expensive cost or/and have to export from overseas.

To this end, there is a growing push to generate low-cost and easy-to-use devices that are extremely low cost (<\$1 US or 30 baths per 1 test) and require minimal external instrumentation to obtain the quantitative information for developed and developing nations, especially Thailand. As an alternative to traditional point-of-care tests, Dungchai and coworkers recently introduced paper-based microfluidic devices (μPAD). There are many advantages in using paper as the platform for POCT. For example, Paper is widely manufactured from renewable resources and is inexpensive. It is combustible and biodegradable. The porous structure of paper enables wicking of liquid which is important for lateral flow assays and chromatography applications. Paper is also suitable for biological applications since cellulose is compatible with biological samples. Paper surface can be easily manipulated through printing,

coating and impregnation and can be fabricated in large quantities. It can be easily stored, transported and disposed. Existing use in analytical chemistry allow for easy transfer of techniques for new applications. Paper properties can be easily altered to suit different applications.

To date, μPAD have been developed for diagnostic tools including glucose, lactate, and uric acid determination.⁴ The results of the assay were quantified by comparing the color intensities generated by unknowns to those generated for known analyte concentrations. In an effort to conduct quantitative analysis for diagnostic tests based on paper microfluidics, several authors have used cameras or scanners to record the color intensity.¹⁰ Camera phones and portable scanners are an attractive format because they can be used by unskilled personnel and provide more accurate results as compared to visual inspection. Hence, μPAD coupled with the colorimetric or/and electrochemical method is one potentially alternative approach for point-of-care testing of contaminant in food, but it has not yet been evaluated.

Our efforts is to develop low-cost and paper-based devices for point-of-care testing of heavy metals such as copper, lead and cadmium ion contaminated in food. Rice, vegetables, fruit, herbal medicines, and water contaminated with heavy metals arise from contaminated agricultural lands and/or the production process. Trace amount of heavy metals in environment can be incorporated into various food chains and accumated to the toxic levels in food. Hence, the determination of trace heavy metals content in food and environmental is important for both toxicology and acceptance criteria of food safety. Several analytical techniques such as atomic absorption spectrometry (AAS), inductive coupled plasma atomic emission spectrometry (ICP-AES), inductively coupled plasma mass spectrometry (ICP-MS), and anodic stripping voltammetry (ASV). These methods aren't suitable for point-of-care testing. Therefore, colorimetric assays based on nanoparticle (NP) assembly have received considerable attention for pointof-care testing of heavy metal due to their easy operation, ability to detect by optical methods, suitability for μPAD, simplicity and high sensitivity. Silver nanoparticles (AgNPs) have been intensively developed as a probe or sensor for the determination of heavy metals, based upon the fact that on the addition of aminothiols, AgNPs become aggregated. 12-13 Only two reports of the AgNPs colorimetric changes in the presence of Hg²⁺ and Ni²⁺ have been reported by using UV-vis spectrometer. The advantage of AgNPs is that the molar extinction coefficient of AqNPs is some 100-fold greater than that for gold nanoparticles and organic indicators. It hence leads to an improved the visibility of AgNPs aggregation in presence of heavy metal on μPAD by naked eyes. Our μPAD will be designed for simultaneous metal detection by untrained personnel without the need to transport food sample and transmit the results to a central laboratory. This approach, which combines many advantages of LPAD with nanoparticles aggregation detection, holds significant potential for POCT due to its low cost, multianalyte capability, low sample volume, and inherent portability. Furthermore, electrochemical detection on LPAD will be developed in this work for the accurate quantifications of contaminated substance in food. Therefore, our proposed devices promise to be low-cost and high-throughput screening test by naked eyes.

Reference

- (1) Chailapakul, O.; Injang, U.; Noyrod, P.; Siangproh, W.; Dungchai, W.; Motomizu, S., Determination of trace heavy metals in herbs by sequential injection analysis-anodic stripping voltammetry using screen-printed carbon nanotubes electrodes. *Anal Chim Acta* **2010**, 668 (1), 54-60.
- (2) Chailapakul, O.; Wonsawat, W.; Siangproh, W.; Grudpan, K.; Zhao, Y. F.; Zhu, Z. W., Analysis of sudan I, sudan II, sudan III, and sudan IV in food by HPLC with electrochemical detection: Comparison of glassy carbon electrode with carbon nanotube-ionic liquid gel modified electrode. *Food Chem* **2008**, *109* (4), 876-882.
- (3) Puchades, R.; Chafer-Pericas, C.; Maquieira, A., Fast screening methods to detect antibiotic residues in food samples. *Trac-Trend Anal Chem* **2010**, *29* (9), 1038-1049.
- (4) Dungchai, W.; Chailapakul, O.; Henry, C. S., Use of multiple colorimetric indicators for paper-based microfluidic devices. *Anal Chim Acta* **2010**, *674* (2), 227-33.
- (5) Dungchai, W.; Chailapakul, O.; Henry, C. S., Electrochemical detection for paper-based microfluidics. *Anal Chem* **2009**, *81* (14), 5821-6.
- (6) Carrilho, E.; Martinez, A. W.; Whitesides, G. M., Understanding Wax Printing: A Simple Micropatterning Process for Paper-Based Microfluidics. *Anal Chem* **2009**, *81* (16), 7091-7095.
- (7) Lin, B. C.; Lu, Y.; Shi, W. W.; Jiang, L.; Qin, J. H., Rapid prototyping of paper-based microfluidics with wax for low-cost, portable bioassay. *Electrophoresis* **2009**, *30* (9), 1497-1500.
- (8) Qin, J. H.; Lu, Y.; Shi, W. W.; Lin, B. C., Fabrication and Characterization of Paper-Based Microfluidics Prepared in Nitrocellulose Membrane By Wax Printing. *Anal Chem* **2010**, *82* (1), 329-335.
- (9) Dungchai, W.; Chailapakul, O.; Henry, C. S., A low-cost, simple, and rapid fabrication method for paper-based microfluidics using wax screen-printing. *Analyst* **2011**, *136* (1), 77-82.
- (10) Martinez, A. W.; Phillips, S. T.; Carrilho, E.; Thomas, S. W.; Sindi, H.; Whitesides, G. M. Simple Telemedicine for Developing Regions: Camera Phones and Paper-Based Microfluidic Devices for Real-Time, Off-Site Diagnosis. *Anal Chem* 2008, 80, 3699-3707.
- (11) Chuanuwatanakul, S.; Dungchai, W.; Chailapakul, O.; Motomizu, S., Determination of trace heavy metals by sequential injection-anodic stripping voltammetry using bismuth film screen-printed printed carbon electrode. *Anal Sci* 2008, 24 (5), 589-94.
- (12) Li, H. B.; Cui, Z. M.; Han, C. P., Glutathione-stabilized silver nanoparticles as colorimetric sensor for Ni²⁺ ion. *Sensor Actuat B-Chem* **2009**, *143* (1), 87-92.
- (13) Roy, B.; Bairi, P.; Nandi, K. A., Selective colorimetric sensing of mercury(II) using turn off–turn on mechanism from riboflavin stabilized silver nanoparticles in aqueous medium. *Analyst* **2011**, *136*, 3605–3607.

CHAPTER II

Silver Nanoparticle Colorimetric Sensing for Paper-Based Devices

1. Introduction

The development of simple, rapid, and inexpensive detection method for diagnostics and environmental monitoring is still needed in developing and undeveloped countries for sustainable development in public health [1]. Currently, paper devices including paper strip tests, paper-based assays, and paper-based microfluidics are attractive for portable point-of-measurement (POM) monitoring and on-site detection due to advantages which include low cost, portability, ease of use, high speed, and low reagent and sample consumption [2-4]. Furthermore, paper provides a high surface area/high optical contrast substrate for colorimetric detection. Paper devices are also suited for use by nontechnical personnel. Finally, paper devices are made from naturally abundant, biodegradable and inexpensive materials (i.e., cellulose) [5-6]. Most commercial paper devices use colorimetric detection and have been applied for qualitative and/or semi-quantitative analyte detection [1, 7-11]. For colorimetric sensing, flow is directed along the paper matrix by capillary action, and analyte reacts with a label or organic dye in the test zone. The assay results are quantified by comparing the color hues and/or intensities generated by unknown analytes to known analyte concentrations. Nontechnical personnel can interpret the result by the naked eye in many cases. Paper devices therefore do not require external instrumentation for interpretation or mechanical forces to drive flow.

Gold nanoparticle (AuNP) colorimetric probes have been widely used for colorimetric assays because their extinction coefficients are high relative to common organic dyes [12-17]. AuNP colorimetric sensing has been used with two approaches. First, the result can be determined by the accumulation of an intense red color that is associated with the color of AuNPs with a diameter of 10-50 nm. The most common example of this mode of detection is the commercial immunochromatographic test strip [18-19]. Alternatively, the color change of AuNP due to aggregation or dispersion with the addition of analyte can be used [20-21]. For example, Lu and coworker first reported the AuNP aggregation in a dipstick assay [22]. Their device detects analyte by immersing a lateral flow device immobilized with blue colored aggregated of AuNPs into a testing solution. The blue aggregated AuNPs turned red when dispersed by the analyte in a concentration dependent manner. Inspired by Lu's work, Zhao and coworkers demonstrated the feasibility of using a AuNP-based colorimetric sensing platform on paper devices [23].

Recently, silver nanoparticles (AgNPs) have been used as an alternative colorimetric sensing system due to lower cost and higher extinction coefficients than AuNPs [24]. The high molar extinction coefficient of AgNPs leads to improved visibility based on the difference in optical brightness and increased sensitivity of UV-visible spectroscopic detection [25]. Although colorimetric applications of AgNP aggregation provide high sensitivity and selectivity for the determination of analytes such as histidine [26], homocysteine [25], cysteine [27],

mercury ions [28-29], and nickel ions [30] using UV-visible spectroscopy, AgNP colorimetric sensing for PADs has not been reported [31]. The only analytical application of AgNPs on cellulose paper that has been reported is for the determination of Rhodamine 6G dye using Raman Spectroscopy [32]. Therefore, the aim of this study was to investigate AgNP colorimetric sensing for PADs. The utility of AgNP aggregation on paper devices was demonstrated for the detection of copper (II) ions based on AgNP aggregation. Copper ions play an important role in living organisms and industry but excess intake of copper ions can be toxic [33]. The World Health Organization (WHO) prescribes the maximum allowable levels of copper (II) ions in drinking water at 1.3 mg L⁻¹ or 20.5 μM [34]. In this work, homocysteine and dithiothreitol bind to AgNPs (~10 nm in diameter presenting yellow color) through Ag-S bonds and then binding between Cu²⁺ and the surface-modified AgNPs results in their aggregation (Figure 1A). The aggregation of AgNPs in the presence of copper (II) ions leads to a decrease in the surface plasmon resonance absorption peak and the formation of a new red-shifted peak. Both paper-based assay devices and paper-based microfluidic devices for Cu²⁺ detection using AgNP colorimetric sensor were studied. After the addition of Cu²⁺ solution into paper devices, the yellow color of AgNPs changed to orange or green-brown depending on the Cu²⁺ concentration. Finally, our devices were successfully applied to the detection of Cu²⁺ in real water samples.

2. Experimental

2.1 Chemicals and Materials

All chemicals used in experiment were analytical reagent (AR) grade and solutions were prepared using high pure water with a resistance of 18 M Ω cm $^{-1}$. Homocysteine (Hcy), dithiothreitol (DTT), cysteine (Cys), glutathione (Glu) and metal ions (As $^{2+}$, Ca $^{2+}$ Cd $^{2+}$, Co $^{2+}$, Cu $^{2+}$, Fe $^{3+}$, Hg $^{2+}$, K $^+$,Mg $^{2+}$, Mn $^{2+}$, Na $^+$,Ni $^{2+}$, Pb $^{2+}$ and Zn $^{2+}$) were bought from Sigma-Aldrich (St. Louis, Missouri). AgNPs was obtained from Sensor Research Unit at Department of Chemistry, Chulalongkorn University, Thailand. Whatman No.1 filter paper was bought from Cole-Parmer (Vernon Hills, IL). All glass ware was thoroughly cleaned with freshly prepared 1:1 HCI/HNO $_3$ and rinsed with Mill-Q 18 M Ω cm $^{-1}$ resistance water prior to use.

2.2 Instrumentation

UV-visible absorption spectra were recorded by a UV-visible spectrometer (Lambda 35, Perkin Elmer Instruments, USA) using 1-cm path length quartz cuvettes. Photographic results were recorded using a digital camera (PowerShot S95, Canon).

2.3 Synthesis of the modified AgNPs

A yellow 0.1 mM AgNP solution (\sim 10 nm in diameter) was prepared from the dilution of AgNPs stock solution with 18 M Ω cm $^{-1}$ water. Then, stock solutions of Hcy and DTT were added to the AgNP solution to

generate final concentrations of 3.5 μ M Hcy and 3.0 μ M DTT. To let the self-assembly of aminothiol compounds onto the surface of AgNPs, the mixture was left for \sim 2 h at the room temperature. After this step, the AgNP aggregation was characterized using UV-visible spectrometry. 1.00 mL of modified AgNP solution was mixed with 1.00 mL of metal ion in 50 mM phosphate buffer at pH 8 (Na₂HPO₄ and NaH₂PO₄). Before analysis using the spectrometer, the mixture solution was incubated for 30 min at the room temperature.

2.4 Preparation of the paper devices

The cutting method was used to pattern Whatman filter paper 1 according to previously reported methods [35]. The pattern was created using CorelDraw and then transferred file to the Silhouette Studio program. Cutting printer (Silhouette America, Inc.) incorporates a knife in place of the traditional ink pen. The knife rotates freely on a turret, enabling precise cutting of various features, including small-radius corners, small channel or holes with 100 μ m resolution. The instrument setup and actual cutting require \sim 60 s and \sim 20 s per device, respectively.

2.5 Detection of copper on the paper devices

Paper-based assay devices (PADs, holes shape with 4 mm in diameter) were modified with 0.5 μ L of homocysteine-dithiothreitol-AgNP solution in the test zone and allowed to dry before use. PADs are differentiated from μ PADs by the lack of a flow channel in PADs. 0.5 μ L of Metal ion solutions (As²⁺, Ca²⁺, Cd²⁺, Co²⁺, Cu²⁺, Fe³⁺, Hg²⁺, K⁺, Mg²⁺, Mn²⁺, Na⁺, Ni²⁺, Pb²⁺ and Zn²⁺) were then added to the paper devices.

Paper-based microfluidic devices (μ PADs) were also prepared for Cu²⁺ detection. The test zone of μ PADs was spotted with 0.2 μ L of homocysteine-dithiothreitol-AgNP solution (Fig. 5A and 5B) and let it dry. For detection, 12 μ L of 15.7 μ M Cu²⁺ solution was dropped into the loading zone. An alternative pattern of μ PADs is shown in Fig. 5C. 0.2 μ L of Cu²⁺ solution at 7.8 nM, 780 nM, 7.8, 15.7, 31.4, 62.8 μ M, and buffer solution was dropped into test zone number 2, 3, 4, 5, 6, 7, and 8, respectively. For detection, 12 μ L of the modified AgNP solution was dropped into the loading zone.

2.6 Applications

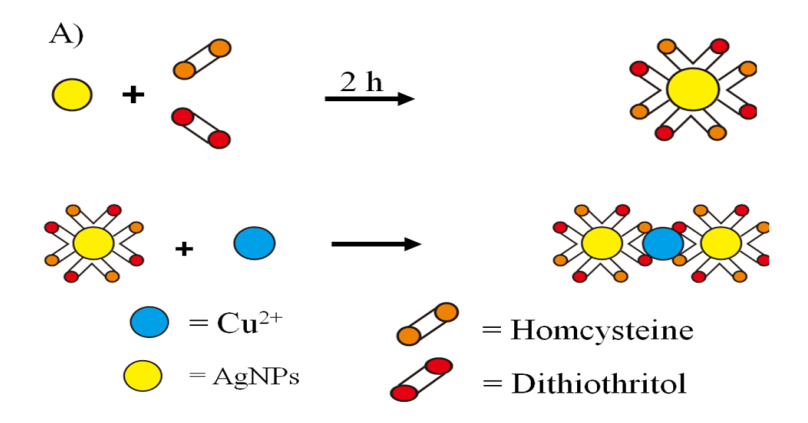
To evaluate the utility of our proposed method, the Cu²⁺ in tap and pond water was quantified. Tap water samples were obtained from a water tap in the chemistry building, Faculty of Science, King Mongkut's University of Technology Thonburi, Bangkok, Thailand. Pond water samples were obtained from a pond in front of King Mongkut's University of Technology Thonburi, Bangkok, Thailand. Prior to analysis, preconcentration was carried out on all samples. 15 mL of sample was mixed with 10 mL of 0.1 M HNO₃ and then heated to evaporate excess water until 2.5 mL of samples remained. Next, 100 mM phosphate buffer pH 8 was added to the sample to generate a final volume of 4 mL. The samples were then adjusted to pH 8 by the addition of 3 M

sodium hydroxide and then water added to reach a final volume of 5 mL and thus a 3-fold higher concentration than the original sample.

3. Results and discussion

3.1 Characterization of AgNP aggregation

We initially investigated the AgNP aggregation by UV-visible spectrometer (Fig. 1A). As is well known, – SH group in aminothiol compounds such as Hcy, DTT, Cys, and Glu can modify the AgNP surface whereas the other functional groups have a strong affinity for metal ions [30]. In this work, four aminothiol compounds, including Hcy, DTT, Cys, and Glu, were studied. After the addition of 7.8 nM Cu²⁺ solution to the modified AqNPs solution, the solution color changed from yellow to orange color only in the mixture of Hcy, DTT and AgNPs. We also found a decrease in the plasmon resonance absorption peak at 404 nm and the formation of a new red-shifted band at 502 nm (Fig. 1B) suggesting that the mixture of Hcy and DTT can induce the aggregation of AgNPs in the presence of Cu2+ is reported to be the excellent catalysts for aminothiol oxidation [36]. After the redox reaction between the aminothiol and Cu^{2+} , Cu^{+} generated in the solution. The Cu²⁺ behaved differently than other metals because of the higher stability constant between DTT and Cu⁺ relative to other metals (log $K = 6.9 \, (Zn^{2+})$, 9.7 (Pb²⁺), 10.8 (Cd²⁺), 6.5 (Ni²⁺) and 11.1 (Cu⁺)) [37]. In the next experiments, the selectivity of this method was evaluated by adding other metal ions at 200 times the Cu2+ concentration (1.6 μ M of As²⁺, Ca²⁺, Cd²⁺, Co²⁺, Fe³⁺, Hg²⁺, K⁺, Mg²⁺, Mn²⁺, Na⁺, Ni²⁺, Pb²⁺ and Zn²⁺) into the AqNP solution. An increase in the absorbance ratio (502 nm/404 nm) was clearly observed in the presence of Cu²⁺, whereas no change was measured in the presence of other metals as shown in Fig. 1B. Next, the parameters affecting the sensitivity and selectivity of Cu²⁺ detection were optimized. The concentration of Hcy and DTT, pH of phosphate buffer and incubation time were studied prior to application on paper devices. The best absorbance ratio was obtained at 50 mM phosphate buffer at pH 8, 3.5 µM of Hcy, 3.0 µM of DTT, and 30 min incubation time of the modified AgNPs and Cu²⁺. Under the optimal conditions, the UV-Vis spectra of AqNPs with different concentrations of Cu²⁺ were investigated as shown in Fig. 2. We expected that AqNPs could be used to quantitatively determine Cu²⁺ levels by monitoring the increase of the absorbance ratio at 502 nm/404 nm. After the addition of different amounts of Cu²⁺ (3.2 nM - 62.8 µM) into the modified AgNP solution, the 502/404 absorbance ratio increased as a function of the Cu^{2+} concentration in the range of 3.2 – 14.2 nM. Then, the absorbance ratio stopped increasing up to 780 nM of Cu²⁺ and then decreased in the range of 780 nM - 7.8 µM. Furthermore, the new red-shifted band slightly changed from blue to red. The plot of absorbance ratio as a function of Cu^{2+} concentration was found to be linear within both the range of 3.2 - 14.2 nM (R^2 = 0.997) and 780 nM - 3.9 μ M ($R^2 = 0.998$).



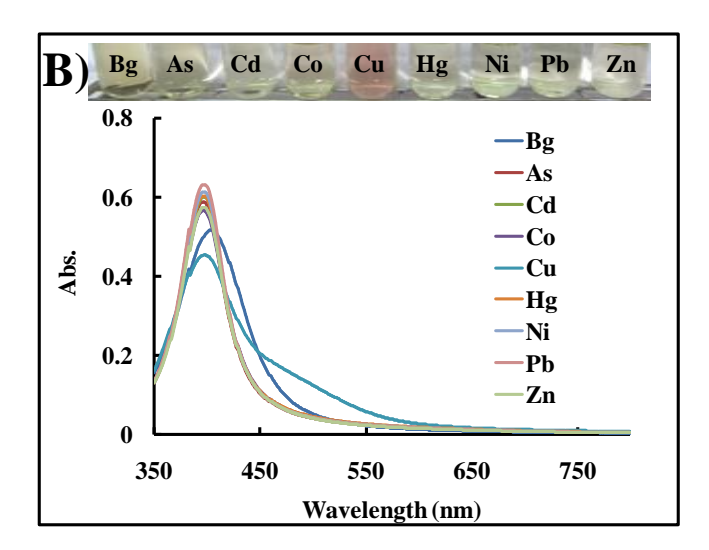


Fig. 1 (A) Schematic of aggregating process of AgNPs induced by adding Cu^{2^+} and (B) UV-visible spectra and photos of homocysteine-dithiothreitol-AgNPs with metal ions (7.8 nM of Cu^{2^+} and 1.6 μ M of other metals).

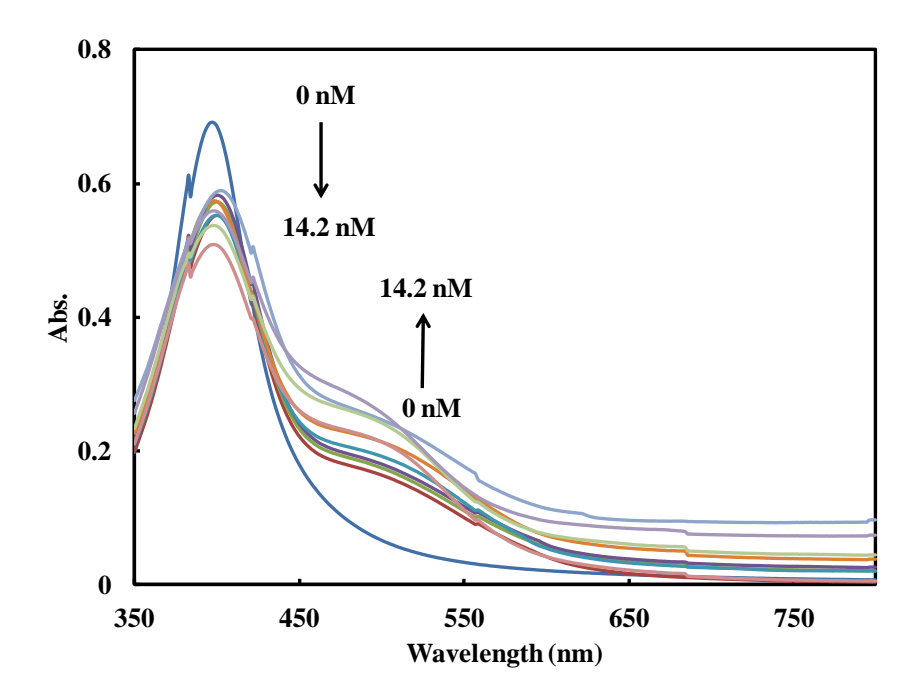


Fig. 2 UV-visible spectra of homocysteine-dithiothreitol-AgNP solutions with various concentrations of Cu^{2^+} in the range from 0 to 14.2 nM increasing in steps of 1.6 nM. The insert figure is various concentrations of Cu^{2^+} in the range from 780 nM to 7.8 μ M (780 nM, 1.6, 3.9, and 7.8 μ M).

3.2 Detection of copper on the paper devices

Colorimetric sensing in paper devices generally uses a higher organic indicator or nanoparticle concentration than is used in solution phase because of the low visibility of colors such as yellow and orange the paper surface. To improve visibility on paper, we investigated the concentration of AgNPs, Hcy, and DTT for nanoparticle aggregation in PADs. It was found that 0.1 mM of AgNPs solution containing 3.5 µM Hcy and 3.0 µM DTT which provided the optimal conditions in solution showed no significant difference when detected by eye between in the presence and absence of Cu²⁺ on the PADs. We hence optimized the AgNP concentration in the range of 0.1 – 20 mM containing 7.0 µM Hcy and 6.0 µM DTT as two time higher aminothiol concentration than in solution phase. We found that 10 mM of AgNP solution mixing with 7.0 µM Hcy and 6.0 µM DTT gave the orange and green-brown color after dropping Cu²⁺ solution and the yellow color after dropping buffer solution on the paper surfaces. The low AgNP concentration (0.1 mM) gave a light yellow color on paper devices while concentrations higher than 15 mM of AgNP concentration gave a dark yellow that prevented color discrimination by naked eye (data not shown). Therefore, we selected 10 mM of AgNP to use in the optimization of aminothiol concentration for PADs in the next experimentation. The optimal aminothiol concentration used in solution also differed for PADs because the aggregation reactions occur in the different media surrounding. The surrounding media has a direct effect on the refractive index and the interparticles distance [24]. We also studied the linearity

of intensity color with the increasing of Cu^{2^+} concentration. PADs exhibited color changes as a function of Cu^{2^+} concentration. Concentrations between 7.8 nM and 3.9 μ M gave an orange color, while concentrations between 15.7 and 62.8 μ M gave a green-brown color as shown in Fig. 3. The detection limit by naked eye was found to be 7.8 nM or 0.5 μ g L⁻¹. Additionally, the green-brown color intensity as a function of the concentration of Cu^{2^+} was measured using Adobe Photoshop CS2 in gray mode. A linear calibration curve between intensity and Cu^{2^+} concentration was obtained in the range of 7.8 – 62.8 μ M (R^2 = 0.992). The World Health Organization (WHO) prescribes the maximum allowable levels of Cu^{2^+} in drinking water at 1.3 mg L⁻¹ or 20.5 μ M. These results clearly show the ability to visually discriminate between the maximum allowable Cu^{2^+} levels and the normal level using the modified AgNPs. Our device should therefore be useful for determining Cu^{2^+} in drinking water. Although the limit of naked-eye detection in paper devices (0.5 μ g L⁻¹ or 7.8 nM) was higher than the previous UV-visible spectra reports (1 nM), [38] it is lower than commercial copper test strips [39-40]. Hence, our paper devices are an attractive, low cost and portable point-of-measurement (POM) as well as on-site test strips.

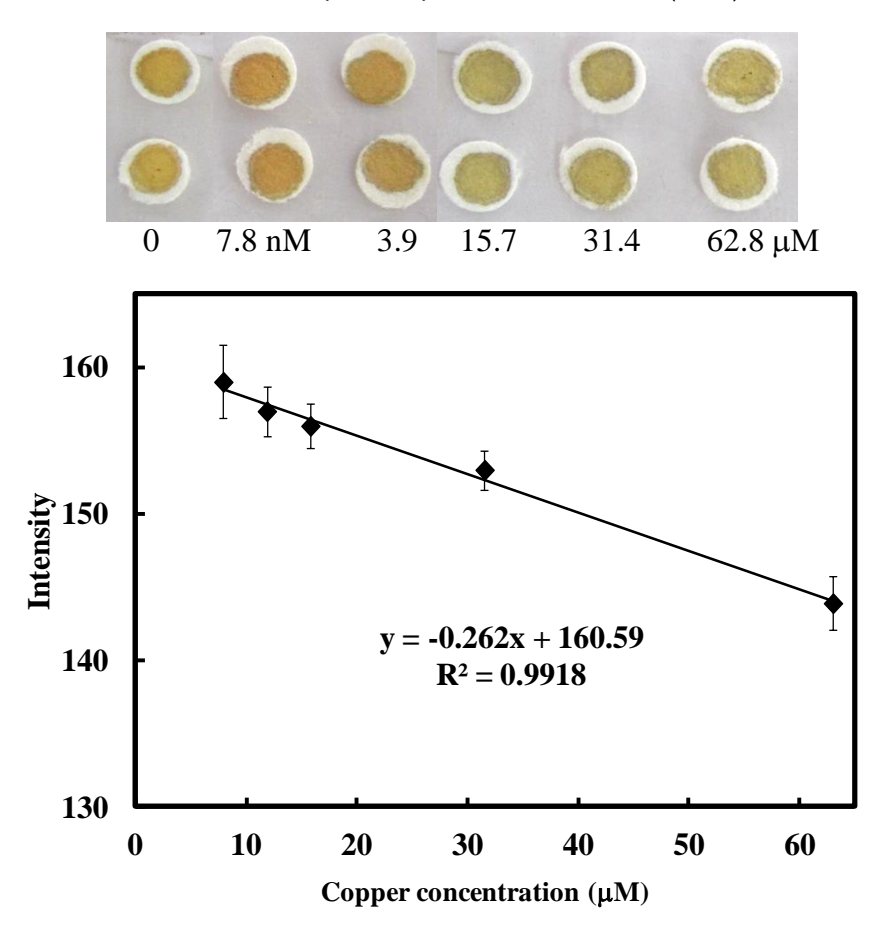


Fig. 3 Paper devices for the quantitative analysis of Cu^{2+} and the calibration plot of color intensity and the concentrations of Cu^{2+} (error bar represented the standard deviation at n = 3).

The selectivity of Cu^{2+} detection on the paper devices was then investigated at the optimal reagent concentrations for the paper devices. Hcy-DTT-AgNPs on the paper surfaces immediately changed the colors in the addition of Cu^{2+} whereas other metal ions did not change color (Fig. 4). Moreover, the analysis time using paper devices is only \sim 5 min, which is \sim 25 min faster than using UV-Vis or atomic absorption spectrometers (AAS).

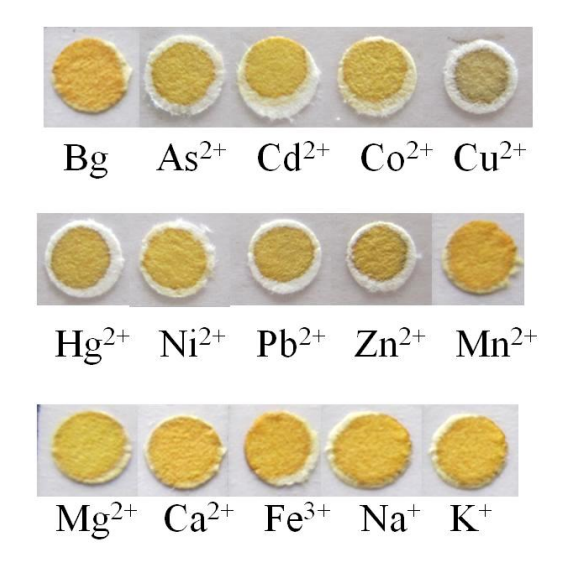


Fig. 4 Study of selectivity of the semi-quantitative analysis of Cu²⁺ toward different heavy-metal ions on paper devices.

Hcy-DTT modified AgNPs were next used with paper-based microfluidic devices using the design shown in Fig. 5. Figure 5A and 5B showed the yellow color of buffer solution and the green-brown color of 15.7 μ M Cu²⁺ solution, respectively. The results indicate that the nanoparticle aggregation reaction generated by the vertical flow of analyte solution was similar to the horizontal flow. However, the horizontal flow of modified AgNP solution to the test zone coated with Cu²⁺ (Fig. 5C) provided a different result from the horizontal flow of Cu²⁺ solution reacted with modified AgNPs at test zone (Fig. 5B). As shown in Fig. 5C, the brown-black color generated at 15.7 – 62.8 μ M of Cu²⁺ while Cu²⁺ concentration at less than 15.7 μ M did not give an orange color. The modified AgNP initially aggregated at the starting point of test zone and the aggregated AgNPs then blocked the horizontal flow of modified AgNP so the AgNP solution cannot flow to the end of the test zone. Although the concentration and flow direction of AgNPs on paper devices affect the sensitivity of AgNP colorimetric sensing, the concept of our method is easy-to-use, versatile, rapid, and suitable for point of care monitoring.

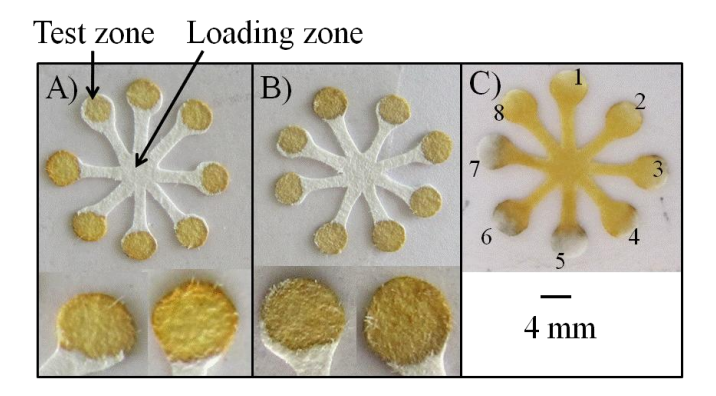


Fig. 5 $\,\mu$ PAD for the semi-quantitative analysis of Cu²⁺ after spotting AgNPs modified with Hcy and DTT into the test zone and then (A) dropping buffer solution and (B) 15.7 $\,\mu$ M of Cu²⁺ solution into the loading zone. (C) $\,\mu$ PAD for the semi-quantitative analysis of Cu²⁺ after spotting (8) 0 (2) 7.8 nM (3) 780 nM (4) 7.8 $\,\mu$ M (5) 15.7 $\,\mu$ M (6) 31.4 $\,\mu$ M (7) 62.8 $\,\mu$ Mof Cu²⁺ solution and then dropping AgNPs modified with Hcy and DTT into loading zone.

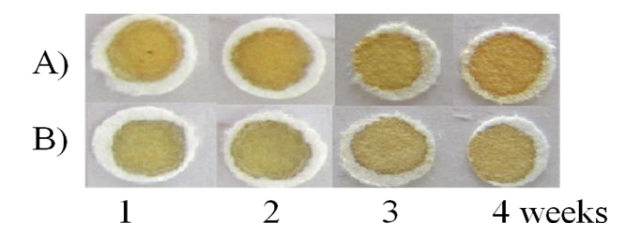


Fig. 6 Lifetime of the paper devices in the addition of (A) 0 and (B) 15.7 μM of Cu $^{^{2+}}$.

3.3 Applications

To evaluate the potential application of AgNP colorimetric sensor in paper devices, the proposed method was applied for the detection of Cu^{2^+} in the real water samples. Pond and tap water samples were analyzed by our devices and AAS. Levels of Cu^{2^+} in tap water samples were measured using the paper devices and AAS to be 2.9 ± 0.24 and 2.8 ± 0.08 μ M, respectively (n = 3). Meanwhile, amount of Cu^{2^+} in pond water samples were measured using the paper devices and AAS to be 3.2 ± 0.30 , and 3.4 ± 0.04 μ M, respectively (n = 3). The paired t-test was used to validate our method versus the standard method. The levels obtained using our approach were in good agreement with those from AAS, falling within the 95% confidence level. Thus, the analyzed values of Cu^{2^+} in pond and tap water sample by our approach can be accepted.

3.4 Lifetime of the devices

For practical use in developing countries, devices must remain stable for weeks. Therefore, we studied the stability of devices after storing the prepared paper devices for 4 weeks. The modified AgNPs coated on paper devices were dried at ambient condition before storage at room temperature (~25 °C). It was found that an observable signal for 15.7 μ M Cu²⁺ solution dropped on the prepared paper over a period of 4 weeks generated no significant difference from the freshly prepared paper devices as shown in Fig. 6. Hence, the devices can be kept for 4 weeks without loss of activity but longer storage time requires refrigeration.

4. Conclusions

This paper demonstrates for the first time the use of AgNP for colorimetric sensing in paper devices to provide rapid, easy to use, inexpensive, and portable devices for point-of-care monitoring. The sensor is based on the aggregation of AgNPs on a paper substrate by the strong affinity between AgNPs modified with thiol conpounds and Cu²⁺, which leads to a shift in the absorption spectrum. Furthermore, the color change of AgNPs on paper substrate can be observable by the naked eye due to the extremely high extinction coefficient of AgNPs. Cu²⁺ was clearly distinguishable color change from the other heavy metal ions under the optimum conditions at the critical level of Cu²⁺ in drinking water prescribed by WHO. Finally, our paper devices were successfully applied to the semi-quantitative analysis of Cu²⁺ in water samples. Both paper-based assay devices and paper-based microfluidic devices would be potentially modified with AgNPs for the detection of a variety of other targets.

5. References

- [1] A.W. Martinez, S.T. Phillips, E. Carrilho, S.W. Thomas, H. Sindi, G.M. Whitesides, Anal. Chem. 80 (2008) 3699-3707.
- [2] W. Zhao, A.V.D. Berg, Lab on a Chip. 8 (2008) 1988-1991.
- [3] S.K. Sia, L.J. Kricka, Lab on a Chip. 8 (2008) 1982-1983.
- [4] A.W. Martinez, S.T. Phillips, M.J. Butte, G.M. Whitesides, Angew. Chem. Int. Ed. 46 (2007) 1318-1320.
- [5] P. Kauffman, E. Fu, B. Lutz, P. Yager, Lab on a Chip. 10 (2010) 2614-2617.
- [6] E. Fu, T. Liang, J. Houghtaling, S. Ramachandran, S.A. Ramsey, B. Lutz, P. Yager, Anal. Chem. 83 (2011) 7941-7946.
- [7] X. Li, J. Tian, T. Nguyen, W. Shen, Anal. Chem. 80 (2008) 9131-9134.
- [8] A. Apilux, W. Dungchai, W. Siangproh, N. Praphairaksit, C.S. Henry, O. Chailapakul, Anal. Chem. 82 (2010) 1727-1732.
- [9] W. Dungchai, O. Chailapakul, C.S. Henry, Anal. Chem. 81 (2009) 5821-5826.
- [10] Z. Nie, C.A. Nijhuis, J. Gong, X. Chen, A. Kumachev, A.W. Martinez, M. Narovlyansky, G.M. Whitesides, Lab on a Chip. 10 (2010) 477-483.

- [11] W. Dungchai, O. Chailapakul, C.S. Henry, Anal. Chim. Acta. 674 (2010) 227-233.
- [12] F.Q. Zhang, L.Y. Zeng, Y.X. Zhang, H.Y. Wang, A.G. Wu, Nanoscale. 3 (2011) 2150-2154.
- [13] Y. Xue, H. Zhao, Z.J. Wu, X.J. Li, Y.J. He, Z.B. Yuan, Analyst. 136 (2011) 3725-3730.
- [14] J. Zhang, Y. Wang, X.W. Xu, X.R. Yang, Analyst. 136 (2011) 3865-3868.
- [15] M.H. Kim, S. Kim, H.H. Jang, S. Yi, S.H. Seo, M.S. Han, Tetra. Lett. 51 (2010) 4712-4716.
- [16] S. Kim, J.W. Park, D. Kim, D. Kim, I.H. Lee, S. Jon, Angew. Chem. Int. Ed. 48 (2009) 4138-4141.
- [17] J.R. Kalluri, T. Arbneshi, S.A. Khan, A. Neely, P. Candice, B. Varisli, M. Washington, S. McAfee, B. Robinson, S. Banerjee, A.K. Singh, D. Senapati, P.C. Ray, Angew. Chem. Int. Ed. 48 (2009) 9668-9671.
- [18] H.L. Xie, W. Ma, L.Q. Liu, W. Chen, C.F. Peng, C.L. Xu, L.B. Wang, Anal. Chim. Acta. 634 (2009) 129-133.
- [19] X.L. Wang, K. Li, D.S. Shi, X. Jin, N. Xiong, F.H. Peng, D.P. Peng, D.R. Bi, J Chromatogr B. 847 (2007) 289-295.
- [20] T.T. Lou, Z.P. Chen, Y.Q. Wang, L.X. Chen, ACS Appl. Mater. Interfaces. 3 (2011) 1568-1573.
- [21] J. Zhang, X.W. Xu, C. Yang, F. Yang, X.R. Yang, Anal. Chem. 83 (2011) 3911-3917.
- [22] J.W. Liu, D. Mazumdar, Y. Lu, Angew. Chem. Int. Ed. 45 (2006) 7955-7959.
- [23] W.A. Zhao, M.M. Ali, S.D. Aguirre, M.A. Brook, Y.F. Li, Anal. Chem. 80 (2008) 8431-8437.
- [24] X.C. Jiang, A.B. Yu, Langmuir. 24 (2008) 4300-4309.
- [25] W. Leesutthiphonchai, W. Dungchai, W. Siangproh, N. Ngamrojnavanich, O. Chailapakul, Talanta. 85 (2011) 870-876.
- [26] H.B. Li, Y.H. Bian, Nanotechnology. 20 (2009)
- [27] A. Ravindran, V. Mani, N. Chandrasekaran, A. Mukherjee, Talanta. 85 (2011) 533-540.
- [28] B. Roy, P. Bairi, A.K. Nandi, Analyst. 136 (2011) 3605-3607.
- [29] Y. Wang, F. Yang, X.R. Yang, ACS Appl. Mater. Interfaces. 2 (2010) 339-342.
- [30] H.B. Li, Z.M. Cui, C.P. Han, Sens. Act. B-Chem. 143 (2009) 87-92.
- [31] Y.H. Ngo, D. Li, G.P. Simon, G. Gamier, Adv. Colloid. Interfac. 163 (2011) 23-38.
- [32] W.W. Yu, I.M. White, Anal. Chem. 82 (2010) 9626-9630.
- [33] A.E. Fisher, D.P. Naughton, Curr. Drug. Deliv. 2 (2005) 261-268.
- [34] B.C. Yin, B.C. Ye, W.H. Tan, H. Wang, C.C. Xie, J. Am. Chem. Soc. 131 (2009) 14624-14625.
- [35] E.M. Fenton, M.R. Mascarenas, G.P. Lopez, S.S. Sibbett, ACS Appl. Mater. Interfaces. 1 (2008) 124-129.
- [36] R.C. Smith, V.D. Reed, Chem. Biol. Inter. 82 (1992) 209-217.

- [37] A. Krezel, W. Lesniak, M. Jezowska-Bojczuk, P. Mlynarz, J. Brasun, H. Kozlowski, W. Bal, J. Inorg. Biochem. 84 (2001) 77-88.
- [38] T.T. Lou, L.X. Chen, Z.P. Chen, Y.Q. Wang, L. Chen, J.H. Li, ACS Appl. Mater. Interfaces. 3 (2011) 4215-4220.
- [39] Copper test strips EM Quant®, catalog number: 10003, Millipore, Germany.
- [40] Copper test strips, catalog number: PT753-50, Freshwatersystems, USA.

CHAPTER III

Colorimetric Determination

of Nitrite and Nitrate in Meat using Paper-based Analytical Device (PAD)

Nitrite and nitrate have also been used as food additives using in processed meat to prevent the spoilage, kept the meat red and produce the good smell. They are food contaminants that as a result of degenerative diseases that effects on human health at high levels caused of Eutrophication, Methemoglobinemia and cancer. Paper was chosen as the substrate for preparing these devices, which they have been shown to be effective testing for a simple, rapid, inexpensive and easy-to-use. A simple colorimetric method for the detection of nitrite and nitrate using paperbased analytical device (PAD) is reported in this work. These Griess reaction can be applied for the determination of nitrite while nitrate was reduced to nitrite on PAD in the section of hydrophilic channel coated with zinc dust. The optimal conditions for the determination of both nitrite and nitrate including the concentration of N-(1-naphthyl)-ethylenediamine dihydrochloride (NED) and sulfanilamide, reaction time, as well as three patterns of PAD were studied. Under the optimal conditions, the color intensity gave a linear response in the range 0-20 mgL^{-1} (R² = 0.993 for nitrite and $R^2 = 0.981$ for nitrate) and the limits of detection was found at 0.1 mgL⁻¹. The purple color in the presence of nitrite and nitrate can be clearly observed in PAD (pattern 1) by the naked eye within 25 minutes. Moreover, our PAD was applied for the determination of nitrite and nitrate in real samples such as poke sausage, smoked poke sausage, and ham.

1. Introduction

Nitrite and nitrate are a versatile chemical agent which has found numerous applications ranging from dye manufacture to food additives. They are also added to meat to preserve its color, stop bacteria from growing, and prevent fats from going rancid [1]. Nitrite is one of the pollutants found in the atmosphere and natural water [2] and is an important intermediate in biological nitrogen cycle. Nitrite and nitrate cause harm to consumers. Especially, those who are sensitive to this chemical reaction are to have nausea, vomiting, abdominal pain, diarrhea, headache, blood in the feces, and eutrophication. Nitrite can react with amines (amine) in a serious carcinogen nitrosamines, which causes liver cancer, gastric cancer, and esophageal cancer. The health effect for children is the "blue baby syndrome" (methemoglobinemia) would to hypoxia because it was not transport oxygen. If methemoglobin had more than 60% of the amount of hemoglobin in the blood, it caused of death. In addition, nitrite is also causing problems for the functioning of the thyroid gland as well [3]. In New Zealand may contain up to 125 mg of total nitrite and nitrate per kg of the

food such as bacon, ham, sausage, pizza, and hamburger [4]. The Joint Expert Committee on Food Additives (JECFA) of the Food and Agriculture Organization of the United Nations/World Health Organization and the European Commission's Scientific Committee on Food have set an acceptable daily intake (ADI) for nitrate of 0-3.7 mg/kg. The same is also true of the EPA reference dose (RFD) for nitrate of 1.6 mg/kg per day (equivalent to about 7.0 mg/kg per day) and the amount of sodium nitrite to not more than 200 mg/kg in the finished meat product. [5].

A previous analytical method such as UV-VIS spectrophotometry [3], flow injection spectrophotometry [6], fluorimetry [7], polarography [8], and voltammetry [9] has been used for nitrite and nitrate determination. Several reported spectrophotometric methods involve the use a reduction reaction followed by diazotization, [10] nitration reactions, [11] or the other.

Paper-based analytical devices have been widely used for biomedical, environmental and food-quality testing [12]. Paper was used as the substrate, which has been shown to be effective testing, a high surface area for colorimetric detection and also suited for using by nontechnical personnel. In addition, they are made from naturally abundant, biodegradable and inexpensive materials. Paper devices are detection due to advantages which include low cost, portability, easy to use, fast patterning techniques, high speed, low reagent and sample consumption.

A simple colorimetric method for the detection of nitrite and nitrate using paper-based analytical device (PAD) is reported in this work. Sulfanilamide was diazotized by nitrite in acidic medium and coupled with N-(1-naphthyl)-ethylenediamine dihydrochloride (NED) to give a colored of azo dye while nitrate was reduced to nitrite on PAD in the section of hydrophilic channel coated with zinc dust. The produced nitrite is subsequently diazotized with sulfanilamide and then coupled with NED to form azo dye. Both nitrite and nitrate were determinated on PAD by Image J program. The developed method has been successfully applied to the determination of nitrite and nitrate in real meat samples.

2. Materials and Methods

2.1 Materals and reagents

N-(1-Naphthyl)-ethylenediamine dihydrocloride, sulfanilamide and zinc dust were bought from Sigma-Aldrich (St.Louis, Missouri). Whatman No.1 filter paper was bought from Cole-Parmer (Vernon Hills, IL). All glassware was thoroughly cleaned with freshly prepared 1:1 HCl/HNO $_3$ and rinsed with high pure water prior to use. All chemicals used in experiment were analytical reagent (AR) grade and solutions were prepared using high pure water with a resistance of 18 M Ω cm $^{-1}$.

2.2 Instrumentation

UV-Visible absorption spectra were recorded in a quartz cuvette (1-cm pathlength) using a UV-Visible spectrometer (Lambda 35, Perkin Elmer Instruments, USA). Photographic results were recorded using scanner (Scx-3405, Samsung).

2.3 Preparation of PAD for the detection of nitrite and nitrate

The pattern was created in Corel Draw three designs of PAD (pattern of paper 1, 2 and 3) and then transferred to the wax printing (ColorQube, Xerox, Thailand) using Whatman No.1. This PAD was followed by baking at 110 °C in an oven for 5 minutes.

The determination of nitrite, the loading zone (1) of PAD (Fig. 1a-c), was dropped with 2 μ L of sulfanilamide solution and allowed dry. Then, 0.5 μ L of NED (Fig. 1a-c, (2)) was dropped into test zone and 30 μ L of sample or standard was dropped into loading zone (Fig. 1a-c, (4)). Nitrate was determined same nitrite, except for the reduction step that coated 2 μ L of zinc dust at the transport channel (Fig. 1a-c, (3)) for changed nitrate to nitrite. All of patterns were incubated for 25 minutes at the room temperature and analysis by Image J program.

2.3 Applications

To evaluate the utility of our proposed method, nitrite and nitrate in the real samples such as poke sausage, smoked poke sausage, and ham. Our method was validated against UV-VIS spectroscopy. 10.00 g of sample was mixed with 25.00 mL of deionized water and stirred it for 2h and then filtered through filter paper. All of samples were adjusted to a final volume of 50.00 mL with deionized water.

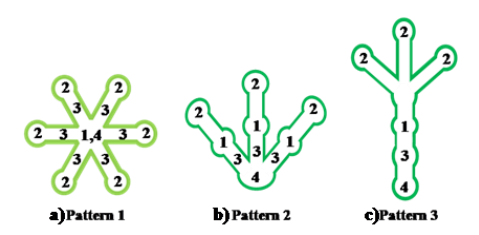


Figure 1 Pattern of paper a) pattern 1, b) pattern 2 and c) pattern 3

3. Results and Discussion

3.1 Effect of NED and sulfanilamide concentrations

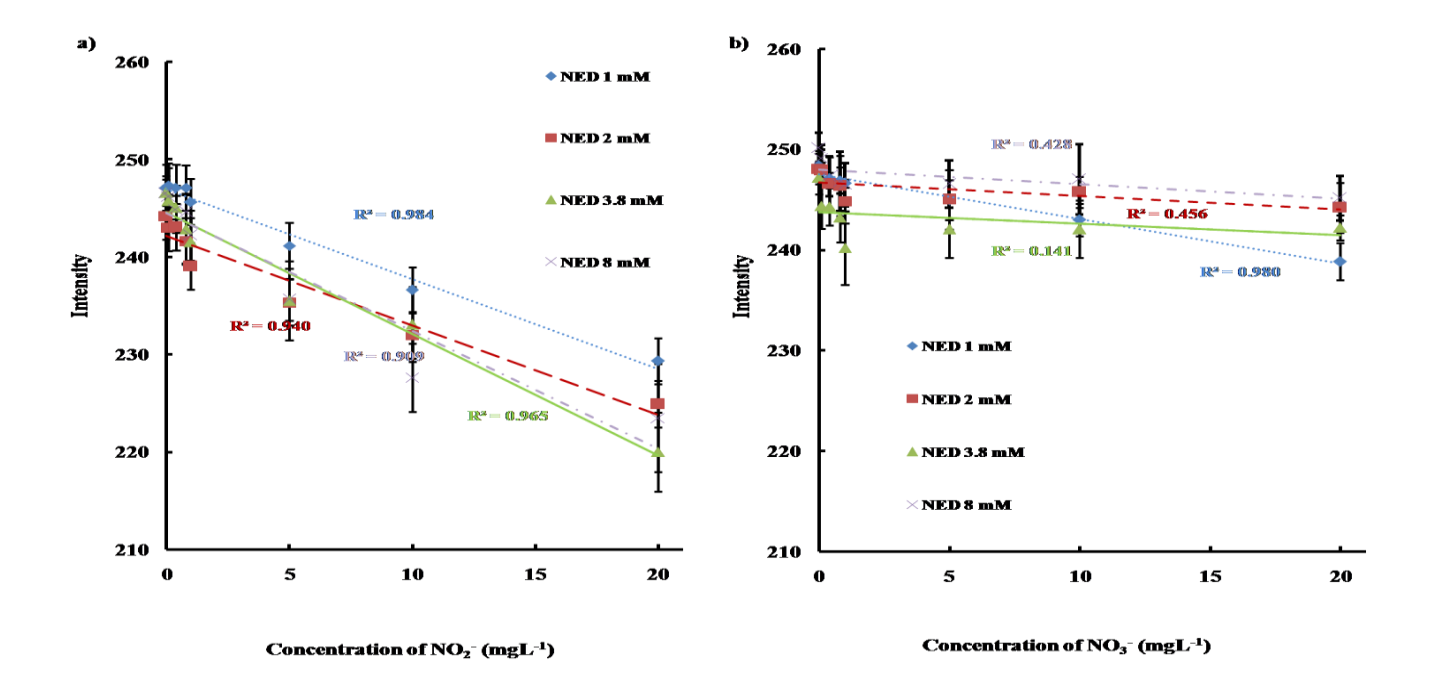


Figure 2 The calibration plot of color intensity with various concentrations of a) NO₂ and b) NO₃ (error bar represented the standard deviation at n=6) and the concentration of NED in the range 1-8 mM (60 mM of sulfanilamide, at 25 minutes) added zinc dust only determined NO₃

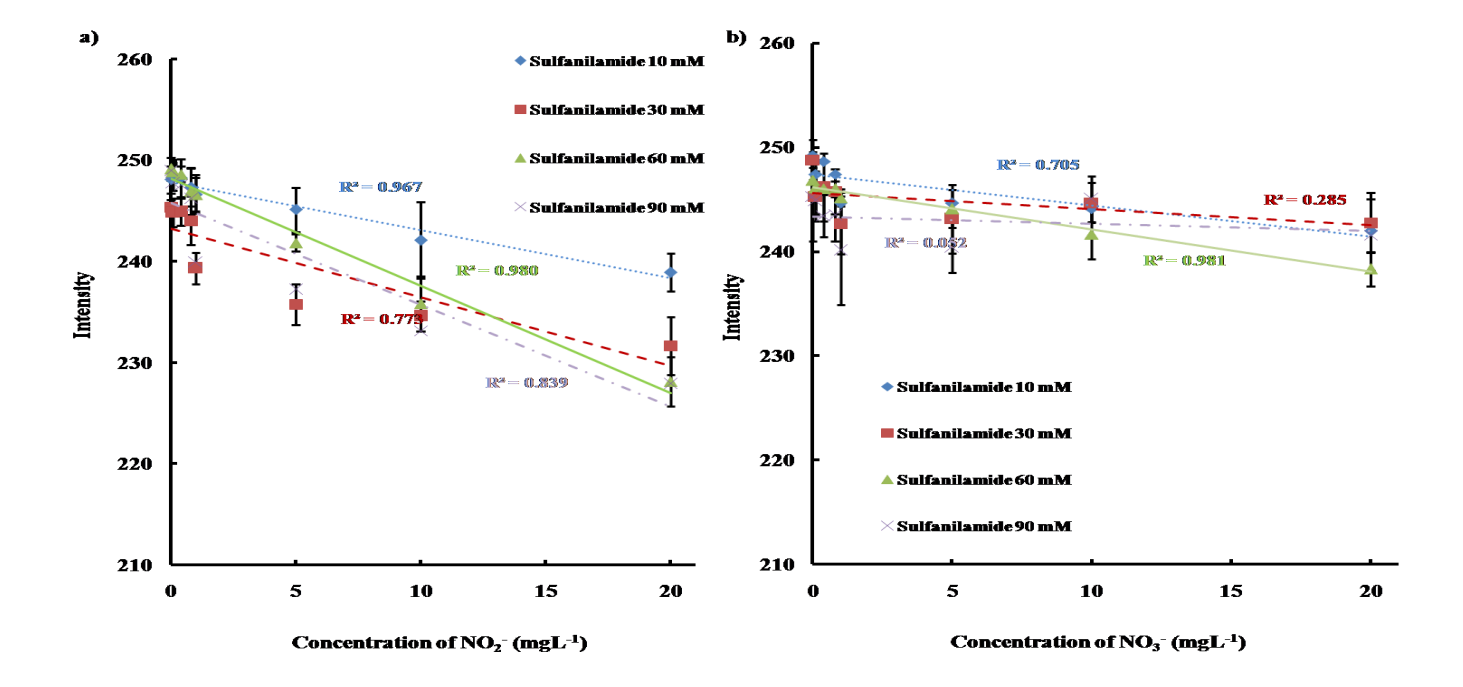


Figure 3 The calibration plot of color intensity with various concentrations of a) NO_2 and b) NO_3 (error bar represented the standard deviation at n=6) and the concentration of sulfanilamide in the range 10-90 mM (1 mM of NED, at 25 minutes) added zinc dust only determined NO_3

The results of these experiment concentrations of NED and sulfanilamide for determinations of nitrite and nitrate were studied by the Griess assay reaction on PAD [Fig. 1a, pattern 1]. When 60 mM of sulfanilamide is dropped to PAD [Fig. 1a, pattern 1] at the loading zone [Fig. 1a, number 1], dropped 1mM of NED at test zone [Fig. 1a, number 2] allowing to dry and then dropped nitrite and nitrate at the loading zone [Fig. 1a, number 4], nitrite will form a complex with the sulfanilamide that are diazonium salt and produces a purple precipitate with NED. In case of nitrate is no color after the addition of sulfanilamide and NED, purple color develops after the addition of zinc dust at the transport channel [Fig. 1a, number 3]. The presence of a purple color in the test nitrate indicates that nitrite is present as a result of the reduction of nitrate on PAD.

The color intensity gave a linear response to the highest R^2 both of nitrite and nitrate compared with other concentrations of sulfanilamide and NED are added to nitrate and nitrite [Fig.2 and 3]. They were reacted and appeared of color on PDA that R^2 value is less than the concentration of NED and sulfanilamide were 1mM and 60 mM, respectively. This concentration of the conditions, which will make the ability of a complex and best the color for determined of nitrite and nitrate.

3.2 Effect of reaction time

The reaction time was varied from 15 to 60 minutes [Fig. 4]. Both of nitrite and nitrate were determinate and found that the maximum reduction of nitrate to nitrite and nitrite in the concentration at 20 mgL⁻¹. Both of nitrate and nitrite were found that can be observed color on PAD by the naked eye within 25 minutes. The differences of average intensity of the color formed have the highest when compare the difference of average intensity of other times. However, in Figure 4 was found to decrease the difference of average intensity when increased time more than 25 minutes indicating a decomposition of complex and might be due to reduction of nitrite. Therefore, 25 minutes was selected as the optimum duration of the reaction time.

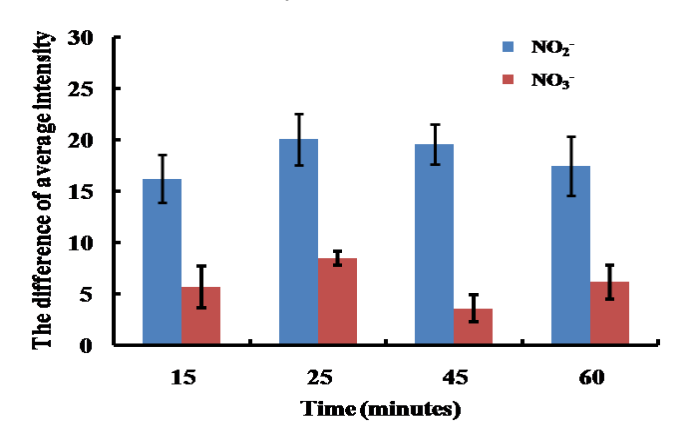


Figure 4 Effect of reaction time between 15-60 minutes (60 mM of sulfanilamide 2 μ L, 1 mM of NED 0.5 μ L and 30 μ L of NO₂ and NO₃ (20 mgL⁻¹, (error bar represented the standard deviation at n=6)) added 2 μ L of zinc dust only determined NO₃)

3.3 Type of patterns

The patterns of PDA were varied 3 types. Our PAD is the vertical with reagents and samples coated on paper surface whereas flows on PAD are horizontal. More detailed information on the direction flow can be found in Fig. 1. Patterns 2 and 3 of PDA were not used because the reaction between sample and reagent were detected at the detection zone, which resulted in poor reproducibility. It may also depend on the position, distribution, distance and reaction sequence to react between reagent and sample. This problem was solved in the pattern 1 of PAD. Nitrite was transported from the sample zone [Fig. 1a, number 1] to the detection zone [Fig. 1a, number 2]. The same procedure, except for the reduction step zinc dust was added on PAD [number 3 all of patterns]. This was used for the determination of nitrite only and the pattern 1 of PAD has the differences of average intensity the highest of color when compare the difference of average intensity of other patterns of PAD [Fig. 5]. Therefore, PDA pattern 1 was selected as the optimum duration of the reaction.

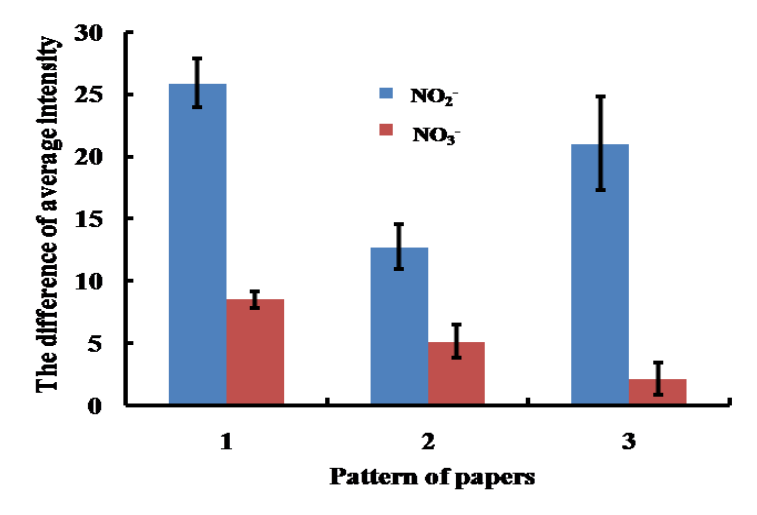


Figure 5 Type of pattern a) pattern 1, b) pattern 2 and c) pattern 3 (60 mM of sulfanilamide 2 μ L, 1 mM of NED 0.5 μ L and 30 μ L of NO₂ and NO₃ (20 mgL⁻¹) added 2 μ L of zinc dust only determined NO₃) at 25 minutes.

3.4 Calibration

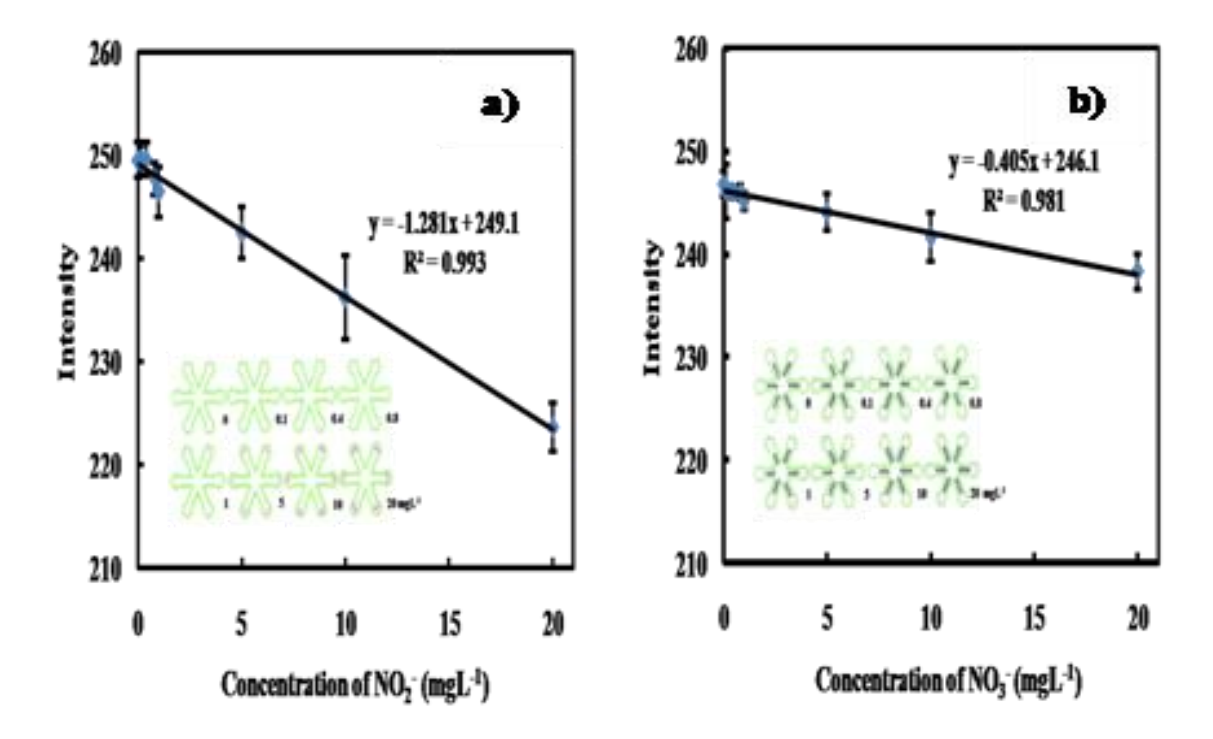


Figure 6 PAD for the quantitative analysis of a) NO_2 and b) NO_3 (error bar represented the standard deviation at n=6) at concentration in the range 0-20 mgL⁻¹. Conditions: 1 mM of NED with 60 mM of sulfanilamide solution at 25 minutes (added zinc dust only determined NO_3).

Nitrite was detected by diazotization in the Griess assay reaction, which gave a purple color on PAD. Nitrate was detected by the same reaction after it was reduced to nitrite by zinc dust within PAD device. Quantitative measurements were possible based on the intensity of the color formed. These devices were scanned after drying to obtain the color values by the RGB color mode was chosen to represent the color reflected from the devices for observed that the concentration of nitrite and nitrate. A calibration was developed using nitrite and nitrate standards. The devices were able to detect nitrite and nitrate have the range of linearity 0 - 20 mgL⁻¹ (R² = 0.993 for nitrite and R² = 0.981 for nitrate) and the detection limit of nitrite and nitrate are found to be 0.1 mgL⁻¹ as shown in Fig. 6.

3.5 Analytical Applications

These devices can be applied to determinations of nitrite and nitrate in meat samples such as poke sausage, smoked poke sausage, and ham. Levels of nitrite and nitrate in meat samples were measured using our PAD and UV-VIS spectroscopy at λ_{max} = 543 nm to show Table.1. The result of meat samples were not statistically significant different from the standard methods at the 95% confidence level and statistical analyses of the results by pair *t*-tests [*t*-test value = 0.77, *t* critical value = 4.30 for nitrite and *t*-test value = 0.95, *t* critical value = 4.30 for nitrate]. The precision of

this method is evaluated by replicate analysis of samples containing nitrite and nitrate at three different samples [Table 1]. The reagents provide a simple and sensitive method for determination of nitrite and nitrate. This method has been successfully applied to the determination of levels of nitrite and nitrate in meat samples.

Table 1: Levels of NO₂ and NO₃ in meat samples were measured using UV-VIS spectroscopy and our method.

Solumo S	Concentration	Concentration of NO ₂ (mg/g)
Section 1	SIA-AN	Our method
Poke sausage	6.57×10 ⁻³ ±8.9×10 ⁻³	$6.74 \times 10^{-3} \pm 3.4 \times 10^{-3}$
Smoked poke sausage	16.52 x10 ⁻³ <u>+</u> 2.8x10 ⁻³	12.81x10 ⁻³ <u>+</u> 9.8x10 ⁻³
Нат	29.13 x10 ⁻³ ±1.7x10 ⁻³	29.57x10 ⁻³ +3.4x10 ⁻³
ool a me o	Concentration	Concentration of NO ₃ (mg/g)
Sell Dies	SIV-VU	Our method
Poke sausage	49.16x10 ⁻³ <u>+</u> 3.2x10 ⁻³	45.76x10 ⁻³ +6.3x10 ⁻³
Smoked poke sausage	134.08×10 ⁻³ +3.8×10 ⁻³	143.26x10 ⁻³ +20.6x10 ⁻³
Нат	174.28x10 ⁻³ +4.9x10 ⁻³	179.10x10 ⁻³ +14.9x10 ⁻³

The standard deviation of meat samples at n=6.

4. Conclusions

This report describes PDA is a devices, which a simple and sensitive method for colorimetric determination of nitrite and nitrate. A great advantage of PAD is the proposed paper-based method, which is characterized by high sensitivity, acceptable repeatability, a high degree of portability, very low cost of analysis, no requires complex equipment or extensive training and the processes do. The paper-based method also exhibited acceptable this method is the first use a PAD, which has been successfully applied to the determination of levels of nitrite and nitrate in

meat samples. These methods suggest a path for the development of portable diagnostic assays that may be useful in remote settings, and simple assays are becoming increasingly important for detecting monitoring health and contaminating in the future.

References

- [1] Kazemzadeh, A., Ensaf, A.A., 2001, Anal. Chim.Acta., 442, 319–326.
- [2] Manzoori, J. L., Sorouraddin, M. and Haji-Shabani, A.M., 1998, Talanta, 46, 1379.
- [3] Badiadka, N. and Kenchaiah, Sunil., 2009, Eurasian J. Anal. Chem., 4, 204-214.
- [4] Thomson, B., 2004, Nitrates and nitrites dietary exposure and risk assessment, Institute of environmental Science & Research Limited.
- [5] [EPA] US Environmental Protection Agency. Integrated Risk Information System (IRIS) database. Nitrate (CASRN 14797-55-8). Washington DC [updated 2002 December 03; accessed July 2012].
- [6] Kazemzadeh, A. and Ensaf, A.A., 2001, *Anal. Chim. Acta.*, 442, 319–326.
- [7] Diallo, S., Bastard, P., Prognon, P., Dauphin, C. and Hamon, M., 1996, *Talanta.*, 43, 359.
- [8] Qiong, L., Tong, Z., Yong, L., Dandan, S. and Guanghan, L., 2002, J. AOAC. Inter., 85, 456-459.
- [9] Xu, G.R., Xu, G., Xu, M.L., Zhang, Z., Tian, Y., Choi, H.N. and Lee, W.Y., 2012, Bull. Korean Chem. Soc., 33,415.
- [10] Moorcroft, M.J., Devis, J. and Compton, R.G., 2001, *Talanta.*, 54, 785.
- [11] Hoggett, J.G., Moodiej, R.B., Penton, J.R. and Schofield, K., 1971, Nitration and aromatic reactivity, University of Exeter.
- [12] Shah, P., Zhu, X. and Li, C. Z., 2013, Expert Rev. Mol.Diagn., 13, 83–91.

CHAPTER IV

Determination of Aerosol Oxidative Activity using Silver Nanoparticle Aggregation on Paper-Based Analytical Devices

1. Introduction

Epidemiological studies have shown that human exposure to airborne particulate matter (PM) is associated with numerous health effects including diseases of the cardiovascular, respiratory, and immune systems (1-5). Although a definitive mechanism of PM-induced toxicity remains elusive, it is generally agreed that PM induces oxidative stress (either directly or through induction of biological systems), causing systematic both inflammation and cellular dysfunction. Recently, both cell-based and cell-free systems have been used to investigate the capacity of PM to induce oxidative stress. Cell-based assays using fluorescence (6), chemiluminescence (7, 8), electron spin resonance (9), glutathione ratio (10, 11), lipid peroxidation, immunoassay and/or macrophage-based methods (12, 13) have shed important light into the mechanisms of PM-induced oxidative stress. However, these methods are expensive, complex, and difficult to use in the field. These assays also tend to require large amounts of PM (tens to hundreds of micrograms), which, in turn, requires long sampling and analysis times. Cell-free measurements of PM reactivity (oxidative load) typically use filter collection of PM and sample extraction prior to analysis. Traditionally, oxidative stress markers such as PAHs, quinones and transition metal have been measured using chromatography, electrophoresis, spectroscopy and mass spectrometry (14, 15). More recently, a method for estimating total oxidative load using dithiotheitol (the so called DTT assay) has been demonstrated (16, 17). The method has been convincingly shown to correlate with oxidative stress in vitro and thus, has been suggested as an appropriate surrogate when biological assays are not suitable. In the DTT assay, aqueous or solvent-based extracts of PM are mixed with DTT and allowed to react for a fixed period of time. The reaction is then quenched and Elman's reagent is added, reacting with the remaining reduced DTT to produce a yellow solution that absorbs light at 412 nm. The rate of DTT consumption measured in this way is directly proportional to the oxidative capacity of the PM sample. The DTT assay provides higher throughput than cell-based measurements, provided sufficient PM sample is available (10-100 ☐ g of PM per test), but also requires laboratory-based equipment to operate.

Microfluidic paper-based analytical devices (μ PADs) have gained interest for point-of-use diagnostics due to their low cost, ease of operation, and ability to function without external power supplies or supporting equipment (18-24). Moreover, μ PADs were recently introduced as an alternative for measuring oxidative load, providing a relatively simple method that requires less sample and reagent relative to traditional methods (25). Unlike the traditional DTT assay, the μ PAD method does not require a separate PM extraction step. Instead, a

small punch taken from a filter sample of PM is spotted with DTT and allowed to react for a specified time (~20 min). The residual DTT present on filter punch is then eluted onto a μ PAD that contains Elman's reagent (which reacts with remaining DTT). The intensity of the yellow color product is used to infer the DTT consumption rate. With the μ PAD-based approach, the oxidative load of PM was measured in less than 30 min. The μ PAD method also requires minimal reagent (1 μ L) due to its small size (approximately 6.25 cm² per device). Finally, because the μ PAD requires only 3 μ g of PM mass, shorter air sampling times and/or collection at lower flow rates (i.e., for personal sampling) is possible, making the device particularly attractive for exposure and risk assessment.

Although previous examples of the DTT assay have used Elman's reagent, the method is less than ideal because the extinction coefficient of the yellow product is low. In recent years, nanoparticles have been widely used for colorimetric assays due to higher extinction coefficients than common organic dyes. Gold nanoparticle (AuNP) and silver nanoparticle (AgNP)-based colorimetric sensors have been reported for measuring thiols such as homocysteine (Hcy) (26-28), glutathione (GSH) (26), and cysteine (Cys) (29-31) in biological samples. The use of AgNPs has gained popularity for colorimetric sensing because AgNPs are inexpensive and have higher extinction coefficients than AuNPs (32-34). The change color intensity or/and color hue of AgNPs on paper-based devices can be visualized with the naked eye making them attractive for many applications (35, 36). Here, we present the first use of AgNP for colorimetric sensing on µPAD for rapid, simple, and sensitive determination of PM oxidative load based upon aggregation of AgNP in the presence of residual GSH. GSH is more biologically relevant as a probe for PM oxidative load (than DTT) because GSH is an abundant endogenous antioxidant. We demonstrate here the ability of an AgNP-based µPAD assay to quantify aerosol oxidative load via the GSH consumption. The effect of reaction time was studied using 1,4-naphthoguinone (1,4-NQ) as a standard oxidant for GSH consumption. The versatility of the µPADs technique was demonstrated by measuring PM oxidative load using two different detection motifs: traditional colorimetric intensity analysis and a recently reported distance-based detection paradigm (37). Distance-based detection eliminates the need for an external scanner or camera because color length can be interpreted by the naked eye. Finally, our μPAD device was also validated against a conventional assay (UV-visible spectroscopy) using GSH instead DTT, and no significant difference was observed (P < 0.05, paired t-test) between the methods.

2. Experimental

Reagent and Materials

Glutathione, reduced 98%, rhodamine B (RB), and 1, 4-naphthoquinone were obtained from Sigma-Aldrich (St. Louis, MO). Dimethylsulfoxide (DMSO) was purchased from EMD Chemical Inc. (Gibbstown, NJ). Tris-hydrochloride (Tri-HCl) was obtained from Mallinckrodt Barker, Inc. (Phillipsburg, NJ). Whatman No. 1

qualitative grade filter paper was purchased from General Electric Company (Schenectady, New York, USA). All chemicals were used as received without further purification.

Preparation of AgNPs

A suspension of silver nanoparticles (AgNPs), obtained from the Sensor Research Unit at Department of Chemistry, Chulalongkorn University, Thailand, was synthesized using chemical reduction (*38-40*). Sodium borohydride (NaBH₄) and methylcellulose solutions were used as the reducing agent and stabilizer, respectively. A 20 mM solution of AgNO₃ (10 mL) was combined with 10 mL freshly prepared methylcellulose solution and the mixture was stirred for 10 min in an ice bath. Then 0.1 M NaBH₄ (2 mL) was added dropwise with continuous stirring at 0°C to the mixture. After the complete addition of NaBH₄ yellow colored silver nanoparticles were obtained. The shapes and particle size distributions of the AgNPs with nominal mean diameters of 10 nm were confirmed by transmission electron microscopy.

GSH quantification using AgNP aggregation

Suspensions of silver nanoparticles will aggregate in the presence of reduced GSH (41). This aggregation results in a color shift of the AgNP suspension, moving from orange to reddish-brown. The amount of GSH present can be measured by color intensity or color length, depending on the type of µPAD used (described in more detail below). Color intensity is quantified using ImageJ software (NIH) and color length is quantified using the naked eye, respectively. All quantified color intensities were measured as a difference between the assay spot and a corresponding control spot. To generate a standard curve, varying levels of a standard oxidant species, 1, 4-naphthoquinone (1,4-NQ) and a fixed amount of GSH were pipetted sequentially onto filter paper and allowed to react for 20 min. The color product on the filter paper was then analyzed using the process described above. The relationship between the 1,4-NQ concentration and the GSH consumption was plotted and used as the standard curve of GSH consumption for real sample analysis.

Designs and procedure

The approaches used to measure GSH with a traditional μPAD or a distance-based μPAD are shown in Figures 1A and 1B, respectively. All μPADs were designed and drawn using standard vector-based drawing software (CorelDraw). A wax printer (Xerox Phaser 8860) was used to print wax on Whatman #1 filter paper following previously reported methods (*42*, *43*). The conventional μPAD consisted of three layers: a top layer for sample loading, a middle layer as a flow valve, and a bottom layer for detection (Figure 1A). Double-sided tape (Scotch ™) was used to hold various layers of the μPAD together. The middle (valve) layer consisted of a polymer film to provide a hydrophobic barrier that prevented sample from moving between layers until desired. This layer prevented sample leakage and also controlled overall reaction time. The top layer consisted of a 6 mm diameter opening for sample addition (i.e., placement of the filter punch) with two channels (2 mm width) leading to sample reaction regions (Figure 1A). Samples for oxidative load analyses consisted of 6 mm diameter punches that were cut from air sampling filters used to collect PM. With the middle layer in place, a PM-laden filter punch

was placed over the sample addition region. Two 5 μ L aliquots of H₂O were then added to the punch to extract the water soluble portion of the PM and elute it onto the two reaction zones. One zone was spotted with 5 μ L of GSH while the other zone received no GSH (acting as a reference blank). After 20 min, the valve was opened by removing the middle layer and 20 μ L of buffer was added to each reaction zone to elute the remaining GSH downwards to the bottom (detection) layer. The detection layer consists of two collection reservoirs (6 mm each; one sample, one reference) that received flow from layer one; each collection reservoir was also connected to four detection regions (each 4.3 mm in diameter) to allow for multiple measurements per sample. Prior to adding the sample punch, the detection spots were modified with a 0.5 μ L aliquot containing 1,000 mg/L AgNPs and 16 μ M RB solution. The residual GSH reacted with AgNPs in the detection layer and generated a reddish-brown color. Once dry, the detection reservoirs were imaged using a desktop scanner. The overall device shown in Figure 1A measures 55×25 mm (L×W). With this approach, the oxidative load of PM was measured in less than 35 min.

The distance-based detection system consisted of a sample addition region (6 mm diameter) connected to a detection channel (3×60 mm). The detection channel was patterned with a series of horizontal baffles (0.3×2 mm, and spaced at 3 mm intervals) designed to reduce flow velocity and increase reaction time between GSH and AgNPs (Figure 1B) (44). The detection channel was modified using a solution that had 1,000 mg/L AgNPs. For analysis, a filter punch (6 mm diameter) containing a PM sample was placed into a petri dish and allowed to react with a 5 μ L drop of GSH for 20 min. The filter punch was then transferred to the sample addition region and the remaining GSH eluted into the detection channel with 20 μ L of buffer. The residual GSH then flowed down the detection channel and reacted with AgNPs present along the flow path. Color develops along the flow path until all of the GSH is consumed. Quantification is achieved by measuring color length. This assay finished within 30 min.

Analysis of oxidative load of various aerosols

Sample collection

Two types of aerosol samples were collected for device validation: high-volume and low-volume filter samples. The high-volume samples were collected at fixed sites representing specific PM sources. The low-volume samples were collected using a miniature pump and filter-cassette assembly, carried by volunteers on different days. The high-loading aerosol samples were collected from three different sources: biomass burning, urban air, and second-hand cigarette smoke. Two biomass burning PM_{2.5} samples (samples B1 and B2) from the combustion of vegetation commonly-burned in North American wildfires were collected using a Hi-volume filter sampler at the USDA Forest Service's Fire Science Laboratory in Missoula, Montana as part of the Third Fire Lab at Missoula Experiment study (45). Three urban aerosol samples (C1–C3 samples) were collected on quartz filters over separate, integrated three-day sampling periods in Cleveland, OH during the winter of 2008 using a Thermo Anderson Hi-Volume Air Sampler (Windsor, NJ, USA). The quartz filters were pre-baked in an

oven at 550 °C for 12 h and wrapped in aluminum foil before use. Additionally, two samples of second-hand tobacco smoke (S1 and S2 samples) were created in a 1.0 m³ aerosol chamber and sampled onto 37 mm filters (Mixed Cellulose Ester Membrane, Millipore, Billerica, MA) at 10 L/min and 1 atm. After sampling, the filters were stored at -20 °C. These 'real-world' samples were used to demonstrate the technique and also served as the basis for comparing the paper-based methods with the traditional spectroscopic methods.

The low-volume samples were collected using a personal air sampler for PM $_{10}$ (PM size $\leq 10~\mu m$) on two separate days spent in Fort Collins, CO. A Teflon-coated glass-fiber filter (Pallflex T40A60, 37 mm, Pall Corporation, Ann Arbor, MI) was used in conjunction with a personal aerosol sampler (Personal Environmental Monitors, 761-203A or 761-200A, SKC, Inc.). A small sampling pump (Omni-400, BGI Incorporated, Waltham, MA) was used to draw air through each sampler at 4 L min $^{-1}$. Volunteers carried the personal sampler in a backpack over a 24 h period during two distinctly different events: (1) a restaurant sample collected across an 8 h work shift in a restaurant kitchen followed 16 h doing normal activities (mixture of indoor and outdoor exposure over 24 hrs) and (2) a sample collected across a 24 h period within a volunteer's home in Fort Collins (a relatively clean environment that was free from other combustion or cooking sources). All filters were weighed before and after sample collection with a microbalance (Mettler-Toledo, model MX5) to determine total mass loading. No additional sample preparation was required for these experiments.

Analysis and validation

To validate our devices with the traditional DTT and GSH assay using UV-visible spectrometer, the high-volume filter samples (B1—B2 and C1—C3) were extracted into de-ionized water. Briefly, two 25 mm diameter punches from each filter sample were extracted into 5 mL of de-ionized water in a Nalgene Amber High Density Polyethylene (HDPE) bottle using sonication with heat (70 ± 5 °C) for 75 min. The aerosol extract was filtered through a 0.2 µm PTFE membrane (Millipore, Billerica, MA, USA) to remove insoluble materials. The filtered extract was kept in the dark at 4 °C until analysis by conventional μ PAD, distance-based μ PAD or UV-visible spectrometer. For the UV-visible spectrometer, the extracted solution was reacted with DTT or GSH for 20 min. The detection of residual DTT or GSH using Elman's reagent was achieved using a UV-visible spectrometer at 412 nm (Thermo Spectronic, Genesys 10 UV) (46). For both paper-based devices, 5 μ L aliquots of sample extract and GSH were sequentially pipetted onto the filter paper and allowed to react for 20 min. To quantify GSH consumption, the filter paper was transferred to the μ PAD (conventional or distance-based) containing AgNPs, and the residual GSH from the filter punch was eluted onto the μ PAD with 20 μ L of buffer. For field samples, sample punches were placed directly into paper devices without extraction. All remaining steps were carried out as described above for the comparison experiments.

3. Results and discussion

Two paper-based analytical devices were developed to measure PM oxidative load. Unlike prior efforts in this field, GSH was used as the reactive thiol because it is an endogenous antioxidant and, thus, more biologically relevant than dithiothreitol. In this assay, reduced GSH is oxidized to its disulfide in the presence of reactive species associated with PM. The remaining reduced GSH reacts with AgNPs (Figure 1C) to generate a colored product.

A conventional μ PAD was designed that contained three layers to allow both sample analysis as well as blank subtraction from a single filter sample. The μ PAD has four detection areas coated with AgNPs to improve the precision of each measurement. The resulting color product was captured using an office scanner and the color intensity was analyzed using ImageJ software. The alternative μ PAD utilizes distance-based detection. The AgNPs were pipetted onto paper in 0.5 μ L increments along the length of the detection channel. The residual GSH flowed along the channel by capillary action, and the GSH reacted with AgNPs giving a reddish-brown color product. Once all of the GSH has reacted, the color development stopped even as solution continued to flow along the channel. GSH quantification is achieved by measuring the length of the color along the channel using the naked eye.

Optimization of AgNP concentration

AqNPs are an alternative colorimetric reagent for determination of residual GSH because they have a high extinction coefficient relative to many molecular dyes. The -SH group in aminothiol compounds such as homocysteine, cysteine, and GSH is known to react with the AgNP surface causing nanoparticle aggregation (41, 47). This aggregation leads to significant shifting in the absorption spectrum with concomitant visible color changes from yellow/orange to reddish-brown. The relationship between GSH concentration and color intensity/length was measured first. For intensity measurements, a background correction was applied to all samples. To enhance the sensitivity, Rhodamine B (RB) was added to the AgNP solution, as this compound (as well as Rhodamine 6G) can affect the plasmon and molecular resonances of AgNPs (48, 49). According to previous reports, RB attaches to the surface of AgNPs through carboxyl group and non-covalent interactions whereas Rhodamine 6G attaches to the surface via non-covalent interaction (50). The AgNP surface modified with RB in Tri-HCl buffer shifted the absorption spectrum of the AgNPs because of the increased electrostatic repulsion between modified RB-AgNPs relative to AgNPs without RB. This phenomenon increased the change in color intensity upon addition of GSH. The effect of RB concentration on slope of GSH calibration was also measured. The maximum slope for a GSH calibration curve was found at 16 μ M of RB and 1,000 mg/L of AgNPs as shown in Figure 2. Moreover, other anions in the aerosol sample or buffer including Cl, SO_4^{2} and NO₃ did not significantly change the color intensity (data not shown). Thus, a final concentration of 16 μM of RB and 1,000 mg/L of AgNPs was selected all further experiments using the conventional μPAD.

Analytical figures of merit

The intensity of the color product in the conventional μ PAD was proportional to the GSH concentration over the range of 0 to 2.5 nmol (Intensity = 12.54*GSH + 0.51, R²=0.99) as shown in Figure 3A using the optimized conditions. The relative standard deviation (RSD, n = 3) of GSH calibration slope was found to be 9.2%. Although this standard deviation is higher than commonly reported for the traditional absorbance method, it is in-line with other μ PADs (*51-53*).

Aerosol oxidative activity was next measured using the distance-based μ PAD. With distance-based detection, no background correction was needed because a distinct color change can be seen visually. The detection channel was coated with only 1,000 mg/L of AgNP. A plot of sample reaction length as a Log function of the analyte concentration is shown in Figure 3B. Reaction length was log-linear in the range of 0.12 to 2 nmol GSH (Distance = 6.4*log-GSH + 7.5, R² = 0.99) and the RSD of GSH calibration slope was 5.3% (n = 3). The improvement in reproducibility for the distance-based μ PAD relative to the traditional μ PAD is most likely the result of the improved ability to distinguish the end point of the distance-based detection relative to the intensity change of the traditional device.

Performance of aerosol oxidative activity measurement

The effect of reaction time on GSH consumption rate was studied using 1,4-NQ as a model oxidant in the range of 0 to 15 ng 1,4-NQ with 2.5 nmol of initial GSH. The sensitivity of the assay demonstrated a significant improvement with increasing reaction time from 15 min (slope = 0.037) to 20 min (slope = 0.062). No further improvement in slope was found at 25 min (slope = 0.066) as shown in Figure 4. As a result, 20 min was selected as the optimal reaction time. The impact of starting GSH amount on detection limit and working range was measured next. The detection limit (Table 1) was estimated as the concentration that produced a signal at 3 times greater than the standard deviation of a blank (n = 10). The working range was taken as the linear range between the intensity or distance and 1,4-NQ amount (Table 1). The lowest detection limit of 1,4-NQ was obtained at low starting GSH (0.5 nmol) but the largest working range was found at higher initial GSH. Meanwhile, the distance-based µPAD gave both the lowest detection limit and the widest working range at high initial GSH (1.25 nmol). Sensitivity is increased for high initial GSH concentrations because the length of the colored region is longer than at lower GSH concentrations. As a result, it was easier to distinguish changes in color at high initial GSH by the eye in the presence of smaller amounts of 1,4-NQ. These results show that the devices can be used for a range of aerosol oxidative reactivities by tuning the initial amount of GSH. For the low oxidative load of our samples, 0.5 nmol and 1.25 nmol of GSH were used to obtain the lowest detection limit for µPAD and distance-based detection, respectively.

Analytical applications

To validate the devices for aerosol oxidative activity determination with real samples, results for the traditional assay using either DTT or GSH with Elman's reagent were compared to the colorimetric and distanced-based μ PADs. Five different samples of aerosol extracts (Figure 5A) were analyzed using all four

methods. The DTT consumption rate measured by the traditional assay in all five samples (black bar in Figure 5A) was higher than the GSH consumption rate (red bar in Figure 5A) according to the stronger reducing power of DTT relative to GSH (54). The GSH consumption rate measured by all three methods (colorimetric and distance-based μ PAD and traditional Elman's reagent assay) was compared using ANOVA (single factor) and plotted for correlation. No significant difference between the three methods was obtained at the 95% confidence level (*p-value* = 0.98). A good correlation between the traditional GSH assay and both μ PAD devices was obtained with R^2 = 0.98 and 0.99 for μ PAD and distance-based detection, respectively.

To further demonstrate the utility of our devices for real samples, four filter samples (S1–S2, ambient aerosols around Fort Collins and in the restaurant) were analyzed using the μ PAD methods. The results shown in Figure 5B show a strong correlation between the traditional and distance-based μ PAD methods (R^2 = 0.99); both devices could distinguish the high and low oxidative activity between cigarette smoke and ambient aerosols, respectively. Both μ PAD devices can also be applied to filter samples collected in the field. The advantages of the traditional μ PAD over distance-based μ PAD include lower detection limit of 1,4-NQ and wider working range. However, the distance-based μ PAD eliminates the need for an external scanner or camera. The analysis time of both our devices without any sample extraction was also less than 35 min, which marks a significant improvement over traditional spectroscopic assays.

4. Conclusion

We demonstrate here the development of an AgNP colorimetric sensing method for aerosol oxidative activity using paper-based analytical devices. The determination of aerosol oxidative activity on paper devices was previously based on the use of Elman's reagent with DTT. Here, the reddish-brown color intensity and distance produced from the aggregation of AgNPs by GSH was used to estimate aerosol reactivity. The reddish-brown color intensity on μ PAD provided a low detection limit for aerosol oxidative activity relative to previously reported methods. With distance-based detection, the length of reddish-brown color product can be readily discriminated by the naked eye. No significant differences for the aerosol oxidative activity measurement in filter samples between using our devices and the traditional GSH assay were observed. Both the distance-based detection and μ PAD represent a highly sensitive, rapid and simple technique that should be applicable to personal exposure monitoring.

5. References

1. A. K. Prahalad *et al.*, Air pollution particles mediated oxidative DNA base damage in a cell free system and in human airway epithelial cells in relation to particulate metal content and bioreactivity. *Chem Res Toxicol* **14**, 879 (Jul, 2001).

- C. A. Pope, 3rd, D. V. Bates, M. E. Raizenne, Health effects of particulate air pollution: time for reassessment? *Environ Health Perspect* 103, 472 (May, 1995).
- 3. Q. H. Sun, X. R. Hong, L. E. Wold, Cardiovascular Effects of Ambient Particulate Air Pollution Exposure. *Circulation* **121**, 2755 (Jun 29, 2010).
- 4. J. Crapo, F. J. Miller, B. Mossman, W. A. Pryor, J. P. Kiley, NHLBI workshop summary. Environmental lung diseases. Relationship between acute inflammatory responses to air pollutants and chronic lung disease. *American Review of Respiratory Disease* **145**, 1506 (1992).
- 5. A. Spira-Cohen, L. C. Chen, M. Kendall, R. Lall, G. D. Thurston, Personal exposures to traffic-related air pollution and acute respiratory health among Bronx schoolchildren with asthma. *Environ Health Perspect* **119**, 559 (Apr, 2011).
- 6. J. J. Sauvain *et al.*, Biomarkers of oxidative stress and its association with the urinary reducing capacity in bus maintenance workers. *J Occup Med Toxicol* **6**, 18 (2011).
- 7. A. Boveris *et al.*, Organ chemiluminescence: noninvasive assay for oxidative radical reactions. *Proc Natl Acad Sci U S A* **77**, 347 (Jan, 1980).
- 8. A. J. Ghio, Z. H. Meng, G. E. Hatch, D. L. Costa, Luminol-enhancedchemiluminescence after in vitro exposures of rat alveolar macrophages to oil fly ash is metal dependent. *Inhalation Toxicology* **9**, 255 (1997).
- M. B. Kadiiska, R. P. Mason, K. L. Dreher, D. L. Costa, A. J. Ghio, In Vivo Evidence of Free Radical Formation in the Rat Lung after Exposure to an Emission Source Air Pollution Particle†. *Chem Res Toxicol* 10, 1104 (1997/10/01, 1997).
- 10. F. Tietze, Enzymic method for quantitative determination of nanogram amounts of total and oxidized glutathione: Applications to mammalian blood and other tissues. *Analytical Biochemistry* **27**, 502 (1969).
- G. G. Xiao, M. Y. Wang, N. Li, J. A. Loo, A. E. Nel, Use of proteomics to demonstrate a hierarchical oxidative stress response to diesel exhaust particle chemicals in a macrophage cell line. *Journal of Biological Chemistry* 278, 50781 (Dec, 2003).
- J. Tamarit, E. Cabiscol, J. Ros, Identification of the Major Oxidatively Damaged Proteins in Escherichia coli Cells Exposed to Oxidative Stress. *J Biol Chem* 273, 3027 (January 30, 1998, 1998).
- 13. E. Shacter, J. A. Williams, M. Lim, R. L. Levine, Differential susceptibility of plasma proteins to oxidative modification: examination by western blot immunoassay. *Free Radic Biol Med* **17**, 429 (Nov, 1994).
- 14. H. Jung, B. Guo, C. Anastasio, I. M. Kennedy, Quantitative measurements of the generation of hydroxyl radicals by soot particles in a surrogate lung fluid. *Atmospheric Environment* **40**, 1043 (2006).
- E. Vidrio, C. H. Phuah, A. M. Dillner, C. Anastasio, Generation of Hydroxyl Radicals from Ambient Fine Particles in a Surrogate Lung Fluid Solution. *Environmental Science & Technology* 43, 922 (2009/02/01, 2009).

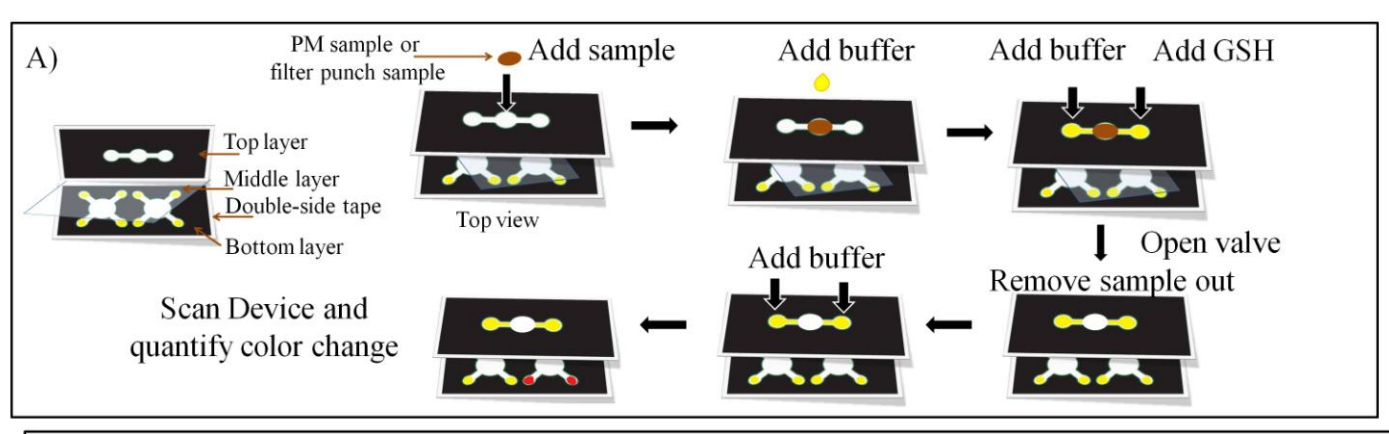
- 16. Y. Sameenoi *et al.*, Microfluidic Electrochemical Sensor for On-Line Monitoring of Aerosol Oxidative Activity. *J Am Chem Soc* **134**, 10562 (2012/06/27, 2012).
- 17. Q. Li, A. Wyatt, R. M. Kamens, Oxidant generation and toxicity enhancement of aged-diesel exhaust. Atmospheric Environment 43, 1037 (2009).
- 18. J. C. Jokerst *et al.*, Development of a Paper-Based Analytical Device for Colorimetric Detection of Select Foodborne Pathogens. *Analytical Chemistry* **84**, 2900 (Mar 20, 2012).
- M. M. Mentele, J. Cunningham, K. Koehler, J. Volckens, C. S. Henry, Microfluidic Paper-Based Analytical Device for Particulate Metals. *Analytical Chemistry* 84, 4474 (May 15, 2012).
- W. Dungchai, O. Chailapakul, C. S. Henry, Electrochemical Detection for Paper-Based Microfluidics.
 Analytical Chemistry 81, 5821 (Jul 15, 2009).
- A. W. Martinez, S. T. Phillips, B. J. Wiley, M. Gupta, G. M. Whitesides, FLASH: A rapid method for prototyping paper-based microfluidic devices. *Lab Chip* 8, 2146 (2008).
- A. W. Martinez, S. T. Phillips, G. M. Whitesides, E. Carrilho, Diagnostics for the Developing World:
 Microfluidic Paper-Based Analytical Devices. *Analytical Chemistry* 82, 3 (Jan 1, 2010).
- 23. C. M. Cheng et al., Paper-Based ELISA. Angew Chem Int Edit 49, 4771 (2010).
- 24. X. X. Yang, O. Forouzan, T. P. Brown, S. S. Shevkoplyas, Integrated separation of blood plasma from whole blood for microfluidic paper-based analytical devices. *Lab Chip* **12**, 274 (2012).
- Y. Sameenoi et al., Microfluidic Paper-Based Analytical Device for Aerosol Oxidative Activity.
 Environmental Science & Technology 47, 932 (Jan 15, 2013).
- 26. M. Hepel, M. Stobiecka, in *Fine Particles in Medicine and Pharmacy,* E. MatijeviĆ, Ed. (Springer US, 2012), pp. 241-281.
- 27. I. I. S. Lim *et al.*, Homocysteine-Mediated Reactivity and Assembly of Gold Nanoparticles. *Langmuir* **23**, 826 (2007/01/01, 2006).
- 28. W. Leesutthiphonchai, W. Dungchai, W. Siangproh, N. Ngamrojnavanich, O. Chailapakul, Selective determination of homocysteine levels in human plasma using a silver nanoparticle-based colorimetric assay. *Talanta* **85**, 870 (2011).
- Z. P. Li, X. R. Duan, C. H. Liu, B. A. Du, Selective determination of cysteine by resonance light scattering technique based on self-assembly of gold nanoparticles. *Analytical Biochemistry* 351, 18 (2006).
- 30. X. Wei, L. Qi, J. Tan, R. Liu, F. Wang, A colorimetric sensor for determination of cysteine by carboxymethyl cellulose-functionalized gold nanoparticles. *Analytica Chimica Acta* **671**, 80 (2010).
- Z. Chen, S. Luo, C. Liu, Q. Cai, Simple and sensitive colorimetric detection of cysteine based on ssDNAstabilized gold nanoparticles. *Analytical and Bioanalytical Chemistry* 395, 489 (2009).

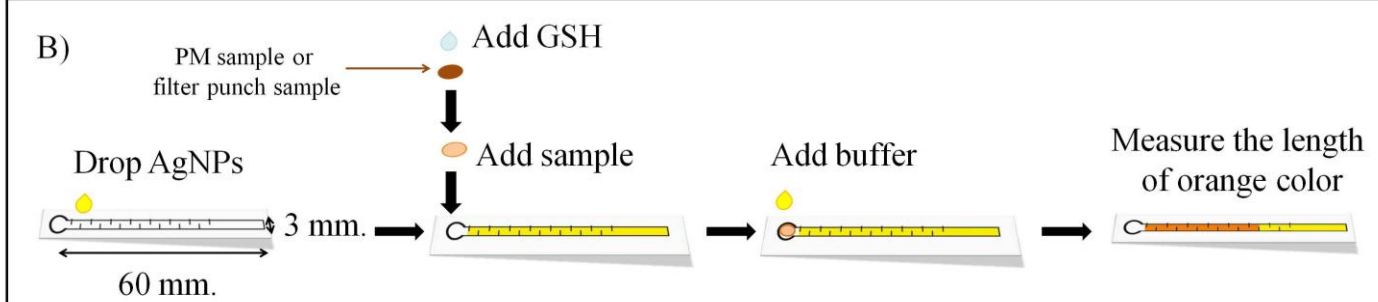
- 32. R. J. Stokes *et al.*, Quantitative enhanced raman scattering of labeled DNA from gold and silver nanoparticles. *Small* **3**, 1593 (2007).
- 33. K. Shrivas, H. F. Wu, Applications of silver nanoparticles capped with different functional groups as the matrix and affinity probes in surface-assisted laser desorption/ionization time-of-flight and atmospheric pressure matrix-assisted laser desorption/ionization ion trap mass spectrometry for rapid analysis of sulfur drugs and biothiols in human urine. *Rapid Communications in Mass Spectrometry* 22, 2863 (2008).
- 34. H. Li, Z. Cui, C. Han, Glutathione-stabilized silver nanoparticles as colorimetric sensor for Ni 2+ ion. Sensors and Actuators, B: Chemical 143, 87 (2009).
- 35. A. Apilux, W. Siangproh, N. Praphairaksit, O. Chailapakul, Simple and rapid colorimetric detection of Hg(II) by a paper-based device using silver nanoplates. *Talanta* **97**, 388 (2012).
- 36. N. Ratnarathorn, O. Chailapakul, C. S. Henry, W. Dungchai, Simple silver nanoparticle colorimetric sensing for copper by paper-based devices. *Talanta*.
- D. M. Cate, W. Dungchai, J. C. Cunningham, J. Volckens, C. S. Henry, Simple, distance-based measurement for paper analytical devices. *Lab Chip* 13, 2397 (Jun 21, 2013).
- 38. W. Leesutthiphonchai, W. Dungchai, W. Siangproh, N. Ngamrojnavanich, O. Chailapakul, Selective determination of homocysteine levels in human plasma using a silver nanoparticle-based colorimetric assay. *Talanta* **85**, 870 (Aug 15, 2011).
- 39. D. K. Bhui, A. Misra, Synthesis of worm like silver nanoparticles in methyl cellulose polymeric matrix and its catalytic activity. *Carbohyd Polym* **89**, 830 (Jul 1, 2012).
- 40. P. Sarkar *et al.*, Aqueous-Phase Synthesis of Silver Nanodiscs and Nanorods in Methyl Cellulose Matrix: Photophysical Study and Simulation of UV-Vis Extinction Spectra Using DDA Method. *Nanoscale Res Lett* **5**, 1611 (Oct, 2010).
- M. Stobiecka, K. Coopersmith, M. Hepel, Resonance elastic light scattering (RELS) spectroscopy of fast non-Langmuirian ligand-exchange in glutathione-induced gold nanoparticle assembly. *J Colloid Interf Sci* 350, 168 (Oct 1, 2010).
- 42. E. Carrilho, A. W. Martinez, G. M. Whitesides, Understanding Wax Printing: A Simple Micropatterning Process for Paper-Based Microfluidics. *Analytical Chemistry* **81**, 7091 (Aug 15, 2009).
- 43. Z. W. Zhong, Z. P. Wang, G. X. D. Huang, Investigation of wax and paper materials for the fabrication of paper-based microfluidic devices. *Microsyst Technol* **18**, 649 (May, 2012).
- 44. A. Apilux, Y. Ukita, M. Chikae, O. Chailapakul, Y. Takamura, Development of automated paper-based devices for sequential multistep sandwich enzyme-linked immunosorbent assays using inkjet printing. *Lab Chip* 13, 126 (2013).
- 45. C. J. Hennigan *et al.*, Chemical and physical transformations of organic aerosol from the photo-oxidation of open biomass burning emissions in an environmental chamber. *Atmos Chem Phys* **11**, 7669 (2011).

- 46. J. Sedlak, R. H. Lindsay, Estimation of total, protein-bound, and nonprotein sulfhydryl groups in tissue with Ellman's reagent. *Analytical Biochemistry* **25**, 192 (1968).
- 47. H. B. Li, Z. M. Cui, C. P. Han, Glutathione-stabilized silver nanoparticles as colorimetric sensor for Ni(2+) ion. Sensor Actuat B-Chem 143, 87 (Dec 4, 2009).
- 48. J. Zhao *et al.*, Interaction of plasmon and molecular resonances for rhodamine 6G adsorbed on silver nanoparticles. *J Am Chem Soc* **129**, 7647 (Jun 20, 2007).
- S. Kruszewski, M. Cyrankiewicz, Aggregated Silver Sols as SERS Substrates. Acta Phys Pol A 121, A68 (Jan, 2012).
- 50. Z. M. Cui, C. P. Han, H. B. Li, Dual-signal fenamithion probe by combining fluorescence with colorimetry based on Rhodamine B modified silver nanoparticles. *Analyst* **136**, 1351 (2011).
- 51. M. M. Mentele, J. Cunningham, K. Koehler, J. Volckens, C. S. Henry, Microfluidic paper-based analytical device for particulate metals. *Anal Chem* **84**, 4474 (May 15, 2012).
- 52. A. W. Martinez, S. T. Phillips, G. M. Whitesides, E. Carrilho, Diagnostics for the developing world: microfluidic paper-based analytical devices. *Anal Chem* **82**, 3 (Jan 1, 2010).
- 53. A. W. Martinez, S. T. Phillips, M. J. Butte, G. M. Whitesides, Patterned paper as a platform for inexpensive, low-volume, portable bioassays. *Angew Chem Int Ed Engl* **46**, 1318 (2007).
- 54. P. A. Johnston *et al.*, Development of a 384-well colorimetric assay to quantify hydrogen peroxide generated by the redox cycling of compounds in the presence of reducing agents. *Assay Drug Dev Techn* **6**, 505 (Aug, 2008).

Figure captions

- Figure 1: Schematic drawings of the device designs and general analytical methods of $\,$ (A) a traditional $\,$ PAD and $\,$ (B) a distance-based $\,$ μ PAD for the determination of the aerosol oxidative load. (C) Schematic diagram of the AgNP aggregation mechanism for determination of residual GSH.
- Figure 2: Optimization of RB and AgNP concentrations on the two different types of µPADs.
- Figure 3: (A) Calibration of GSH using the μPADs. (B) Calibration of GSH using the distance-based μPAD.
- Figure 4: Optimization of reaction time between GSH and 1,4-NQ at 2.5 nmol of the initial GSH.
- Figure 5: Method validation using (A) an extracted sample and (B) a filter sample.
- Table 1: Linearity and LOD of 1,4-NQ in the presence of various initial GSH amount with 20 min of reaction time.





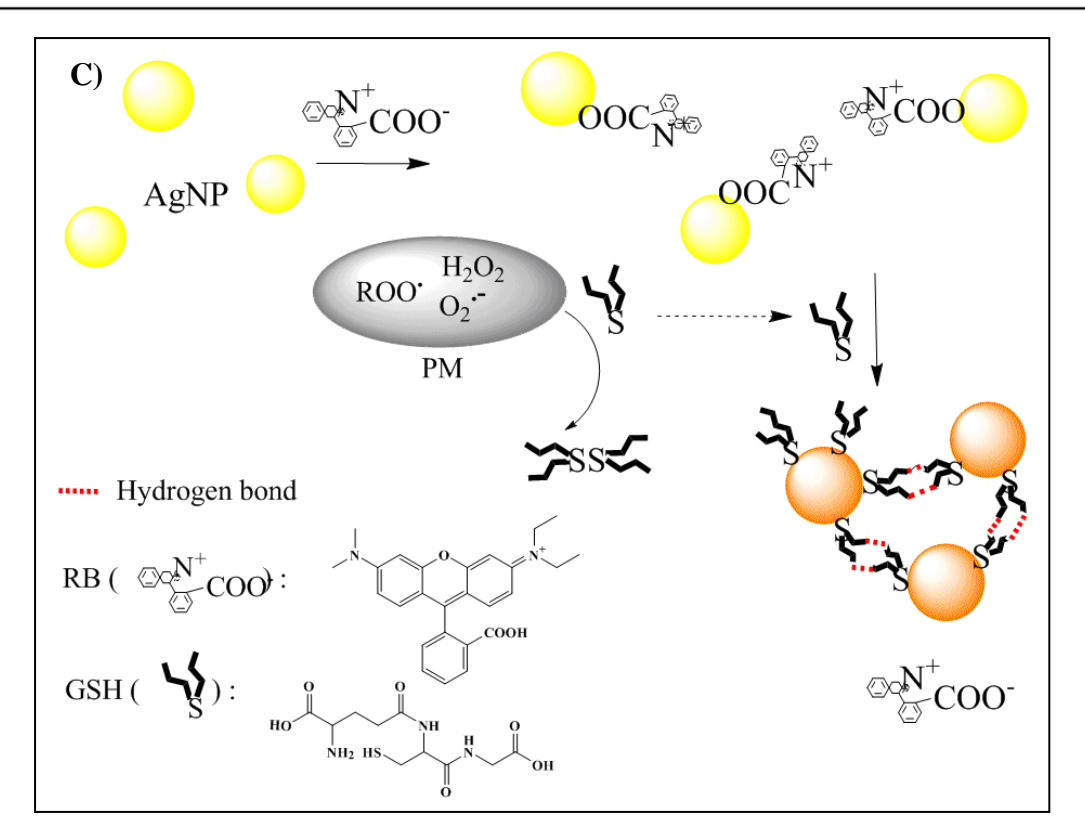


Figure 1: Schematic drawings of the device designs and general analytical methods of (A) colorimetric

PAD and (B) distance-based μPAD for the determination of the aerosol oxidative load. (C) Schematic diagram of the AgNP aggregation for determination of residual GSH.

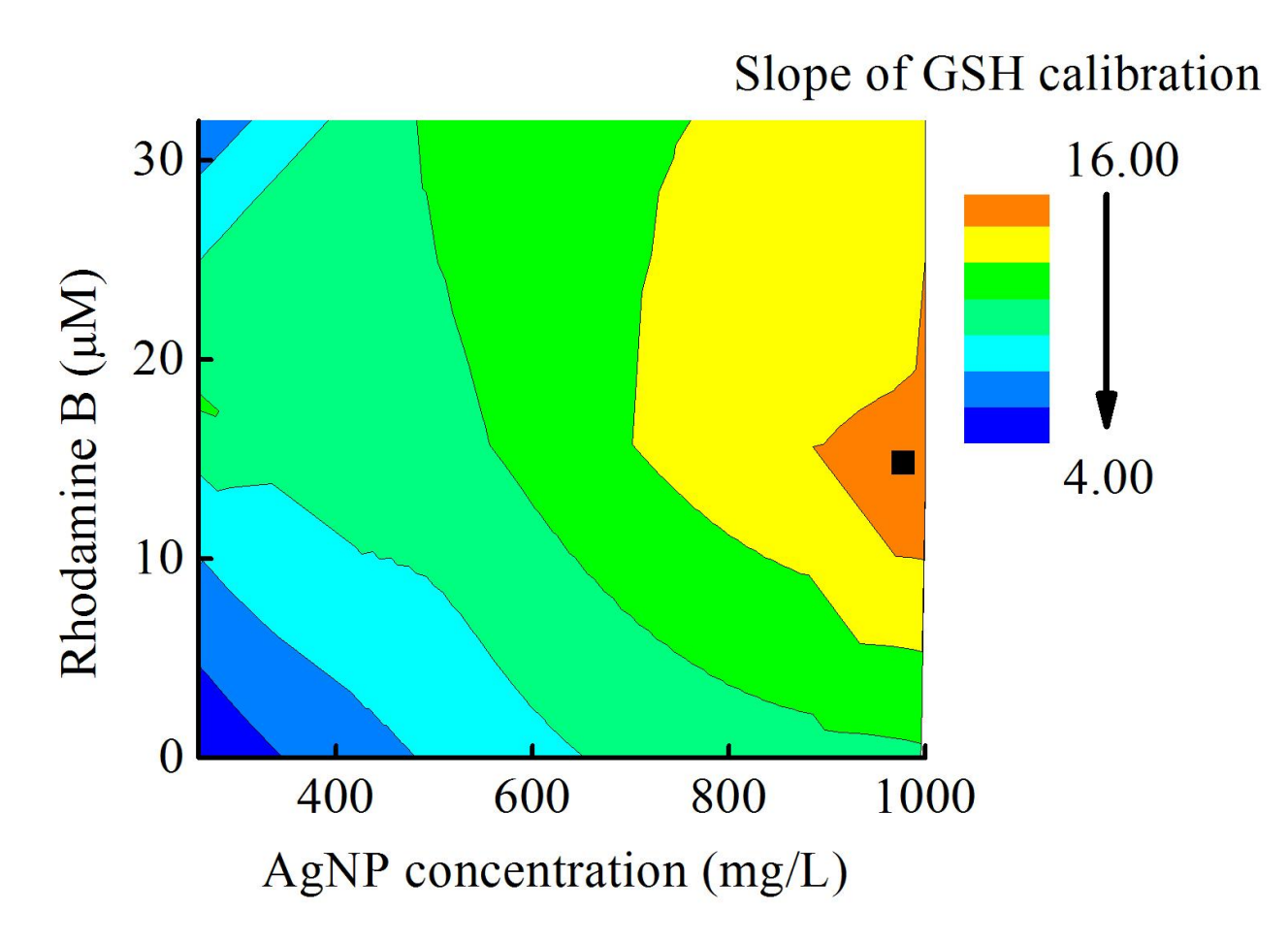
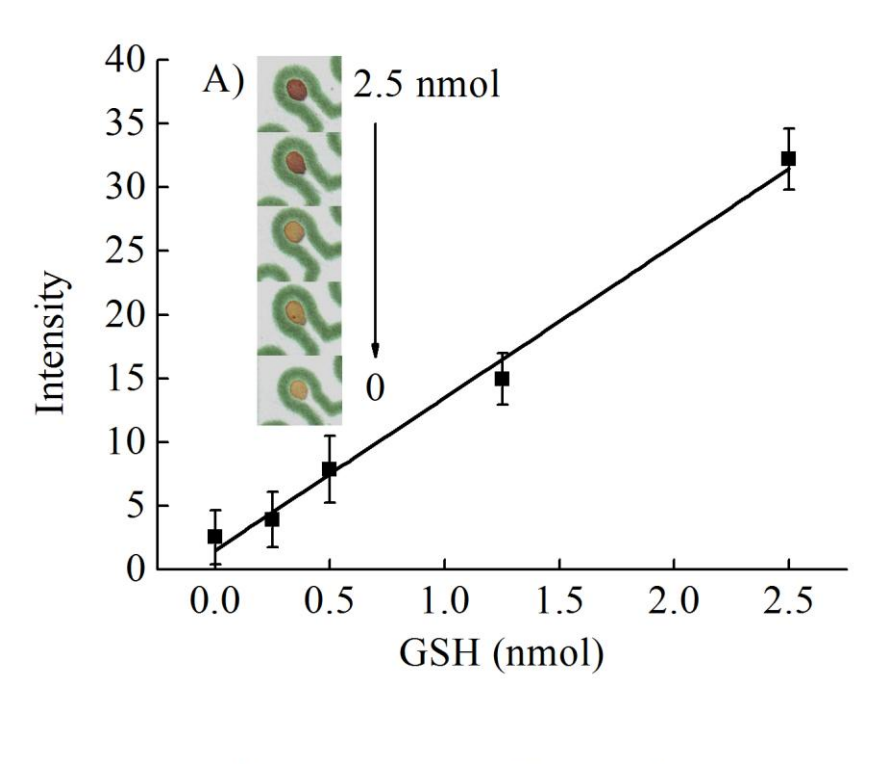


Figure 2: Optimization of RB and AgNP concentrations on the two different types of μ PADs. The optimized condition represented by in this figure.



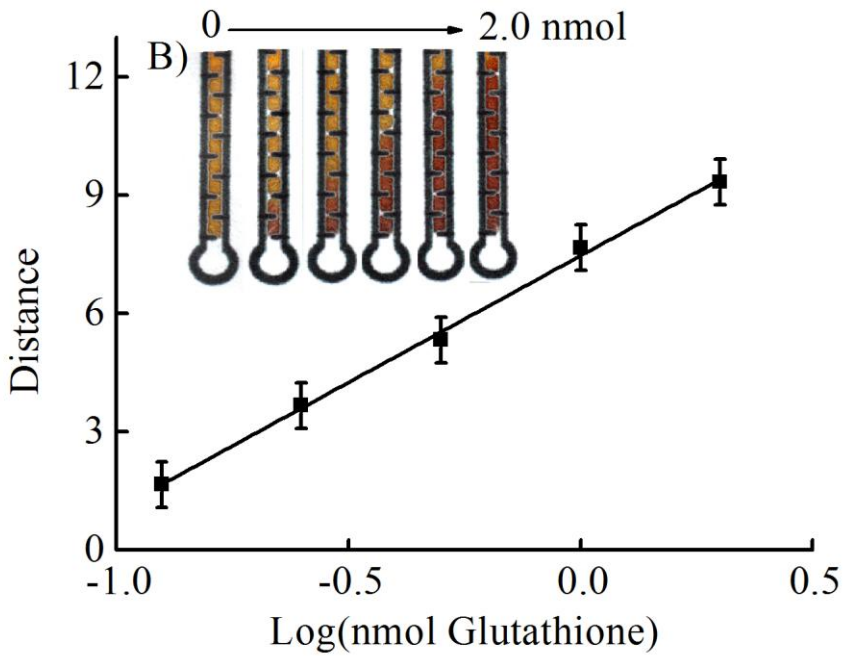


Figure 3: (A) Calibration of GSH using the μ PADs. (B) Calibration of GSH using the distance-based μ PAD.

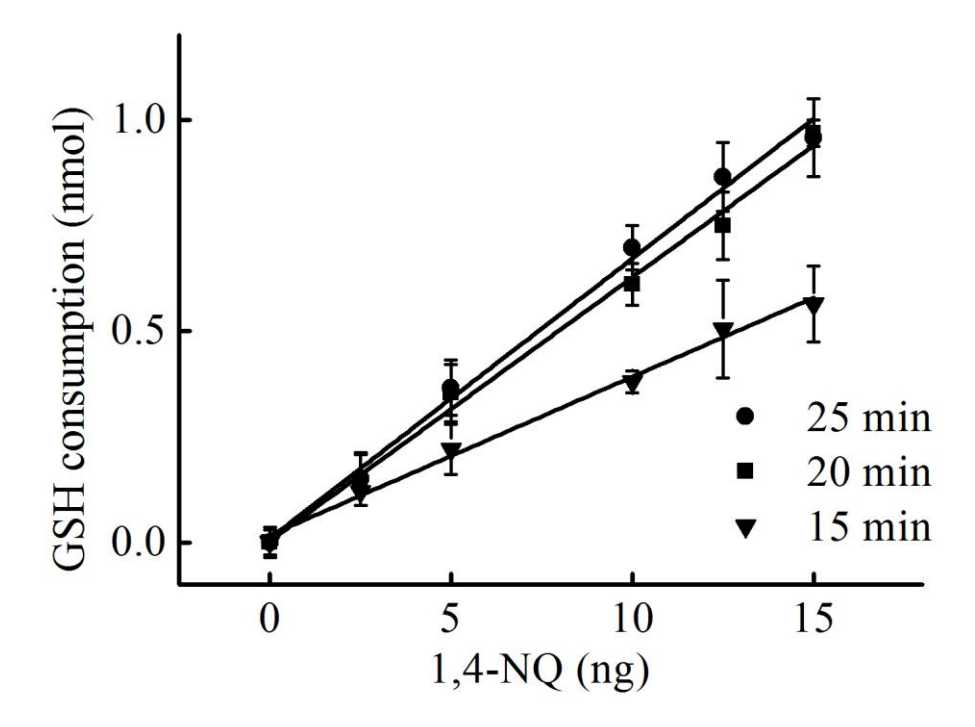
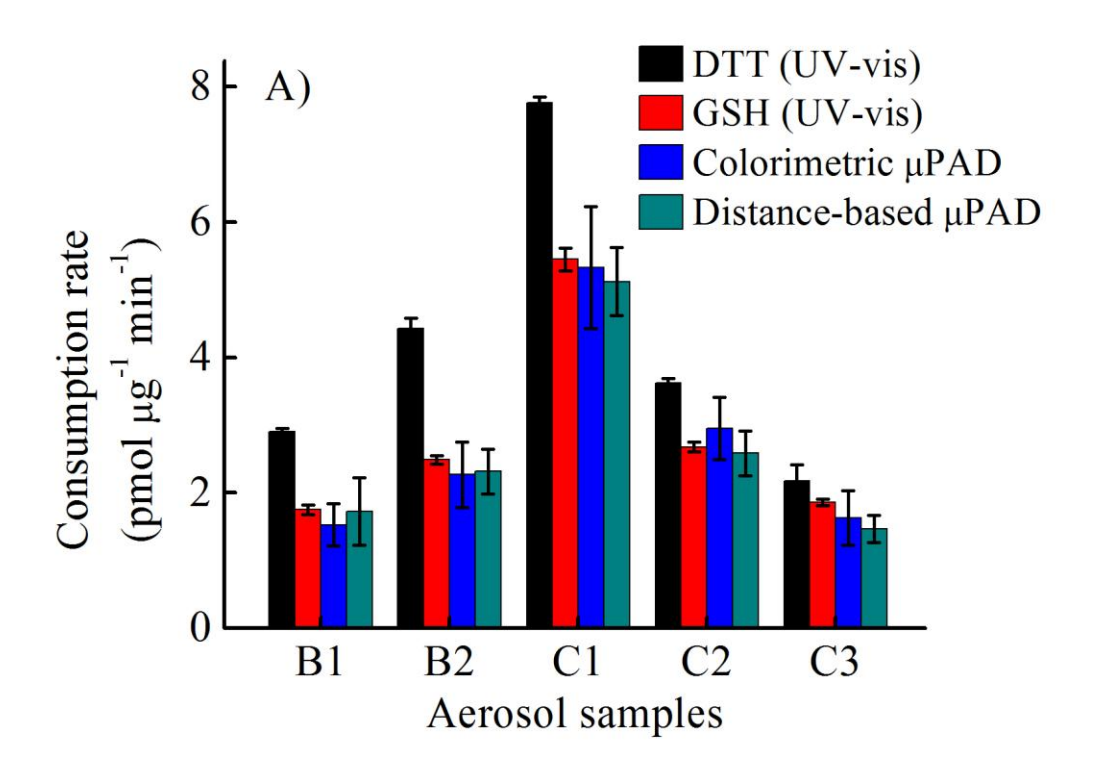


Figure 4: Optimization of reaction time between GSH and 1,4-NQ at 2.5 nmol of the initial GSH.



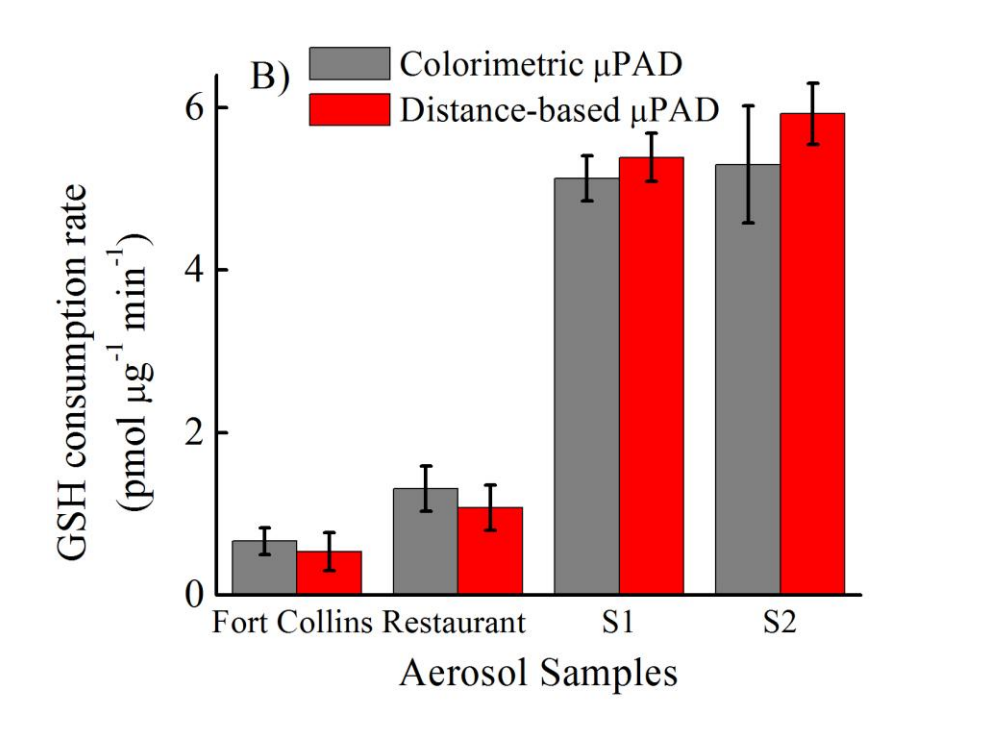


Figure 5: Method validation using (A) an extracted sample (B) a filter sample.

Table 1: Linearity and LOD of 1,4-NQ in the presence of various initial GSH amount with 20 min of reaction time.

Devices	GSH (nmol)	LOD of 1,4-NQ (ng)	Linearity of 1,4-NQ (ng)
	2.5	11.0	0 - 75
μPADs	1.25	6.5	0 - 35
	0.5	3.7	0 - 25
Distance-based	1.25	10.0	5-25
detection	0.5	20.0	15-30

CHAPTER V

CONCLUSIONS AND FUTURE PERSPECTIVE

1. Conclusion

In this proposed work, the first time the use of silver nanoparticles for determination of copper (II) ion on paper device was presented. The sensor is based on the aggregation of AqNPs on a paper substrate by the strong affinity between AgNPs modified with thiol conpounds and Cu²⁺, which leads to a shift in the absorption spectrum. Furthermore, the color change of AgNPs on paper substrate can be observable by the naked eye due to the extremely high extinction coefficient of AgNPs. Cu²⁺ was clearly distinguishable color change from the other heavy metal ions under the optimum conditions at the critical level of Cu2+ in drinking water prescribed by WHO. Finally, our paper devices were successfully applied to the semiquantitative analysis of Cu2+ in water samples. Both paper-based assay devices and paper-based microfluidic devices would be potentially modified with AgNPs for the detection of a variety of other targets. Moreover, A simple colorimetric method for the detection of nitrite and nitrate using paper-based analytical device (PAD) was also reported in this work. These Griess reaction can be applied to the determination of nitrite while nitrate was reduced to nitrite on PAD in the section of hydrophilic channel coated with Zn dust. The optimal conditions for the determination both nitrite and nitrate including the concentration of N-(1naphthyl)-ethylenediamine dihydrochloride (NED) and sulfanilamide, time, as well as three pattern of PAD (pattern 1, 2 and 3) were studied. Under the optimal conditions, the color intensity gave a linear response in the range 0-20 mgL⁻¹ ($R^2 = 0.993$ for nitrite and $R^2 = 0.981$ for nitrate) and the limits of detection was found at 0.1 mgL⁻¹. The purple color in the presence of nitrite and nitrate can be observed in PAD (pattern 1) by the naked eye within 25 minutes. Moreover, our PAD was applied for the determination of nitrite and nitrate in real samples such as poke sausage, smoked poke sausage, and ham.

2. Future perspective

This developed method is versatile, offers enhanced performance and can be easily extended to other metal detection. Moreover, the proposed aggregation pattern may be used for the development of immunochromatogrpic paper.

ภาคผนวก

Output ที่ได้จากโครงการคือ International Journal Publication จำนวน 2 ฉบับ ตาม ภาคผนวกแนบนี้ Analyst

PAPER

1

Cite this: DOI: 10.1039/c3an01235b

Determination of aerosol oxidative activity using silver nanoparticle aggregation on paper-based analytical devices

Wijitar Dungchai,^a Yupaporn Sameenoi,^{bd} Orawon Chailapakul,^e John Volckens^c and Charles S. Henry^{*b}

Airborne particulate matter (PM) pollution significantly impacts human health, but the cellular mechanisms of PM-induced toxicity remain poorly understood. A leading hypothesis on the effects of inhaled PM involves the generation of cellular oxidative stress. To investigate PM-induced oxidative stress, analytical methods have been developed to study the chemical oxidation of dithiothreitol (DTT) in the presence of PM. Although DTT readily reacts with several forms of reactive oxygen species, this molecule is not endogenously produced in biological systems. Glutathione (GSH), on the other hand, is an endogenous antioxidant that is produced throughout the body and is directly involved in combating oxidative stress in the lungs and other tissues. We report here a new method for measuring aerosol oxidative activity that uses silver nanoparticle (AqNP) aggregation coupled to glutathione (GSH) oxidation in a paper-based analytical device. In this assay, the residual reduced GSH from the oxidation of reduced GSH to its disulfide induces the aggregation of AgNPs on a paper-based analytical device, which produces a reddish-brown product. Two methods for aerosol oxidative reactivity are presented: one based on change in color intensity using a traditional paper-based techniques and one based on the length of the color product formed using a distance-based device. These methods were validated against traditional spectroscopic assays for DTT and GSH that employ Elman's reagent. No significant difference was found between the levels measured by all three GSH methods (our two paper-based devices and the traditional method) at the 95% confidence level. PM reactivity towards GSH was less than towards DTT most likely due to the difference in the oxidation potential between the two molecules.

2

10

15

20

25

30

35

40

45

50

DOI: 10.1039/c3an01235b

Received 25th June 2013

Accepted 10th September 2013

www.rsc.org/analyst

Introduction

Epidemiological studies have shown that human exposure to airborne particulate matter (PM) is associated with numerous health effects including diseases of the cardiovascular, respiratory, and immune systems.^{1–5} Although a definitive mechanism of PM-induced toxicity remains elusive, it is generally agreed that PM induces oxidative stress (either directly or through induction of biological systems), causing systematic both inflammation and cellular dysfunction. Recently, both cell-based and cell-free systems have been used to investigate

the capacity of PM to induce oxidative stress. Cell-based assays using fluorescence,6 chemiluminescence,7,8 electron spin resonance,9 glutathione ratio,10,11 lipid peroxidation, immunoassay and/or macrophage-based methods12,13 have shed important light into the mechanisms of PM-induced oxidative stress. However, these methods are expensive, complex, and difficult to use in the field. These assays also tend to require large amounts of PM (tens to hundreds of micrograms), which, in turn, requires long sampling and analysis times. Cell-free measurements of PM reactivity (oxidative load) typically use filter collection of PM and sample extraction prior to analysis. Traditionally, oxidative stress markers such as polyaromatic hydrocarbons (PAHs), quinones and transition metal have been measured using chromatography, electrophoresis, spectroscopy and mass spectrometry. 14,15 More recently, a method for estimating total oxidative load using dithiothreitol (the so called DTT assay) has been demonstrated. 16,17 The method has been convincingly shown to correlate with oxidative stress in vitro and thus, has been suggested as an appropriate surrogate when biological assays are not suitable. In the DTT assay, aqueous or solvent-based extracts of PM are mixed with DTT and allowed to

5

10

15

30

35

40

45

^aDepartment of Chemistry, Faculty of Science, King Mongkut's University of Technology Thonburi, Prachautid Road, Thungkru, Bangkok, 10140, Thailand

^bDepartment of Chemistry, Colorado State University, Fort Collins, Colorado, 80523-1872, USA. E-mail: chuck.henry@colostate.edu; Fax: +1-970-491-1801; Tel: +1-970-491-2852

Department of Environmental and Radiological Health Sciences, Colorado State University, Fort Collins, Colorado, 80523-1872, USA

^dDepartment of Chemistry, Faculty of Science, Burapha University, Chonburi, 20131, Thailand

^eDepartment of Chemistry, Faculty of Science, Chulalongkorn University, 10330, Thailand

react for a fixed period of time. The reaction is then quenched and Elman's reagent is added, reacting with the remaining reduced DTT to produce a yellow solution that absorbs light at 412 nm. The rate of DTT consumption measured in this way is directly proportional to the oxidative capacity of the PM sample. The DTT assay provides higher throughput than cell-based measurements, provided sufficient PM sample is available (10–100 $\,\mu g$ of PM per test), but also requires laboratory-based equipment to operate.

10

15

20

30

35

40

55

Microfluidic paper-based analytical devices (µPADs) have gained interest for point-of-use diagnostics due to their low cost, ease of operation, and ability to function without external power supplies or supporting equipment. 18-24 Moreover, µPADs were recently introduced as an alternative for measuring oxidative load, providing a relatively simple method that requires less sample and reagent relative to traditional methods.25 Unlike the traditional DTT assay, the uPAD method does not require a separate PM extraction step. Instead, a small punch taken from a filter sample of PM is spotted with DTT and allowed to react for a specified time (\sim 20 min). The residual DTT present on filter punch is then eluted onto a µPAD that contains Elman's reagent (which reacts with remaining DTT). The intensity of the yellow color product is used to infer the DTT consumption rate. With the µPAD-based approach, the oxidative load of PM was measured in less than 30 min. The μPAD method also requires minimal reagent (1 µL) due to its small size (approximately 6.25 cm² per device). Finally, because the μPAD requires only 3 μg of PM mass, shorter air sampling times and/or collection at lower flow rates (i.e., for personal sampling) is possible, making the device particularly attractive for exposure and risk assessment.

Although previous examples of the DTT assay have used Elman's reagent, the method is less than ideal because the extinction coefficient of the yellow product is low ($\sim 10^4 \text{ M}^{-1}$ cm⁻¹). In recent years, nanoparticles have been widely used for colorimetric assays due to higher extinction coefficients than common organic dyes. Gold nanoparticle (AuNP) and silver nanoparticle (AgNP)-based colorimetric sensors have been reported for measuring thiols such as homocysteine (Hcy), 26-28 glutathione (GSH),26 and cysteine (Cys)29-31 in biological samples. The use of AgNPs has gained popularity for colorimetric sensing because AgNPs are inexpensive and have higher extinction coefficients than AuNPs.32-34 The change color intensity or/and color hue of AgNPs on paper-based devices can be visualized with the naked eye making them attractive for many applications. 35,36 Here, we present the first use of AgNP for colorimetric sensing on µPAD for rapid, simple, and sensitive determination of PM oxidative load based upon aggregation of AgNP in the presence of residual GSH. GSH is more biologically relevant as a probe for PM oxidative load (than DTT) because GSH is an abundant endogenous antioxidant.37,38 We demonstrate here the ability of an AgNP-based µPAD assay to quantify aerosol oxidative load via the GSH consumption. The effect of reaction time was studied using 1,4-naphthoquinone (1,4-NQ) as a standard oxidant for GSH consumption. The versatility of the µPADs technique was demonstrated by measuring PM oxidative load using two different detection motifs: traditional colorimetric intensity analysis and a recently reported distance-based detection paradigm.³⁹ Distance-based detection eliminates the need for an external scanner or camera because the length of the colored region can be interpreted by the naked eye. Finally, our μ PAD device was also validated against a conventional assay (UV-visible spectroscopy) using GSH instead DTT, and no significant difference was observed (P < 0.05, paired t-test) between the methods.

1

5

10

15

20

25

30

35

40

45

55

Experimental

Reagent and materials

Glutathione, reduced 98%, rhodamine B (RB), and 1,4-naphthoquinone were obtained from Sigma-Aldrich (St. Louis, MO). Dimethylsulfoxide (DMSO) was purchased from EMD Chemical Inc. (Gibbstown, NJ). Tris-hydrochloride (Tris-HCl) was obtained from Mallinckrodt Baker, Inc. (Phillipsburg, NJ). Whatman No. 1 qualitative grade filter paper was purchased from General Electric Company (Schenectady, New York, USA). All chemicals were used as received without further purification.

Preparation of AgNPs

A suspension of silver nanoparticles (AgNPs), obtained from the Sensor Research Unit at Department of Chemistry, Chulalongkorn University, Thailand, was synthesized using chemical reduction. Hold Sodium borohydride (NaBH4) and methylcellulose solutions were used as the reducing agent and stabilizer, respectively. A 20 mM solution of AgNO3 (10 mL) was combined with 10 mL freshly prepared methylcellulose solution and the mixture was stirred for 10 min in an ice bath. Then 0.1 M NaBH4 (2 mL) was added dropwise with continuous stirring at 0 °C to the mixture. After the complete addition of NaBH4 yellow colored silver nanoparticles were obtained. The shapes and particle size distributions of the AgNPs with nominal mean diameters of 10 nm were confirmed by transmission electron microscopy.

GSH quantification using AgNP aggregation

Suspensions of silver nanoparticles will aggregate in the presence of reduced GSH.43 This aggregation results in a color shift of the AgNP suspension, moving from orange to reddish-brown. The amount of GSH present can be measured by color intensity or color length, depending on the type of µPAD used (described in more detail below). Color intensity is quantified using ImageJ software (national institutes of health, NIH) and the length of the colored region is quantified using the naked eye, respectively. All quantified color intensities were measured as a difference between the assay spot and a corresponding control spot. To generate a standard curve, varying levels of a standard oxidant species, 1,4-naphthoquinone (1,4-NQ) and a fixed amount of GSH were pipetted sequentially onto filter paper and allowed to react for 20 min. The color product on the filter paper was then analyzed using the process described above. The relationship between the 1,4-NQ concentration and the GSH Paper Analyst

consumption was plotted and used as the standard curve of GSH consumption for real sample analysis.

Designs and procedure

1

5

10

15

20

The approaches used to measure GSH with a traditional µPAD or a distance-based µPAD are shown in Fig. 1A and B, respectively. All µPADs were designed and drawn using standard vector-based drawing software (CorelDraw). A wax printer (Xerox Phaser 8860) was used to print wax on Whatman #1 filter paper following previously reported methods. 44,45 The conventional µPAD consisted of three layers: a top layer for sample loading, a middle layer as a flow valve, and a bottom layer for detection (Fig. 1A). Double-sided tape (ScotchTM) was used to hold various layers of the µPAD together. The middle (valve) layer consisted of a polymer film to provide a hydrophobic barrier that prevented sample from moving between layers until desired. This layer prevented sample leakage and also controlled overall reaction time. The top layer consisted of a 6 mm diameter opening for sample addition (i.e., placement of the filter punch) with two channels (2 mm width) leading to sample reaction regions (Fig. 1A). Samples for oxidative load analyses consisted of 6 mm diameter punches that were cut from air sampling filters used to collect PM. With the middle layer in place, a PM-laden filter punch was placed over the sample addition region. Two 5 µL aliquots of H₂O were then added to the punch to extract the water soluble portion of the PM and elute it onto the two reaction zones. One zone was spotted with 5 µL of GSH while the other zone received no GSH (acting as a reference blank). After 20 min, the valve was opened by removing the middle layer and 20 µL of buffer was added to each reaction zone to elute the remaining GSH downwards to the bottom (detection) layer. The detection layer consists of two collection reservoirs (6 mm each; one sample, one reference) that received flow from layer one; each collection reservoir was also connected to four detection regions (each 4.3 mm in diameter) to allow for multiple measurements per sample. Prior to adding the sample punch, the detection spots were modified with a 0.5 μ L aliquot containing 1000 mg L⁻¹ AgNPs and 16 μ M RB solution. The residual GSH reacted with AgNPs in the detection layer and generated a reddish-brown color. Once dry, the detection reservoirs were imaged using a desktop scanner (Xerox DocuMate 3220 Scanner, color photo setting, 600 dpi). Then, color intensity is quantified using Image I software (NIH). The overall device shown in Fig. 1A measures 55×25 mm (length \times width). With this approach, the oxidative load of PM was measured in less than 35 min.

1

5

10

15

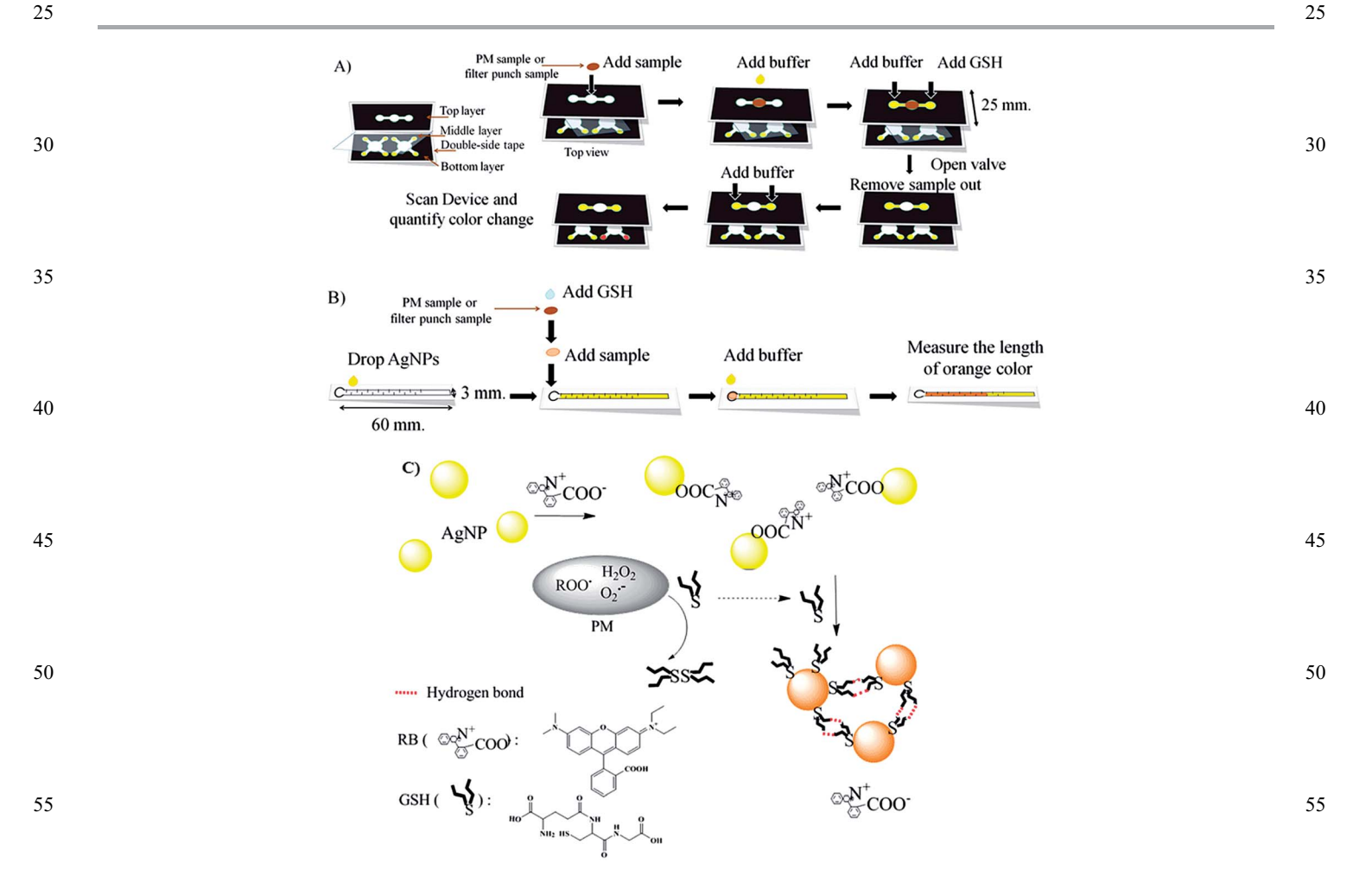


Fig. 1 Schematic drawings of the device designs and general analytical methods of (A) a traditional μPAD and (B) a distance-based μPAD for the determination of the aerosol oxidative load. (C) Schematic diagram of the AgNP aggregation mechanism for determination of residual GSH.

The distance-based detection system consisted of a sample addition region (6 mm diameter) connected to a detection channel (3 \times 60 mm). The detection channel was patterned with a series of horizontal baffles (0.3 \times 2 mm, and spaced at 3 mm intervals) designed to reduce flow velocity and increase reaction time between GSH and AgNPs (Fig. 1B).46 The detection channel was modified using a solution that had 1000 mg L⁻¹ AgNPs. For analysis, a filter punch (6 mm diameter) containing a PM sample was placed into a Petri dish and allowed to react with a 5 µL drop of GSH for 20 min. The filter punch was then transferred to the sample addition region and the remaining GSH eluted into the detection channel with 20 µL of buffer. The residual GSH then flowed down the detection channel and reacted with AgNPs present along the flow path. Color develops along the flow path until all of the GSH is consumed. Quantification is achieved by measuring color length. This assay finished within 30 min.

Analysis of oxidative load of various aerosols

10

15

20

35

40

50

55

Sample collection. Two types of aerosol samples were collected for device validation: high-volume and low-volume filter samples. The high-volume samples were collected at fixed sites representing specific PM sources. The low-volume samples were collected using a miniature pump and filter-cassette assembly, carried by volunteers on different days. The highloading aerosol samples were collected from three different sources: biomass burning, urban air, and second-hand cigarette smoke. Two biomass burning PM2.5 samples (samples B1 and B2) from the combustion of vegetation commonly-burned in North American wildfires were collected using a Hi-volume filter sampler at the USDA Forest Service's Fire Science Laboratory in Missoula, Montana as part of the Third Fire Lab at Missoula Experiment study.47 Three urban aerosol samples (C1-C3 samples) were collected on quartz filters over separate, integrated three-day sampling periods in Cleveland, OH during the winter of 2008 using a Thermo Anderson Hi-Volume Air Sampler (Windsor, NJ, USA). The quartz filters were pre-baked in an oven at 550 °C for 12 h and wrapped in aluminum foil before use. Additionally, two samples of second-hand tobacco smoke (S1 and S2 samples) were created in a 1.0 m³ aerosol chamber and sampled onto 37 mm filters (Mixed Cellulose Ester Membrane, Millipore, Billerica, MA) at 10 L min⁻¹ and 1 atm. After sampling, the filters were stored at -20 °C. These 'real-world' samples were used to demonstrate the technique and also served as the basis for comparing the paper-based methods with the traditional spectroscopic methods.

The low-volume samples were collected using a personal air sampler for PM $_{10}$ (PM size $\leq 10~\mu m$) on two separate days spent in Fort Collins, CO. A Teflon-coated glass-fiber filter (Pallflex® T40A60, 37 mm, Pall Corporation, Ann Arbor, MI) was used in conjunction with a personal aerosol sampler (Personal Environmental Monitors, 761-203A or 761-200A, SKC, Inc.). A small sampling pump (Omni-400, BGI Incorporated, Waltham, MA) was used to draw air through each sampler at 4 L min $^{-1}$. Volunteers carried the personal sampler in a backpack over a 24 h period during two distinctly different events: (1) a

restaurant sample collected across an 8 h work shift in a restaurant kitchen followed 16 h doing normal activities (mixture of indoor and outdoor exposure over 24 h) and (2) a sample collected across a 24 h period within a volunteer's home in Fort Collins (a relatively clean environment that was free from other combustion or cooking sources). All filters were weighed before and after sample collection with a microbalance (Mettler-Toledo, model MX5) to determine total mass loading. No additional sample preparation was required for these experiments.

1

5

10

15

20

35

55

Analysis and validation. To validate our devices with the traditional DTT and GSH assay using UV-visible spectrometer, the high-volume filter samples (B1 and B2 and C1-C3) were extracted into de-ionized water. Briefly, two 25 mm diameter punches from each filter sample were extracted into 5 mL of deionized water in a Nalgene Amber High Density Polyethylene (HDPE) bottle using sonication with heat (70 \pm 5 °C) for 75 min. The aerosol extract was filtered through a 0.2 µm PTFE membrane (Millipore, Billerica, MA, USA) to remove insoluble materials. The filtered extract was kept in the dark at 4 °C until analysis by conventional µPAD, distance-based µPAD or UVvisible spectrometer. For the UV-visible spectrometer, the extracted solution was reacted with DTT or GSH for 20 min. The detection of residual DTT or GSH using Elman's reagent was achieved using a UV-visible spectrometer at 412 nm (Thermo Spectronic, Genesys 10 UV).48 For both paper-based devices, 5 μL aliquots of sample extract and GSH were sequentially pipetted onto the filter paper and allowed to react for 20 min. To quantify GSH consumption, the filter paper was transferred to the µPAD (conventional or distance-based) containing AgNPs, and the residual GSH from the filter punch was eluted onto the μPAD with 20 μL of buffer. For field samples, sample punches were placed directly into paper devices without extraction. All remaining steps were carried out as described above for the comparison experiments.

Results and discussion

Two paper-based analytical devices were developed to measure PM oxidative load. Unlike prior efforts in this field, GSH was used as the reactive thiol because it is an endogenous antioxidant and, thus, more biologically relevant than dithiothreitol. In this assay, reduced GSH is oxidized to its disulfide in the presence of reactive species associated with PM. The remaining reduced GSH reacts with AgNPs (Fig. 1C) to generate a colored product.

A conventional μPAD was designed that contained three layers to allow both sample analysis as well as blank subtraction from a single filter sample. The μPAD has four detection areas coated with AgNPs to improve the precision of each measurement. The resulting color product was captured using an office scanner and the color intensity was analyzed using ImageJ software. The alternative μPAD utilizes distance-based detection. The AgNPs were pipetted onto paper in 0.5 μL increments along the length of the detection channel. The residual GSH flowed along the channel by capillary action, and the GSH reacted with AgNPs giving a reddish-brown color product. Once

Paper Analyst

all of the GSH has reacted, the color development stopped even as solution continued to flow along the channel. GSH quantification is achieved by measuring the length of the color along the channel using the naked eye.

Optimization of AgNP concentration

5

10

15

20

25

30

35

40

45

50

55

AgNPs are an alternative colorimetric reagent for determination of residual GSH because they have a high extinction coefficient $(\sim 10^{10} \text{ M}^{-1} \text{ cm}^{-1})$ relative to many molecular dyes. The -SH group in aminothiol compounds such as homocysteine, cysteine, and GSH is known to react with the AgNP surface causing nanoparticle aggregation. 43,49 This aggregation leads to significant shifting in the absorption spectrum with concomitant visible color changes from yellow/orange to reddish-brown. The relationship between GSH concentration and color intensity/length was measured first. For intensity measurements, a background correction was applied to all samples. To enhance the sensitivity, rhodamine B (RB) was added to the AgNP solution, as this compound (as well as rhodamine 6G) can affect the plasmon and molecular resonances of AgNPs. 50,51 According to previous reports, RB attaches to the surface of AgNPs through carboxyl group and non-covalent interactions whereas rhodamine 6G attaches to the surface via non-covalent interaction.⁵² The AgNP surface modified with RB in Tri-HCl buffer shifted the absorption spectrum of the AgNPs because of the increased electrostatic repulsion between modified RB-AgNPs relative to AgNPs without RB. This phenomenon increased the change in color intensity upon addition of GSH. The effect of RB concentration on slope of GSH calibration was also measured. The maximum slope for a GSH calibration curve was found at 16 μ M of RB and 1000 mg L⁻¹ of AgNPs as shown in Fig. 2. Moreover, other anions in the aerosol sample or buffer including Cl⁻, SO₄²⁻ and NO₃⁻ did not significantly change the color intensity (data not shown). Thus, a final concentration of 16 μ M of RB and 1000 mg L⁻¹ of AgNPs was selected all further experiments using the conventional µPAD.

Analytical figures of merit

The intensity of the color product in the conventional μ PAD was proportional to the GSH concentration over the range of 0 to 2.5 nmol (intensity = 12.54GSH + 0.51, R^2 = 0.99) as shown in

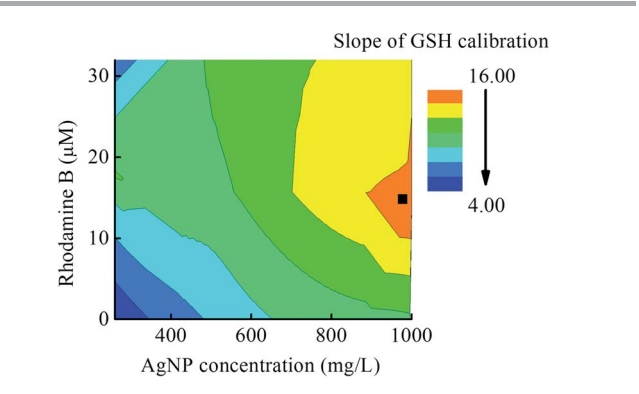
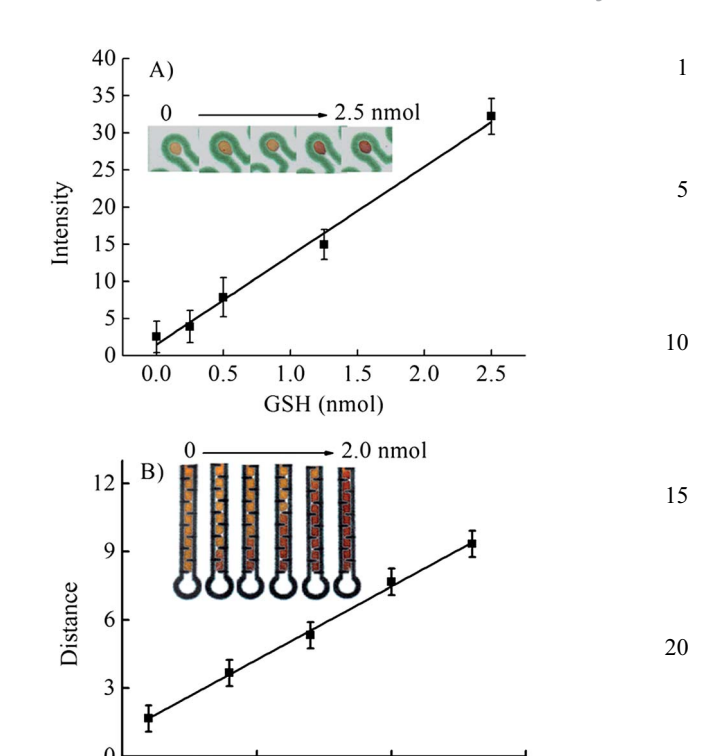


Fig. 2 Optimization of RB and AgNP concentrations on the two different types of μ PADs. The optimized condition represented by \blacksquare in this figure.



0.0

0.5

25

30

35

40

45

50

55

Fig. 3 (A) Calibration of GSH using the μ PADs. (B) Calibration of GSH using the distance-based μ PAD, n=3.

Log(nmol Glutathione)

-0.5

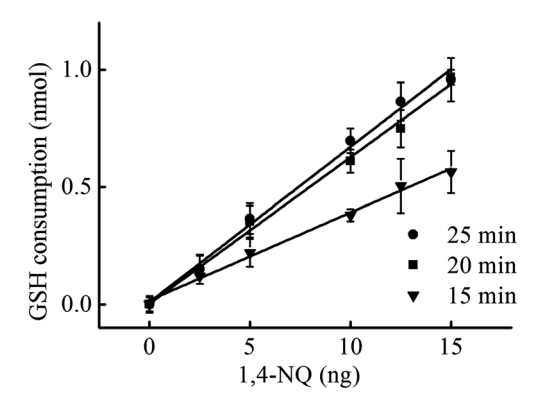
-1.0

Fig. 3A using the optimized conditions. The relative standard deviation (RSD, n=5) of GSH calibration slope was found to be 8.7%. Although this standard deviation is higher than commonly reported for the traditional absorbance method, it is in-line with other μ PADs. ^{53–55}

Aerosol oxidative activity was next measured using the distance-based μ PAD. With distance-based detection, no background correction was needed because a distinct color change can be seen visually. The detection channel was coated with only 1000 mg per L of AgNP. A plot of sample reaction length as a log function of the analyte concentration is shown in Fig. 3B. Reaction length was log-linear in the range of 0.12 to 2 nmol GSH (distance = 6.4 log GSH + 7.5, $R^2 = 0.99$) and the RSD of GSH calibration slope was 5.1% (n = 5). The improvement in reproducibility for the distance-based μ PAD relative to the traditional μ PAD is most likely the result of the improved ability to distinguish the end point of the distance-based detection relative to the intensity change of the traditional device.

Performance of aerosol oxidative activity measurement

The effect of reaction time on GSH consumption rate was studied using 1,4-NQ as a model oxidant in the range of 0 to 15 ng 1,4-NQ with 2.5 nmol of initial GSH. The sensitivity of the assay demonstrated a significant improvement with increasing reaction time from 15 min (slope = 0.037) to 20 min (slope = 0.062). No further improvement in slope was found at 25 min (slope = 0.066) as shown in Fig. 4. As a result, 20 min was



1

10

15

20

25

30

35

40

45

50

55

Fig. 4 Optimization of reaction time between GSH and 1,4-NQ at 2.5 nmol of the initial GSH, n=3.

selected as the optimal reaction time. The impact of starting GSH amount on detection limit and working range was measured next. The detection limit (Table 1) was estimated as the concentration that produced a signal at 3 times greater than the standard deviation of a blank (n = 10). The working range was taken as the linear range between the intensity or distance and 1,4-NO amount (Table 1). The lowest detection limit of 1,4-NQ was obtained at low starting GSH (0.5 nmol) but the largest working range was found at higher initial GSH. Meanwhile, the distance-based µPAD gave both the lowest detection limit and the widest working range at high initial GSH (1.25 nmol). Sensitivity is increased for high initial GSH concentrations because the length of the colored region is longer than at lower GSH concentrations. As a result, it was easier to distinguish changes in color at high initial GSH by the eye in the presence of smaller amounts of 1,4-NQ. These results show that the devices can be used for a variety range of aerosol oxidative reactivities in the field by tuning the initial amount of GSH on paper devices. For the low oxidative load of our samples, 0.5 nmol and 1.25 nmol of GSH were used to obtain the lowest detection limit for µPAD and distance-based detection, respectively.

Analytical applications

To validate the devices for aerosol oxidative activity determination with real samples, results for the traditional assay using either DTT or GSH with Elman's reagent were compared to the colorimetric and distanced-based $\mu PADs$. Five different samples of aerosol extracts (Fig. 5A) were analyzed using all four methods. The DTT consumption rate measured by the

Table 1 Linearity and LOD of 1,4-NQ in the presence of various initial GSH amount with 20 min of reaction time

Devices	GSH (nmol)	LOD of 1,4-NQ (ng)	Linearity of 1,4-NQ (ng)
μPADs	2.5	11.0	0-75
	1.25	6.5	0-35
	0.5	3.7	0-25
Distance-based μPAD	1.25, 0.5	10.0, 20.0	5-25, 15-30

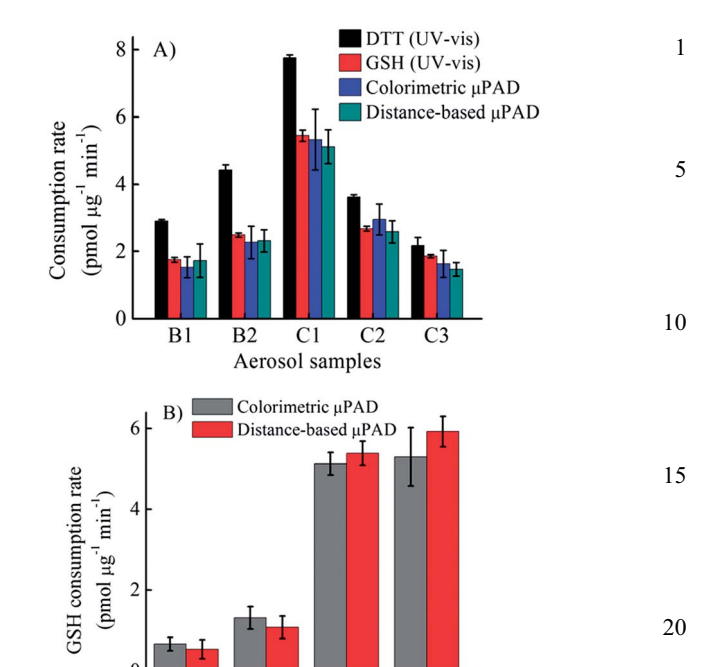


Fig. 5 Method validation using (A) an extracted sample and (B) a filter sample, n = 3.

Aerosol Samples

S1

S2

25

30

35

40

45

50

55

Fort Collins Restaurant

traditional assay in all five samples (black bar in Fig. 5A) was higher than the GSH consumption rate (red bar in Fig. 5A) according to the stronger reducing power of DTT relative to GSH. 56 The GSH consumption rate measured by all three methods (colorimetric and distance-based μPAD and traditional Elman's reagent assay) was compared using analysis of variance (ANOVA, single factor) and plotted for correlation. No significant difference between the three methods was obtained at the 95% confidence level (p-value=0.98). A good correlation between the traditional GSH assay and both μPAD devices was obtained with $R^2=0.98$ and 0.99 for μPAD and distance-based detection, respectively.

To further demonstrate the utility of our devices for real samples, four filter samples (S1 and S2, ambient aerosols around Fort Collins and in the restaurant) were analyzed using the µPAD methods. The results shown in Fig. 5B show a strong correlation between the traditional and distance-based µPAD methods ($R^2 = 0.99$); both devices could distinguish the high and low oxidative activity between cigarette smoke and ambient aerosols, respectively. Both µPAD devices can also be applied to filter samples collected in the field. The advantages of the traditional µPAD over distance-based µPAD include lower detection limit of 1,4-NQ and wider working range. However, the distance-based µPAD eliminates the need for an external scanner or camera. The analysis time of both our devices without any sample extraction was also less than 35 min, which marks a significant improvement over traditional spectroscopic assays (2 h).14

Paper Analyst

Conclusion

10

15

20

50

55

We demonstrate here the development of an AgNP colorimetric sensing method for aerosol oxidative activity using paper-based analytical devices. The determination of aerosol oxidative activity on paper devices was previously based on the use of Elman's reagent with DTT. Here, the reddish-brown color intensity and distance produced from the aggregation of AgNPs by GSH was used to estimate aerosol reactivity. The reddishbrown color intensity on µPAD provided a low detection limit for aerosol oxidative activity relative to previously reported methods. With distance-based detection, the length of reddishbrown color product can be readily discriminated by the naked eye. No significant differences for the aerosol oxidative activity measurement in filter samples between using our devices and the traditional GSH assay were observed. Both the distancebased detection and µPAD represent a highly sensitive, rapid and simple technique that should be applicable to personal exposure monitoring.

Acknowledgements

WD gratefully acknowledges the financial support from Chemistry department, Science Faculty, King Mongkut's University of Technology Thonburi and the Thailand Research Fund (MRG5580234). This work was supported by grants from the National Institute for Occupational Safety and Health (OH010050) and the National Institute of Environmental Health Sciences (ES019264).

References

- 35 1 A. K. Prahalad, J. Inmon, L. A. Dailey, M. C. Madden, A. J. Ghio and J. E. Gallagher, *Chem. Res. Toxicol.*, 2001, 14, 879–887.
 - 2 C. A. Pope, 3rd, D. V. Bates and M. E. Raizenne, *Environ. Health Perspect.*, 1995, **103**, 472–480.
- 40 3 Q. H. Sun, X. R. Hong and L. E. Wold, *Circulation*, 2010, **121**, 2755–2765.
 - 4 J. Crapo, F. J. Miller, B. Mossman, W. A. Pryor and J. P. Kiley, Am. Rev. Respir. Dis., 1992, 145, 1506–1512.
 - 5 A. Spira-Cohen, L. C. Chen, M. Kendall, R. Lall and G. D. Thurston, *Environ. Health Perspect.*, 2011, 119, 559–565.
 - 6 J. J. Sauvain, A. Setyan, P. Wild, P. Tacchini, G. Lagger, F. Storti, S. Deslarzes, M. Guillemin, M. J. Rossi and M. Riediker, J. Occup. Med. Toxicol., 2011, 6(18), 1–13.
 - 7 A. Boveris, E. Cadenas, R. Reiter, M. Filipkowski, Y. Nakase and B. Chance, *Proc. Natl. Acad. Sci. U. S. A.*, 1980, 77, 347–351.
 - 8 A. J. Ghio, Z. H. Meng, G. E. Hatch and D. L. Costa, *Inhalation Toxicol.*, 1997, **9**, 255–271.
 - 9 M. B. Kadiiska, R. P. Mason, K. L. Dreher, D. L. Costa and A. J. Ghio, *Chem. Res. Toxicol.*, 1997, 10, 1104–1108.
 - 10 F. Tietze, Anal. Biochem., 1969, 27, 502-522.
 - 11 G. G. Xiao, M. Y. Wang, N. Li, J. A. Loo and A. E. Nel, *J. Biol. Chem.*, 2003, **278**, 50781–50790.

- 12 J. Tamarit, E. Cabiscol and J. Ros, *J. Biol. Chem.*, 1998, 273, 3027–3032.
- 13 E. Shacter, J. A. Williams, M. Lim and R. L. Levine, *Free Radical Biol. Med.*, 1994, 17, 429–437.
- 14 H. Jung, B. Guo, C. Anastasio and I. M. Kennedy, *Atmos. Environ.*, 2006, **40**, 1043–1052.
- 15 E. Vidrio, C. H. Phuah, A. M. Dillner and C. Anastasio, *Environ. Sci. Technol.*, 2009, 43, 922–927.
- 16 Y. Sameenoi, K. Koehler, J. Shapiro, K. Boonsong, Y. Sun, J. Collett, J. Volckens and C. S. Henry, *J. Am. Chem. Soc.*, 2012, **134**, 10562–10568.

10

15

20

25

30

35

40

45

50

- 17 Q. Li, A. Wyatt and R. M. Kamens, *Atmos. Environ.*, 2009, 43, 1037–1042.
- 18 J. C. Jokerst, J. A. Adkins, B. Bisha, M. M. Mentele, L. D. Goodridge and C. S. Henry, *Anal. Chem.*, 2012, 84, 2900–2907.
- 19 M. M. Mentele, J. Cunningham, K. Koehler, J. Volckens and C. S. Henry, *Anal. Chem.*, 2012, **84**, 4474–4480.
- 20 W. Dungchai, O. Chailapakul and C. S. Henry, *Anal. Chem.*, 2009, **81**, 5821–5826.
- 21 A. W. Martinez, S. T. Phillips, B. J. Wiley, M. Gupta and G. M. Whitesides, *Lab Chip*, 2008, **8**, 2146–2150.
- 22 A. W. Martinez, S. T. Phillips, G. M. Whitesides and E. Carrilho, *Anal. Chem.*, 2010, **82**, 3–10.
- 23 C. M. Cheng, A. W. Martinez, J. L. Gong, C. R. Mace, S. T. Phillips, E. Carrilho, K. A. Mirica and G. M. Whitesides, *Angew. Chem., Int. Ed.*, 2010, **49**, 4771–4774.
- 24 X. X. Yang, O. Forouzan, T. P. Brown and S. S. Shevkoplyas, *Lab Chip*, 2012, **12**, 274–280.
- 25 Y. Sameenoi, P. Panymeesamer, N. Supalakorn, K. Koehler, O. Chailapakul, C. S. Henry and J. Volckens, *Environ. Sci. Technol.*, 2013, 47, 932–940.
- 26 M. Hepel and M. Stobiecka, *Fine Particles in Medicine and Pharmacy*, ed. E. Matijević, Springer, US, 2012, pp. 241–281.
- 27 I. I. S. Lim, W. Ip, E. Crew, P. N. Njoki, D. Mott, C.-J. Zhong, Y. Pan and S. Zhou, *Langmuir*, 2006, **23**, 826–833.
- 28 W. Leesutthiphonchai, W. Dungchai, W. Siangproh, N. Ngamrojnavanich and O. Chailapakul, *Talanta*, 2011, **85**, 870–876.
- 29 Z. P. Li, X. R. Duan, C. H. Liu and B. A. Du, *Anal. Biochem.*, 2006, **351**, 18–25.
- 30 X. Wei, L. Qi, J. Tan, R. Liu and F. Wang, *Anal. Chim. Acta*, 2010, **671**, 80–84.
- 31 Z. Chen, S. Luo, C. Liu and Q. Cai, *Anal. Bioanal. Chem.*, 2009, 395, 489–494.
- 32 R. J. Stokes, A. Macaskill, P. Johan Lundahl, W. Ewen Smith, K. Faulds and D. Graham, *Small*, 2007, 3, 1593–1601.
- 33 K. Shrivas and H. F. Wu, *Rapid Commun. Mass Spectrom.*, 2008, 22, 2863–2872.
- 34 H. Li, Z. Cui and C. Han, Sens. Actuators, B, 2009, 143, 87–92.
- 35 A. Apilux, W. Siangproh, N. Praphairaksit and O. Chailapakul, *Talanta*, 2012, **97**, 388–394.
- 36 N. Ratnarathorn, O. Chailapakul, C. S. Henry and W. Dungchai, *Talanta*, 2012, **99**, 552–557.
- 37 D. Scibior, M. Skrzycki, M. Podsiad and H. Czeczot, *Clin. Biochem.*, 2008, **41**, 852–858.

38 A. F. Banne, A. Amiri and R. W. Pero, *J. Anti-Aging Med.*, 2003, **6**, 327–334.

- 39 D. M. Cate, W. Dungchai, J. C. Cunningham, J. Volckens and C. S. Henry, *Lab Chip*, 2013, 13, 2397–2404.
- 40 W. Leesutthiphonchai, W. Dungchai, W. Siangproh, N. Ngamrojnavanich and O. Chailapakul, *Talanta*, 2011, **85**, 870–876.
 - 41 D. K. Bhui and A. Misra, Carbohydr. Polym., 2012, 89, 830-835.
 - 42 P. Sarkar, D. K. Bhui, H. Bar, G. P. Sahoo, S. Samanta, S. Pyne and A. Misra, *Nanoscale Res. Lett.*, 2010, 5, 1611–1618.

10

30

- 43 M. Stobiecka, K. Coopersmith and M. Hepel, *J. Colloid Interface Sci.*, 2010, **350**, 168–177.
- 44 E. Carrilho, A. W. Martinez and G. M. Whitesides, *Anal. Chem.*, 2009, **81**, 7091–7095.
- 45 Z. W. Zhong, Z. P. Wang and G. X. D. Huang, *Microsyst. Technol.*, 2012, 18, 649-659.
 - 46 A. Apilux, Y. Ukita, M. Chikae, O. Chailapakul and Y. Takamura, *Lab Chip*, 2013, 13, 126–135.
- 20 47 C. J. Hennigan, M. A. Miracolo, G. J. Engelhart, A. A. May, A. A. Presto, T. Lee, A. P. Sullivan, G. R. McMeeking, H. Coe, C. E. Wold, W. M. Hao, J. B. Gilman, W. C. Kuster,

J. de Gouw, B. A. Schichtel, J. L. Collett, S. M. Kreidenweis and A. L. Robinson, *Atmos. Chem. Phys.*, 2011, 11, 7669–7686.

1

5

10

15

20

55

- 48 J. Sedlak and R. H. Lindsay, *Anal. Biochem.*, 1968, **25**, 192–205.
- 49 H. B. Li, Z. M. Cui and C. P. Han, Sens. Actuators, B, 2009, 143, 87–92.
- 50 J. Zhao, L. Jensen, J. H. Sung, S. L. Zou, G. C. Schatz and R. P. Van Duyne, J. Am. Chem. Soc., 2007, 129, 7647–7656.
- 51 S. Kruszewski and M. Cyrankiewicz, *Acta Phys. Pol., A*, 2012, 121, A68–A74.
- 52 Z. M. Cui, C. P. Han and H. B. Li, *Analyst*, 2011, **136**, 1351–1356.
- 53 M. M. Mentele, J. Cunningham, K. Koehler, J. Volckens and C. S. Henry, *Anal. Chem.*, 2012, **84**, 4474–4480.
- 54 A. W. Martinez, S. T. Phillips, G. M. Whitesides and E. Carrilho, *Anal. Chem.*, 2010, **82**, 3–10.
- 55 A. W. Martinez, S. T. Phillips, M. J. Butte and G. M. Whitesides, *Angew. Chem., Int. Ed.*, 2007, 46, 1318–1320.
- 56 P. A. Johnston, K. M. Soares, S. N. Shinde, C. A. Foster, T. Y. Shun, H. K. Takyi, P. Wipf and J. S. Lazo, Assay Drug Dev. Technol., 2008, 6, 505–518.

25

30

35

40

45

50

FISEVIER

Contents lists available at SciVerse ScienceDirect

Talanta

journal homepage: www.elsevier.com/locate/talanta



Simple silver nanoparticle colorimetric sensing for copper by paper-based devices

Nalin Ratnarathorn ^a, Orawon Chailapakul ^b, Charles S. Henry ^c, Wijitar Dungchai ^{a,*}

- a Department of Chemistry, Faculty of Science, King Mongkut's University of Technology Thonburi, Prachautid Road, Thungkru, Bangkok, 10140, Thailand
- b Center of Excellence for Petroleum, Petrochemicals, and Advanced Materials, Chulalongkorn University, Patumwan, Bangkok, 10330, Thailand
- ^c Department of Chemistry, Colorado State University, Fort Collins, Colorado 80523-1872, USA

ARTICLE INFO

Article history: Received 20 April 2012 Received in revised form 14 June 2012 Accepted 15 June 2012 Available online 20 June 2012

Keywords: Silver nanoparticle Colorimetric sensing Paper-based devices Copper

ABSTRACT

The first investigation of silver nanoparticle (AgNP) colorimetric sensing of Cu2+ by paper-based analytical devices (PADs) is reported here. AgNP colorimetric sensing for the detection of Cu²⁺ was first characterized by UV-visible spectroscopy. The -SH groups on homocysteine (Hcy) and dithiothreitol (DTT) were used to modify the AgNP surface whereas the -COOH and -NH2 functional groups have strong affinity to Cu²⁺ relative to other ions in solution. The plasmon resonance absorption peak intensity at 404 nm decreased and a new red-shifted band at 502 nm occurred in the presence of Cu²⁺. Paper devices coated with the modified AgNP solution changed from yellow to orange and green-brown color after the addition of Cu²⁺ due to nanoparticle aggregation. The color intensity change as a function of Cu^{2+} concentration gave a linear response in the range of 7.8-62.8 μ M (R^2 =0.992). The limit of naked-eye detection is 7.8 nM or 0.5 $\mu g L^{-1}$. A color change observed by the naked eye with the addition of Cu^{2+} can be clearly differentiated from the other metals (As³⁺, Cd²⁺, Co²⁺, Hg²⁺, Ni²⁺, Pb^{2+} , Zn^{2+} , Mg^{2+} , Mn^{2+} , Ca^{2+} , Fe^{3+} , Na^+ , and K^+) at 15.7 μ M. The use of different flow directions in the PADs and μ PADs for Cu^{2+} detection was also demonstrated. Levels of Cu^{2+} in real water samples were measured using the paper devices to be $2.9 \pm 0.24 \, \mu M$ (tap water) and $3.2 \pm 0.30 \, \mu M$ (pond water), respectively, and were within error of the values measured using an atomic absorption spectrometer ($2.8 \pm 0.08 \,\mu\text{M}$ in tap water, and $3.4 \pm 0.04 \,\mu\text{M}$ in pond water). Thus, this work shows the successful integration of paper devices and AgNP colorimetric sensing as a simple, rapid, easy-touse, inexpensive and portable alternative point-of-measurement monitoring.

© 2012 Elsevier B.V. All rights reserved.

1. Introduction

The development of simple, rapid, and inexpensive detection method for diagnostics and environmental monitoring is still needed in developing and undeveloped countries for sustainable development in public health [1]. Currently, paper devices including paper strip tests, paper-based assays, and paper-based microfluidics are attractive for portable point-of-measurement (POM) monitoring and on-site detection due to advantages which include low cost, portability, ease of use, high speed, and low reagent and sample consumption [2–4]. Furthermore, paper provides a high surface area/high optical contrast substrate for colorimetric detection. Paper devices are also suited for use by nontechnical personnel. Finally, paper devices are made from naturally abundant, biodegradable and inexpensive materials (i.e.,

cellulose) [5,6]. Most commercial paper devices use colorimetric detection and have been applied for qualitative and/or semi-quantitative analyte detection [1,7–11]. For colorimetric sensing, analyte flow is directed along the paper matrix by capillary action, and analyte then reacts with a label or organic dye in the test zone. The assay results are quantified by comparing the color hues and/or intensities generated by unknown analytes to known analyte concentrations. Nontechnical personnel can interpret the result by the naked eye in many cases. Paper devices therefore do not require external instrumentation for interpretation or mechanical forces to drive flow.

Gold nanoparticle (AuNP) colorimetric probes have been widely used for colorimetric assays because their extinction coefficients are high relative to common organic dyes [12–17]. AuNP colorimetric sensing has been used with two approaches. First, the result can be determined by the accumulation of an intense red color that is associated with the color of AuNPs with a diameter of 10–50 nm. The most common example of this detection mode is the commercial immunochromatographic test strip [18,19]. Alternatively, the color change of AuNPs due to aggregation or

^{*} Corresponding author. Tel.: +66 2 470 9553; fax: +66 2 470 8840. *E-mail addresses*: wijitar.dun@kmutt.ac.th, wijitar_29@hotmail.com (W. Dungchai).

dispersion with the addition of analyte can be used [20,21]. For example, Lu and coworker first reported the AuNP aggregation in a dipstick assay [22]. Their devices detect analyte by immersing a lateral flow device immobilized with aggregated AuNPs into a testing solution. The blue aggregated AuNPs turned red when dispersed by the analyte in a concentration dependent manner. Inspired by Lu's work, Zhao and coworkers demonstrated the feasibility of using a AuNP-based colorimetric sensing platform on paper devices [23].

Recently, silver nanoparticles (AgNPs) have been used as an alternative colorimetric sensing system due to lower cost and higher extinction coefficients than AuNPs [24]. The high molar extinction coefficient of AgNPs leads to improved visibility based on the difference in optical brightness and increased sensitivity of UV-visible spectroscopic detection [25]. Although colorimetric applications of AgNP aggregation provide high sensitivity and selectivity for the determination of analytes such as histidine [26], homocysteine [25], cysteine [27], mercury ions [28,29], and nickel ions [30] using UV-visible spectroscopy, AgNP colorimetric sensing for copper ion by PADs has not been reported [31]. The only analytical application of AgNPs on cellulose paper that has been reported is for the determination of Rhodamine 6 G dye using Raman Spectroscopy [32]. Therefore, the aim of this study was to investigate AgNP colorimetric sensing for PADs. The utility of AgNP aggregation on paper devices was demonstrated for the detection of copper (II) ions. Copper ions play an important role in living organisms and industry but excess intake of copper ions can be toxic [33]. High copper levels in blood and liver are implicated in Alzheimer's disease and inflammatory disorders. Moreover, excessive copper in children is associated with hyperactive behavior, learning disorders such as dyslexia, and ear infections. The World Health Organization (WHO) prescribes the maximum allowable levels of copper (II) ions in drinking water at 1.3 mg L^{-1} or 20.5 μ M [34]. In this work, homocysteine and dithiothreitol bind to AgNPs (~10 nm in diameter presenting yellow color) through Ag-S bonds, and then binding between Cu²⁺ and the surface-modified AgNPs results in their aggregation (Fig. 1A). The aggregation of AgNPs in the presence of copper (II) ions leads to a decrease in the surface plasmon resonance absorption peak and the formation of a new red-shifted peak. Both paper-based assay devices and paper-based microfluidic devices for Cu²⁺ detection using AgNP colorimetric sensor were studied. After the addition of Cu²⁺ solution into paper devices, the yellow color of AgNPs changed to orange or green-brown depending on the Cu²⁺ concentration. Finally, our devices were successfully applied to the detection of Cu²⁺ in real water samples.

2. Experimental

2.1. Chemicals and Materials

All chemicals used in experiment were analytical reagent (AR) grade and solutions were prepared using high pure water with a resistance of $18~M\Omega~cm^{-1}$. Homocysteine (Hcy), dithiothreitol (DTT), cysteine (Cys), glutathione (Glu) and metal ions (As 3 +, Ca 2 + Cd 2 +, Co 2 +, Cu 2 +, Fe 3 +, Hg 2 +, K+,Mg 2 +, Mn 2 +, Na $^+$, Ni 2 +, Pb 2 + and Zn 2 +) were bought from Sigma-Aldrich (St. Louis, Missouri). AgNP solution was obtained from Sensor Research Unit at Department of Chemistry, Chulalongkorn University, Thailand. Whatman No.1 filter paper was bought from Cole-Parmer (Vernon Hills, IL). All glassware was thoroughly cleaned with freshly prepared 1:1 HCl/HNO $_3$ and rinsed with Mill-Q 18 M Ω cm $^{-1}$ water prior to use. All metal ion stock solutions were prepared in 0.1 M HNO $_3$. Working standard solutions of metal ions were

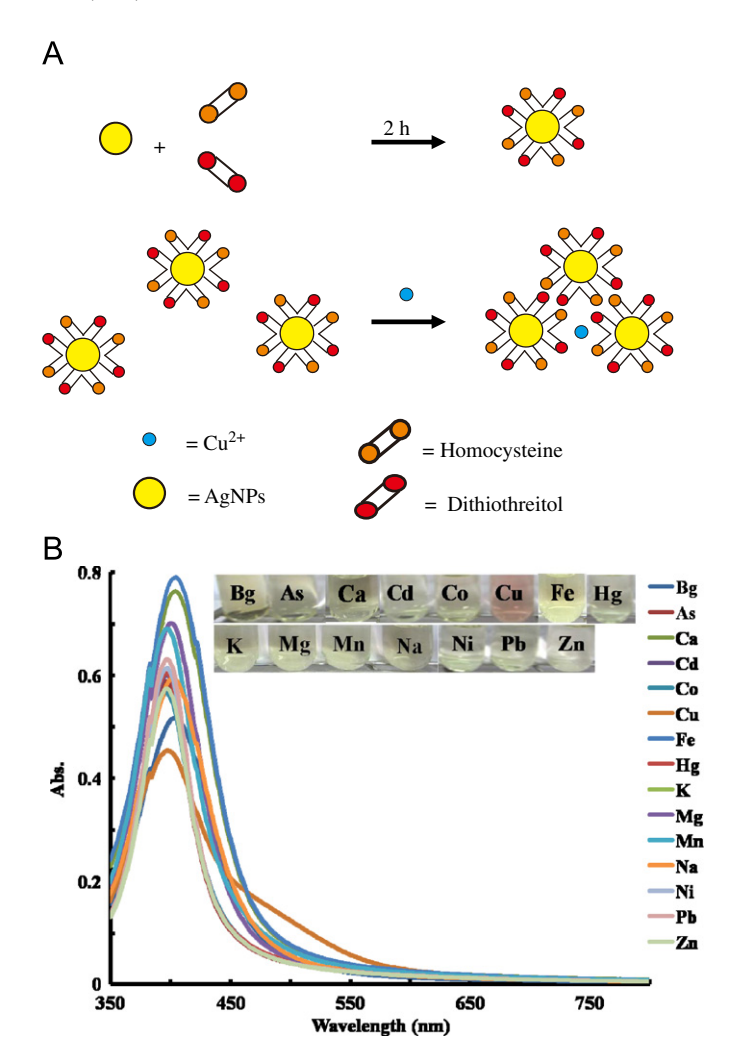


Fig. 1. (A) Schematic of aggregating process of AgNPs induced by adding Cu^{2+} and (B) UV–visible spectra and photos of Hcy-DTT-AgNPs with metal ions (7.8 nM of Cu^{2+} and 1.6 μ M of other metals).

prepared daily by appropriate dilution of 157 μM stock solutions with 0.1 M phosphate buffer pH 8.0.

2.2. Instrumentation

UV-visible absorption spectra were recorded by a UV-visible spectrometer (Lambda 35, Perkin Elmer Instruments, USA) using quartz cuvettes (1-cm pathlength). Photographic results were recorded using a digital camera (PowerShot S95, 10.1 Megapixels, Canon). An atomic absorption spectrometer (AAS) with a hollow cathode lamp and standard air/acetylene flame (Analyst 300, Perkin Elmer Instruments, USA) was used for atomic absorbance measurements. A hollow cathode lamp was used under the following operations conditions: wavelength: 324.8 nm; slitwidth: 0.70 nm; lamp current: 25 mA.

2.3. Synthesis of the modified AgNPs

AgNPs were synthesized using our previously reported methods using the chemical reduction process [25]. Sodium borohydride and methyl cellulose solution were used as the reducing agent and stabilizer, respectively. The shapes and particle size distributions of the AgNPs with nominal mean diameters of 10 nm were measured using TEM.

The Hcy-DTT-AgNP solution was prepared using self-assembly of the aminothiol on the AgNP surface. A yellow 0.1 mM AgNP

solution ($\sim\!10$ nm in diameter) was first prepared from the dilution of 10 mM AgNPs stock solution with 18 M Ω cm $^{-1}$ water. Then, 7 μ M of 0.30 mM Hcy and 6 μ L of 0.30 mM DTT were added into 6 mL of 0.1 mM AgNP solution to generate final concentrations of 3.5 μ M Hcy and 3.0 μ M DTT. Aminothiol compounds were self-assembled onto the surface of AgNPs by incubating the AgNPs with the aminothiol solutions for 2 h at room temperature. After this step, the AgNP aggregation was characterized using UV-visible spectrometry. 1.00 mL of modified AgNP solution was mixed with 1.00 mL of metal ion in 50 mM phosphate buffer at pH 8 (Na₂HPO₄ and NaH₂PO₄). Before analysis by the spectrometer, the mixture was incubated for 30 min at the room temperature.

2.4. Preparation of the paper devices

Whatman filter paper 1 was patterned using a cutting tool according to previously reported methods [35]. The pattern was created in CorelDraw and then transferred to the Silhouette Studio program that operated the cutter. Cutting printers (Silhouette America, Inc.) incorporate a knife in place of the traditional ink pen. The knife rotated freely on a turret, enabling precise cutting of various features, including small-radius corners, small channel or holes with 100 μm resolution. The instrument setup and actual cutting required $\sim\!60\,s$ and $\sim\!20\,s$ per device, respectively.

2.5. Detection of copper on the paper devices

Paper-based assay devices (PADs, holes shape with 4 mm in diameter) were modified with 0.5 μL of Hcy-DTT-AgNP solution in the test zone and allowed to dry before use. PADs were differentiated from μ PADs by the lack of a flow channel in PADs. 0.5 μL of metal ion solutions (As³+, Ca²+, Cd²+, Co²+, Cu²+, Fe³+, Hg²+, K+, Mg²+, Mn²+, Na²+, Ni²+, Pb²+ and Zn²+) were then added to the paper devices.

Paper-based microfluidic devices (μ PADs) were also prepared for Cu²⁺ detection. The test zone of μ PADs was spotted with 0.2 μ L of Hcy-DTT-AgNP solution (Figs. 5A and B) and allowed dry. For detection, 12 μ L of 15.7 μ M Cu²⁺ solution was dropped into the loading zone. An alternative pattern of μ PADs is shown in Fig. 5C. In this pattern, 0.2 μ L of Cu²⁺ solution at 7.8 nM, 780 nM, 7.8, 15.7, 31.4, 62.8 μ M, and buffer solution was dropped into test zone number 2, 3, 4, 5, 6, 7, and 8, respectively. For detection, 12 μ L of the modified AgNP solution was added to the loading zone.

2.6. Applications

To evaluate the utility of our proposed method, the Cu²⁺ in tap and pond water was quantified. Tap water samples were obtained from the chemistry building, Faculty of Science, King Mongkut's University of Technology Thonburi, Bangkok, Thailand. Pond water samples were obtained from a pond in front of King Mongkut's University of Technology Thonburi, Bangkok, Thailand. Our method was validated against AAS. Prior to analysis, preconcentration was carried out on all samples. 15 mL of sample was mixed with 10 mL of 0.1 M HNO3 and then heated to evaporate excess water until 2.5 mL of samples remained. For AAS, samples were adjusted to a final volume of 5 mL with deionized water. For our proposed method, 50 mM phosphate buffer pH 8 was added to the sample to generate a final volume of 4 mL. The samples were then adjusted to pH 8 by the addition of 3 M sodium hydroxide and then water added to reach a final volume of 5 mL and thus a 3-fold higher concentration than the original sample.

3. Results and discussion

3.1. Characterization of AgNP aggregation

We initially investigated the AgNP aggregation by UV-visible spectrometer (Fig. 1A). As is well known, -SH group in aminothiol compounds such as Hcy, DTT, Cys, and Glu can modify the AgNP surface whereas the other functional groups have a strong affinity for metal ions [30]. In this work, four aminothiol compounds. including Hcv. DTT. Cvs. and Glu. were studied. After the addition of 7.8 nM Cu²⁺ solution to the modified AgNPs solution, the solution color changed from vellow to orange color only in the mixture of Hcv. DTT and AgNPs as shown in Fig. S1. We also found a decrease in the plasmon resonance absorption peak at 404 nm and the formation of a new red-shifted band at 502 nm (Fig. 1B) suggesting that the mixture of Hcy and DTT can induce the aggregation of AgNPs in the presence of Cu²⁺. It has been reported Cu²⁺ is an excellent catalysts for Hcy oxidation [36]. After the redox reaction between the Hcy and Cu²⁺, Cu⁺ remained in the solution. Cu²⁺ behaved differently than other metals because of the higher stability constant between DTT and Cu^{+} relative to other metals (log $K=6.9 (Zn^{2+}), 9.7 (Pb^{2+}), 10.8$ (Cd^{2+}) , 6.5 (Ni^{2+}) and 11.1 (Cu^{+})) [37]. Another possible mechanism for AgNP aggregation in the two thiols system is that the number of carbon bond (C-C) on Hcy and DTT molecule are the same. After AgNP surface was modified with the mixture of Hcv and DTT, the distance between nanoparticles at the Hcv active site is similar to the DTT active site. Therefore, the remaining Cu2+ and Cu+ can simultaneously bind with COOHof Hcy and SH- of DTT on the Hcy-DTT-AgNPs surface. The selectivity of this method was evaluated by adding metal ions at 200 times the Cu^{2+} concentration (1.6 μ M of As^{3+} , Ca^{2+} , Cd^{2+} , Co^{2+} , Fe^{3+} , Hg^{2+} , K^+ , Mg^{2+} , Mn^{2+} , Na^+ , Ni^{2+} , Pb^{2+} and Zn^{2+}) into the AgNP solution. An increase in the absorbance ratio (502 nm/404 nm) was clearly observed in the presence of Cu^{2+} , whereas no change was measured in the presence of other metals (Fig. 1B). Next, the parameters affecting the sensitivity and selectivity of Cu²⁺ detection were optimized. The concentration of Hcy and DTT, pH of phosphate buffer and incubation time were studied prior to application on paper devices. The best absorbance ratio was obtained at 50 mM phosphate buffer at pH 8, 3.5 µM of Hcy, 3.0 µM of DTT, and 30 min incubation time of the modified AgNPs and Cu²⁺. Using the optimal conditions, the UV-Vis spectra of AgNPs with different concentrations of Cu²⁺ were investigated (Fig. 2). We expected that AgNPs could be used to quantitatively determine Cu²⁺ levels by monitoring the increase of the absorbance ratio at 502 nm/404 nm. The 502/404 absorbance ratio increased as a function of the Cu²⁺ concentration in the range of 3.2-14.2 nM. Then, the absorbance ratio stopped increasing up to 780 nM of Cu²⁺ and then decreased in the range of 780 nM -7.8μ M. The plot of absorbance ratio as a function of Cu²⁺ concentration was found to be linear within both the range of 3.2–14.2 nM (R^2 =0.997) and 780 nM–3.9 μ M (R^2 =0.998).

3.2. Detection of copper on the paper devices

Colorimetric sensing in paper devices generally uses a higher organic indicator or nanoparticle concentration than is used in solution phase because of the low visibility of colors such as yellow and orange the paper surface. To improve visibility on paper, we investigated the concentration of AgNPs, Hcy, and DTT for nanoparticle aggregation in PADs. It was found that the 0.1 mM of AgNPs solution containing 3.5 μ M Hcy and 3.0 μ M DTT which provided the optimal solution detection conditions showed no significant response in the presence and absence of Cu²+ on the PADs by the naked eye. We therefore optimized the

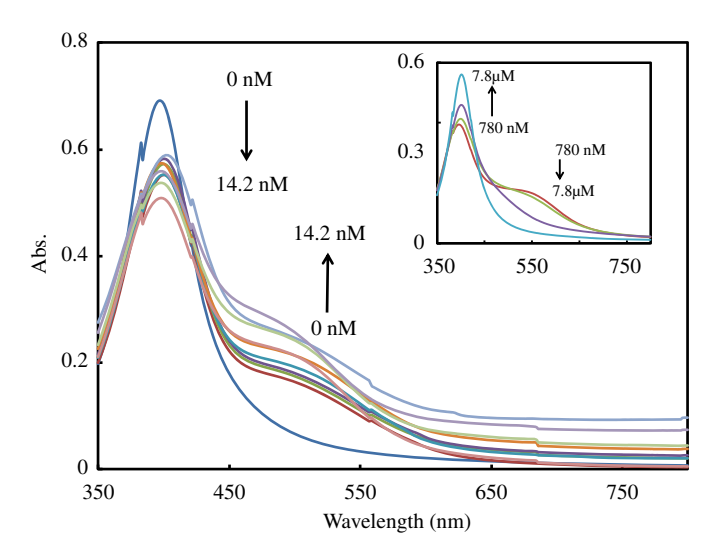


Fig. 2. UV–visible spectra of Hcy–DTT–AgNP solutions with various concentrations of Cu^{2+} in the range from 0 to 14.2 nM μ g L^{-1} increasing in steps of 1.6 nM. The insert figure is various concentrations of Cu^{2+} in the range from 780 nM to 7.8 μ M (780 nM, 1.6, 3.9, and 7.8 μ M).

AgNP concentration in the range of 0.1-20 mM containing 7.0 μM Hcy and 6.0 µM DTT. 0.5 µL of 10 mM AgNP solution was spotted into the paper surface, followed by 0.5 μ L of 7.0 μ M Hcy and 6 μ M DTT. An orange or green-brown color that was distant from the control experiment was observed after adding Cu2+ solution to the Hcy-DTT-AgNP coated paper surface, depending on Cu²⁺ concentration. A low AgNP concentration (0.1 mM) gave a light yellow color on paper devices while concentrations higher than 15 mM of AgNP concentration gave a dark vellow that made color discrimination by naked eve difficult (data not shown). As a result, we selected 10 mM of AgNP to use in the optimization of aminothiol concentration for PADs. The optimal Hcy and DTT concentration for PADs were studied next. 7.0 μ M Hcy and 6 μ M DTT gave the highest difference between the intensity of buffer solution and 15.7 μ M Cu²⁺, thus 7.0 μ M Hcy and 6 μ M DTT were chosen for the AgNP modification on PADs (Fig. S2). The optimal aminothiol concentration used in solution differed for PADs because the aggregation reactions occur in the different media surrounding. The surrounding media has a direct effect on the refractive index and the interparticles distance [24]. We also studied the linearity of color intensity with the increasing of Cu²⁺ concentration. PADs exhibited color changes as a function of Cu²⁺ concentration. Concentrations between 7.8 nM and 3.9 µM gave an orange color, while concentrations between 15.7 and 62.8 μM gave a green-brown color as shown in Fig. 3. The detection limit by the naked eye was found to be 7.8 nM or $0.5 \,\mu g \, L^{-1}$. The green-brown color intensity as a function of the concentration of Cu²⁺ was also measured using Adobe Photoshop CS2 in gray mode. A linear calibration curve between intensity and Cu²⁺ concentration was obtained in the range of 7.8-62.8 µM $(R^2=0.992)$. The World Health Organization (WHO) defines the maximum allowable levels of Cu²⁺ in drinking water at 1.3 mg L^{-1} or 20.5 μ M. These results clearly show the ability to visually discriminate between the maximum allowable Cu²⁺ levels and the normal level using the modified AgNPs. Our device should therefore be useful for determining Cu2+ in drinking water. Although the limit of naked-eye detection in paper devices $(0.5 \,\mu g \,L^{-1} \text{ or } 7.8 \,n\text{M})$ was higher than the previous UV-visible spectra reports (1 nM), [38] it is lower than commercial copper test strips [39,40]. Hence, our paper devices are an attractive, low cost and portable point-of-measurement (POM).

The selectivity of Cu^{2+} detection on the paper devices was then investigated at the optimal reagent concentrations (10 mM

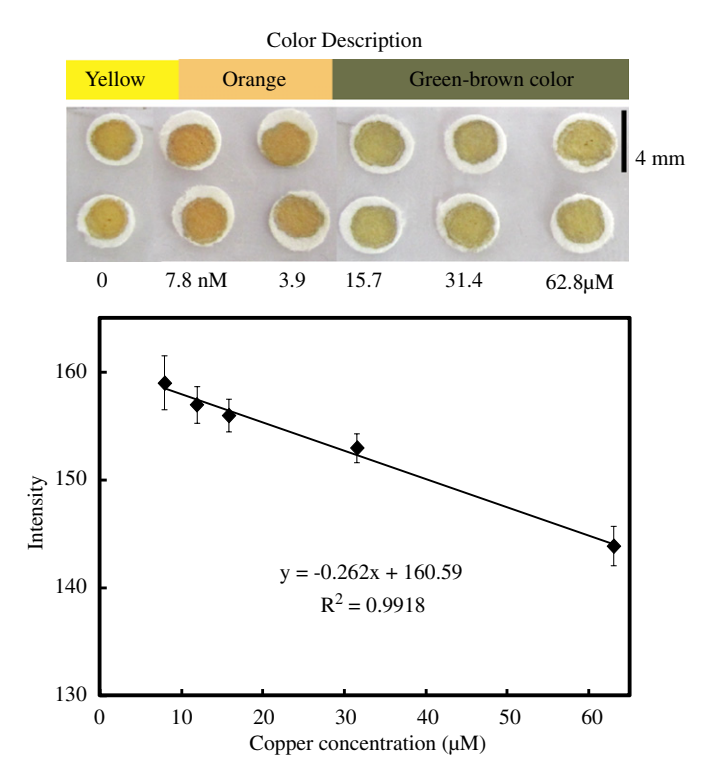


Fig. 3. Paper devices for the quantitative analysis of Cu^{2+} and the calibration plot of color intensity and the concentrations of Cu^{2+} (error bar represented the standard deviation at n=3). We converted one photographed digital image including all copper concentration to gray mode and selected the appropriate test zone for the device. The mean pixel values within the test zones correlate with the concentration of copper. Conditions: 10 mM of AgNP solution modified with 7.0 μ M Hcy and 6.0 μ M DTT. (For interpretation of the references to color in this figure legend, the reader is referred to the web version of this article.)

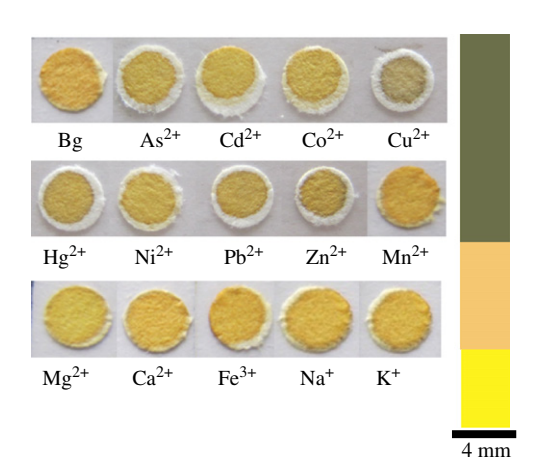


Fig. 4. Study of selectivity of the semi-quantitative analysis of Cu^{2+} toward different heavy-metal ions at 15.7 μM on paper devices. Other experimental conditions are the same as in Fig. 3. (For interpretation of the references to color in this figure legend, the reader is referred to the web version of this article.)

of AgNP modified with 7.0 μ M Hcy, and 6.0 μ M DTT). We evaluated selectivity by adding 0.5 μ L each of 15.7 μ M Cu²⁺ and metal ions onto paper devices coated with 0.5 μ L of AgNPs. Hcy-DTT-AgNPs on the paper surfaces immediately changed colors with the addition of Cu²⁺ whereas other metal ions did not change the color (Fig. 4). Moreover, the analysis time using paper devices is only 5 min, which is 25 min faster than using UV-Vis or AAS.

Hcy-DTT modified AgNPs were next used with μ PADs using the design shown in Fig. 5. The analyte solution flow direction in

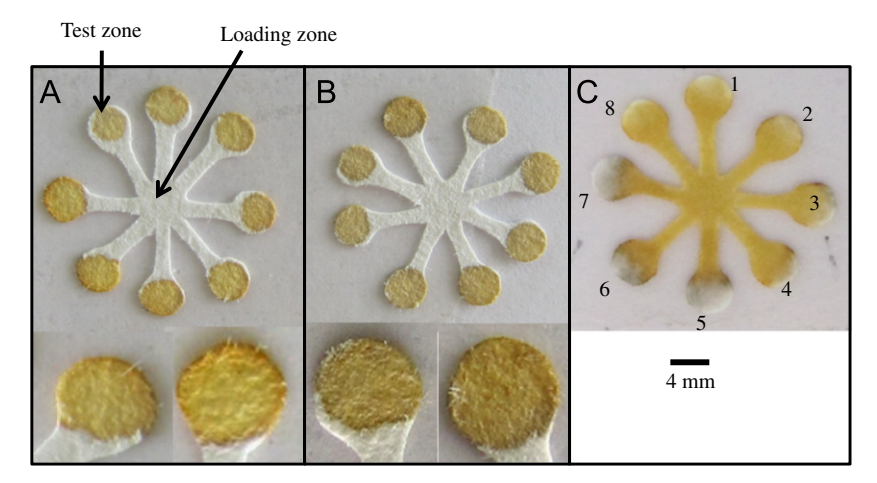


Fig. 5. μ PAD for the semi-quantitative analysis of Cu²⁺ after spotting AgNPs modified with Hcy and DTT into the test zone and then (A) dropping buffer solution and (B) 15.7 μ M of Cu²⁺ solution into the loading zone. (C) μ PAD for the semi-quantitative analysis of Cu²⁺ after spotting (8) 0 (2) 7.8 nM (3) 780 nM (4) 7.8 μ M (6) 31.4 μ M (7) 62.8 μ M of Cu²⁺ solution and then dropping AgNPs modified with Hcy and DTT into loading zone. Other experimental conditions are the same as in Fig. 3. (For interpretation of the references to color in this figure legend, the reader is referred to the web version of this article.)

our PADs is the vertical with AgNP coated on paper surface whereas flow on $\mu PADs$ is horizontal. More detailed information on the direction flow can be found in Fig. S3. Figs. 5A and B show the yellow color formed from buffer and the green-brown color formed from 15.7 μ M Cu²⁺, respectively. The results indicate that the nanoparticle aggregation reaction generated by the vertical flow of analyte solution (Fig. 3) was similar to the horizontal flow (Figs. 5A and B). However, the horizontal flow of modified AgNP solution to the test zone coated with Cu²⁺ (Fig. 5C) gave a different result from the horizontal flow of Cu²⁺ solution reacted with modified AgNPs at test zone (Fig. 5B). The results of the horizontal flow of modified AgNP solution into µPADs are shown in Fig. 5C. The brown-black color generated at 15.7-62.8 µM of Cu²⁺ while Cu²⁺ concentration at less than 15.7 μM did not give an orange color. The modified AgNP initially aggregated at the beginning of the test zone, blocking the horizontal flow of modified AgNP to the end of the test zone so the brown-black color in Fig. 5C obtained instead of green-brown color. Although the flow direction of AgNPs on paper devices affects the sensitivity of AgNP colorimetric sensing, the concept of our method is easy-to-use, versatile, rapid, and suitable for point of care monitoring.

3.3. Applications

To evaluate the potential application of AgNP colorimetric sensor in paper devices, the proposed method was applied for the detection of Cu^{2+} in the real water samples. Pond and tap water samples were analyzed by our devices and AAS. Levels of Cu^{2+} in tap water samples were measured using the paper devices and AAS to be 2.9 ± 0.24 and 2.8 ± 0.08 $\mu\mathrm{M}$, respectively ($n{=}3$). Meanwhile, amount of Cu^{2+} in pond water samples were measured using the paper devices and AAS to be 3.2 ± 0.30 , and 3.4 ± 0.04 $\mu\mathrm{M}$, respectively ($n{=}3$). The paired t-test was used to validate our method versus the AAS method. The levels obtained using our approach were in good agreement with those from AAS, falling within the 95% confidence level. Thus, the analyzed values of Cu^{2+} in pond and tap water sample by our approach can be accepted.

3.4. Lifetime of the devices

For practical use in developing countries, devices must remain stable for weeks. Therefore, we studied the stability of devices after

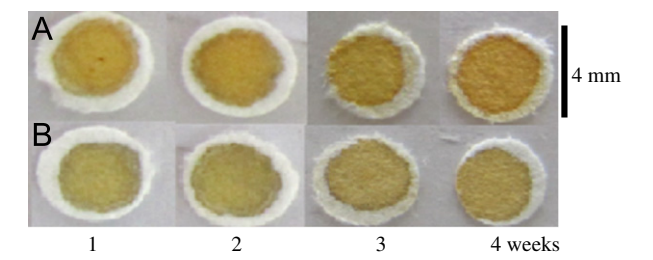


Fig. 6. Lifetime of the paper devices in the addition of (A) 0 and (B) 15.7 μ M of Cu²⁺. Other experimental conditions are the same as in Fig. 3.

storing the prepared paper devices for 4 weeks. The modified AgNPs coated on paper devices were dried at ambient condition before storage at room temperature ($\sim\!25\,^{\circ}\text{C}$). The results were measured by the naked eye and using a digital camera. An observable signal for 15.7 μM Cu $^{2+}$ solution dropped on the prepared paper over a period of 4 weeks (intensity in gray mode=152.32 \pm 5.68) generated no significant difference from the freshly prepared paper devices (intensity in gray mode=157.47 \pm 7.36) as shown in Fig. 6. Hence, the devices can be kept for 4 weeks without loss of activity but longer storage requires refrigeration.

4. Conclusions

This paper demonstrates for the first time the use of AgNP for colorimetric sensing of Cu²⁺ in paper devices to provide rapid, easy to use, inexpensive, and portable devices for point-of-care monitoring. The sensor is based on the aggregation of AgNPs on a paper substrate by the strong affinity between modified AgNPs and Cu²⁺, which leads to a shift in the absorption spectrum. Furthermore, the color change of AgNPs on paper substrate can be observable by the naked eye due to the extremely high extinction coefficient of AgNPs. Cu2+ was clearly distinguishable color change from the other heavy metal ions under the optimum conditions at the critical level of Cu2+ in drinking water prescribed by WHO. Finally, our paper devices were successfully applied to the semi-quantitative analysis of Cu²⁺ in water samples. Both paper-based assay devices and paper-based microfluidic devices would be potentially modified with AgNPs for the detection of a variety of other targets.

Acknowledgments

Wijitar Dungchai gratefully acknowledges the financial support from Science Faculty, King Mongkut's University of Technology Thonburi and the Thailand Research Fund. C. Henry acknowledges support of a grant from the National Institutes of Health, National Institute for Occupational Safety and Health grant number R210H010050. We would also like to thank Assoc. Prof. Dr. Sanong Ekgasit, Sensor Research Unit at the Department of Chemistry, Chulalongkorn University, for the synthesis of AgNPs.

Appendix A. Supporting information

Supplementary data associated with this article can be found in the online version at http://dx.doi.org/10.1016/j.talanta.2012. 06.033.

References

- [1] A.W. Martinez, S.T. Phillips, E. Carrilho, S.W. Thomas, H. Sindi, G.M. Whitesides, Anal. Chem. 80 (2008) 3699-3707.
- [2] W. Zhao, A.V.D. Berg, Lab Chip. 8 (2008) 1988-1991.
- [3] S.K. Sia, L.I. Kricka, Lab Chip, 8 (2008) 1982-1983.
- [4] A.W. Martinez, S.T. Phillips, M.J. Butte, G.M. Whitesides, Angew. Chem. Int. Ed. 46 (2007) 1318-1320.
- [5] P. Kauffman, E. Fu, B. Lutz, P. Yager, Lab Chip 10 (2010) 2614-2617.
- [6] E. Fu, T. Liang, J. Houghtaling, S. Ramachandran, S.A. Ramsey, B. Lutz, P. Yager, Anal. Chem. 83 (2011) 7941–7946.
- [7] X. Li, J. Tian, T. Nguyen, W. Shen, Anal. Chem. 80 (2008) 9131–9134. [8] A. Apilux, W. Dungchai, W. Siangproh, N. Praphairaksit, C.S. Henry, O. Chailapakul, Anal. Chem. 82 (2010) 1727-1732.
- [9] W. Dungchai, O. Chailapakul, C.S. Henry, Anal. Chem. 81 (2009) 5821-5826.
- [10] Z. Nie, C.A. Nijhuis, J. Gong, X. Chen, A. Kumachev, A.W. Martinez, M. Narovlyansky, G.M. Whitesides, Lab Chip 10 (2010) 477–483.
- [11] W. Dungchai, O. Chailapakul, C.S. Henry, Anal. Chim. Acta. 674 (2010) 227-233
- [12] F.Q. Zhang, L.Y. Zeng, Y.X. Zhang, H.Y. Wang, A.G. Wu, Nanoscale 3 (2011) 2150-2154.

- [13] Y. Xue, H. Zhao, Z.J. Wu, X.J. Li, Y.J. He, Z.B. Yuan, Analyst 136 (2011)
- [14] J. Zhang, Y. Wang, X.W. Xu, X.R. Yang, Analyst 136 (2011) 3865-3868
- [15] M.H. Kim, S. Kim, H.H. Jang, S. Yi, S.H. Seo, M.S. Han, Tetra. Lett. 51 (2010) 4712-4716.
- [16] S. Kim, I.W. Park, D. Kim, D. Kim, I.H. Lee, S. Jon, Angew, Chem, Int. Ed. 48 (2009) 4138-4141
- [17] J.R. Kalluri, T. Arbneshi, S.A. Khan, A. Neely, P. Candice, B. Varisli, M. Washington, S. McAfee, B. Robinson, S. Banerjee, A.K. Singh, D. Senapati, P.C. Ray, Angew. Chem. Int. Ed. 48 (2009) 9668-9671.
- [18] H.L. Xie, W. Ma, L.Q. Liu, W. Chen, C.F. Peng, C.L. Xu, L.B. Wang, Anal. Chim. Acta. 634 (2009) 129-133.
- [19] X.L. Wang, K. Li, D.S. Shi, X. Jin, N. Xiong, F.H. Peng, D.P. Peng, D.R. Bi, J. Chromatogr. B. 847 (2007) 289-295.
- [20] T.T. Lou, Z.P. Chen, Y.Q. Wang, L.X. Chen, ACS Appl. Mater. Interfaces 3 (2011) 1568-1573
- [21] J. Zhang, X.W. Xu, C. Yang, F. Yang, X.R. Yang, Anal. Chem. 83 (2011) 3911-3917
- [22] J.W. Liu, D. Mazumdar, Y. Lu, Angew. Chem. Int. Ed. 45 (2006) 7955-7959.
- [23] W.A. Zhao, M.M. Ali, S.D. Aguirre, M.A. Brook, Y.F. Li, Anal. Chem. 80 (2008)
- [24] X.C. Jiang, A.B. Yu, Langmuir 24 (2008) 4300-4309.
- [25] W. Leesutthiphonchai, W. Dungchai, W. Siangproh, N. Ngamrojnavanich, O. Chailapakul, Talanta 85 (2011) 870-876.
- [26] H.B. Li, Y.H. Bian, Nanotechnology 20 (2009)
- [27] A. Ravindran, V. Mani, N. Chandrasekaran, A. Mukherjee, Talanta 85 (2011) 533-540.
- [28] B. Roy, P. Bairi, A.K. Nandi, Analyst 136 (2011) 3605-3607.
- [29] Y. Wang, F. Yang, X.R. Yang, ACS Appl. Mater. Interfaces 2 (2010) 339-342.
- [30] H.B. Li, Z.M. Cui, C.P. Han, Sens, Act. B-Chem, 143 (2009) 87-92.
- [31] Y.H. Ngo, D. Li, G.P. Simon, G. Gamier, Adv. Colloid. Interfac. 163 (2011) 23-38
- [32] W.W. Yu, I.M. White, Anal. Chem. 82 (2010) 9626-9630.
- [33] A.E. Fisher, D.P. Naughton, Curr. Drug. Deliv. 2 (2005) 261-268.
- [34] B.C. Yin, B.C. Ye, W.H. Tan, H. Wang, C.C. Xie, J. Am. Chem. Soc. 131 (2009) 14624-14625
- [35] E.M. Fenton, M.R. Mascarenas, G.P. Lo'pe, S.S Sibbett, ACS Appl. Mater. Interfaces 1 (2008) 124-129.
- [36] R.C. Smith, V.D. Reed, Chem. Biol. Inter. 82 (1992) 209-217.
- [37] A. Krezel, W. Lesniak, M. Jezowska-Bojczuk, P. Mlynarz, J. Brasun, H. Kozlowski, W. Bal, J. Inorg. Biochem. 84 (2001) 77-88.
- [38] T.T. Lou, L.X. Chen, Z.P. Chen, Y.Q. Wang, L. Chen, J.H. Li, ACS Appl. Mater. Interfaces 3 (2011) 4215-4220.
- [39] Copper test strips EM Quant®, catalog number: 10003, Millipore, Germany.
- [40] Copper test strips, catalog number: PT753-50, Freshwatersystems, USA.